NOTE TO USERS

OPTICAL SPECTROSCOPY OF COLON TISSUE AND A BREAST CANCER CELL LINE: POTENTIAL FOR CANCER DETECTION

By

Christina Marie McLaughlin

Submitted in partial fulfillment of the requirements
for the Master of Science degree.

Lakehead University
Thunder Bay, Ontario

2004

Your file Votre référence
ISBN: 0-612-96984-3
Our file Notre référence
ISBN: 0-612-96984-3

ABSTRACT

McLaughlin, C. 2004. Optical Spectroscopy of Colon Tissue and a Breast Cancer Cell Line: Potential for Cancer Detection. 132 pp.

Key words: absorption, colon tissue, fluorescence, green fluorescent protein, breast cancer cell line, optical spectroscopy, tagged.

Two forms of cancer affecting a large number of individuals are breast cancer and colon cancer. In 2003, it was projected that approximately 21000 Canadians would be diagnosed with breast cancer and another18000 would be diagnosed with colorectal cancer (Canadian Cancer Society 2003a, Canadian Cancer Society 2003b). Optical spectroscopy techniques for discerning biochemical and morphological properties have been investigated for potential in detecting these two types of cancer. Techniques based on absorption and fluorescence spectroscopy were developed and preliminary data were obtained using cancerous and normal colon tissue, and using living Actin and H1 GFP tagged MCF-7 breast cancer cells. Analysis of absorption spectra for normal and cancerous colon tissue samples revealed a shift between the two, which may suggest a potential method to distinguish between the two tissue types. Fluorescence spectroscopy and imaging were also performed on the colon tissue samples. Analysis of the spectroscopic data revealed potential methods for differentiating between tissues. Fluorescence measurements were performed with living Actin and H1 GFP tagged MCF-7 breast cancer cells to investigate the value of imaging and spectroscopy under identical conditions. Various stages of mitosis and cellular movement were observed. As an extrapolation of this study some cells were irradiated with 5 Gy of Cobalt-60 gamma rays, but no differences between irradiated and non-irradiated samples were noted. These preliminary results reveal a potential application for optical diagnostic techniques, although further investigations are required.

ACKNOWLEDGEMENTS

This research would not have been possible without the support from the Medical Physics Department and Research Laboratory at the Northwestern Ontario Regional Cancer Centre, the Northern Cancer Research Foundation and the Physics Department at Lakehead University.

First of all, I would like to thank my supervisor Dr. Peter McGhee, who willingly accepted the responsibility as supervisor along with his many other duties as the Head of Medical Physics at the Northwestern Ontario Regional Cancer Centre and Adjunct Professor in the Department of Physics at Lakehead University. For his guidance and encouragement throughout my Master's I am greatly appreciative. He always found a way to challenge my way of thinking and stimulate discussions about physics.

I am especially grateful to Dr. Sylvie Landry for all her assistance with the instrumentation and preparation of cell samples. I appreciate putting up with my invasion into your office/lab often leaving you in the dark. I would like to thank Bans Arjune for his enthusiasm and many ideas for the research. I would also like to thank the remaining members of the Medical Physics Department Dr. Patrick Rapley, Isaac Tavares, Robert Knutson, Michael Tassotto, Lawrence DeGagne, and Dianne Brett for their support and friendship. Also, I would like to thank Curtis Shewchuk for our many discussions and concerns regarding our thesis research.

Further I would like to thank Dr. John Th'ng and Marisa Kubinec in the Research Lab for their collaboration. Without your expertise, resources, and time we would not have had any samples.

A special thanks to the Northern Cancer Research Foundation for financial support. Without your dedication to research in the North none of this would be possible.

I am grateful to all the professors and staff in the Physics Department at Lakehead University for their support and guidance throughout my Honours and Masters of Science in Physics. A special thanks to Dr. Werden Keeler for sharing his ideas, leading to the design and application of the eyepiece/fibre adapter.

Last but not least I would like to thank my family and friends who have supported me for so long. You have always been there to listen and guide me in the right direction when I got lost and for that I am grateful.

CONTENTS

		Page
ABSTRACT		ii
ACKNOWLEDGEMENTS		iii
TABLES		vii
FIGURES		ix
EQUATIONS		xii
1.	INTRODUCTION	1
2.	THEORY	1
	2.1. Light-Tissue Interactions	2
	2.2. Fluorescence Spectroscopy	9
	2.3. Fluorescence Imaging	19
	2.4. Tissue Diagnositics	24
	2.5. Radiobiology	31
3.	INSTRUMENTATION	34
	3.1. Absorption Spectroscopy	34
	3.2. Fluorescence Spectroscopy and Imaging	39
4.	SAMPLE PREPARATION	46
	4.1. References Standards	46
	4.2. Cell Lines	47
	4.3. Tissue	49
5.	METHODS	50
	5.1. Absorption Measurements	51
	5.2. Fluorescence Measurements	52
6.	ANALYSIS/RESULTS	55
	6.1. Absorbance Spectra	55
	6.2. Fluorescence Spectra and Images	70
7.	DISCUSSION	92
	7.1. Absorption Spectroscopy	93
	7.2. Fluorescence Spectroscopy and Imaging	98
8.	CONCLUSION	103
LITERATURE CITED		107

APPENDICES		114
APPENDIX I	ABBREVIATIONS AND ACRONYMS	115
APPENDIX II	UNIT CONVERSIONS	118
APPENDIX III	PRODUCTS	119
APPENDIX IV	DOSE CALCULATIONS	122
APPENDIX V	MEASUREMENT TIMELINES	124
APPENDIX VI.i.	ANALYSIS SUMMARY FOR ABSORPTION SPECTROSCOPY FOR COLON TISSUE	126
APPENDIX VI.ii.	ANALYSIS SUMMARY FOR FLUORESCENCE SPECTROSCOPY FOR ETHIDIUM BROMIDE	128
APPENDIX VI.iii.	ANALYSIS SUMMARY FOR FLUORESCENCE MEASUREMENTS FOR FIXED TAGGED REFERENCE CELLS	129
APPENDIX VI.iv.	ANALYSIS SUMMARY FOR FLUORESCENCE MEASUREMENTS FOR LIVING TAGGED MCF-7 CELLS	130
APPENDIX VI.v.	ANALYSIS SUMMARY FOR FLUORESCENCE MEASUREMENTS FOR COLON TISSUE	131

TABLES

Table		Page
2-1.	Absorption Wavelengths of Tissue Components.	6
2-2.	Biological Endogenous Fluorophores.	14
2-3.	Quantum Yield and Lifetimes for Aromatic Amino Acids.	15
3-1.	Adapter Components.	43
4-1.	Volumes and Concentrations of EtBr.	47
4-2.	Time to Deliver 500 cGy of ^{60}Co gamma rays.	49
5-1.	Spectrometer Integration Times and Light Intensities for Fluorescence Measurements.	54
6-1.	Ratio of the Spectral Area for Absorbance of Colon Tissue.	58
6-2.	Summary of Renormalization Absorbance Parameters for the Same Patient Comparison of Colon Tissue Samples.	60
6-3.	Fitting Parameters of Spectral Difference PAC-PAN, and PBC-PBN for Colon Tissue.	63
6-4.	Ratio of Area of Spectral Difference for Colon Tissue.	64
6-5.	Normalization Parameters for the Inter-patient Comparison.	65
6-6.	Fitting Parameters of Spectral Difference PAN-PBN, and PAC-PBC for Colon Tissue.	68
6-7.	Ratios of Area for Inter-patient Spectral Difference for Colon Tissue.	69
6-8.	Spectral Area for EtBr Concentrations.	71
6-9.	Spectral Areas of Fixed Tagged Reference Cells.	73
6-10.	Fluorescence Images and Spectra Summary for GFP Tagged MCF-7 Cells.	75
6-11.	Ratio of Spectral Area for Actin and HI GFP Tagged MCF-7 Cell Samples.	77
6-12.	Normalization Parameters for Actin and H1 GFP Tagged MCF-7 Cells.	80

Table		Page
6-13.	Ratio of the Spectral Difference for Actin GFP Tagged MCF-7 Cells.	82
6-14.	Ratio of the Spectral Difference for H1 GFP Tagged MCF-7 Cells.	83
6.15.	Ratio of Spectral Area for Fluorescence of Colon Tissue.	85
6-16.	Fluorescence Renormalization Parameters for Colon Tissue.	87
6-17.	Ratio of the Spectral Difference Between Fluorescence Spectra of Cancerous and Normal Colon Tissue.	89
6-18.	Fluorescence Renormalization Parameters for the Inter-patient Comparison of Colon Tissue.	90
6-19.	Absolute Spectral Difference by Inter-patient Comparison of Fluorescence Spectra of Colon Tissue.	92

FIGURES

Figure		Page
2-1.	EM Radiation Spectrum.	2
2-2.	Interactions of Light with Tissue.	3
2-3.	Jablonski Diagram of Absorption.	5
2-4.	Jablonski Diagram of Rayleigh Scattering.	7
2-5.	Jablonski Diagram of Raman Scattering.	8
2-6.	Jablonski Diagram of Fluorescence.	11
2-7.	Molecular Structure of EtBr.	13
2-8.	Aromatic Amino Acids.	15
2-9.	Structural Proteins.	16
2-10.	NADH and Flavin.	17
2-11.	Schematic of an Epi-fluorescence Microscope.	20
2-12.	Filter Cube.	21
2-13.	CCD Pixel.	23
2-14.	Structure of the Breast.	25
2-15.	Structure of Gastrointestinal Tract.	28
2-16.	Compton Interaction.	32
2-17.	Direct and Indirect Action.	33
3-1.	Basic Components for Absorption Spectroscopy.	35
3-2.	Components for Absorption Spectroscopy.	35
3-3.	Sample Holder, Illumination and Collection Fibre.	37
3-4.	Asymmetric Crossed Czerny Turner Design.	37

Figures		Page
3-5.	Components for Combined Fluorescence Spectroscopy and Imaging.	40
3-6.	Microscope Incubator.	42
3-7.	Microscope Eyepiece/Fibre Adapter.	42
3-8.	PVC Collar and Eyepiece/Fibre Adapter.	43
3-9.	Miniature Fibre Optic Spectrometer.	44
3-10.	CCD Camera Sensitivity.	45
4-1.	Cell Irradiation Geometry.	49
6-1.	Raw Absorbance Spectra for Colon Tissue of Patient PA.	56
6-2.	Raw Absorbance Spectra for Colon Tissue of Patient PB.	56
6-3.	Renormalized Spectra of Colon Tissue (N and C) from Patient PA.	61
6-4.	Renormalized Spectra of Colon Tissue (N and C) from Patient PB.	61
6-5.	Plots of Spectral Difference for PAC-PAN, and PBC-PBN Colon Tissue.	63
6-6.	Renormalized Spectra for the Inter-patient of Normal Colon Tissue	66
6-7.	Renormalized Spectra for the Inter-patient of Cancerous Colon Tissue.	66
6-8.	Plot of Inter-patient Spectral Difference PAN-PBN and PAC-PBC for Colon Tissue.	68
6-9.	Raw Fluorescence Spectra for EtBr.	70
6-10.	Raw Fluorescence Spectra for Fixed Tagged Reference Cells.	72
6-11.	Fluorescence Images of Fixed Tagged Reference Cells (a) 40 x Min Iris, (b) 40 x Opt Iris, (c) 60 x Min Iris, and (d) 60 x Opt Iris.	74
6-12.	Average Raw Fluorescence Spectra of Actin GFP Tagged MCF-7 Cell Samples.	75
6-13.	Average Raw Fluorescence Spectra of H1 GFP Tagged MCF-7 Cell Samples.	76

Figures Page

6-14. Image Sequence of Actin GFP Tagged MCF-7 Sample 3. 78

6-15. Image Sequence of Actin GFP tagged MCF-7 Sample 6 (Irradiated with 5 Gy of ^{60}Co gamma rays). 78

6-16. Image Sequence of H1 GFP Tagged MCF-7 Sample 4. 78

6-17. Image Sequence of H1 GFP tagged MCF-7 Sample 5 (Irradiated with 5 Gy of ^{60}Co gamma rays). 79

6-18. Renormalized Spectra of Actin GFP Tagged MCF-7 Cell Samples. 81

6-19. Renormalized Spectra of H1 GFP Tagged MCF-7 Cell Samples. 81

6-20. Raw Fluorescence Spectra of Colon Tissue from Patient PA (Normal – N and Cancerous – C). 84

6-21. Raw Fluorescence Spectra of Colon Tissue from Patient PB (Normal – N and Cancerous – C). 84

6-22. Fluorescence Images of (a) PAN, (b) PAC, (c) PBN, and (d) PBC Samples. 86

6-23. Renormalized Fluorescence Spectra to Compare Colon Tissue Samples of Patient PA. 88

6-24. Renormalized Fluorescence Spectra to Compare Colon Tissue Samples of Patient PB. 88

6-25. Renormalized Fluorescence Spectra for the Inter-patient Comparison of Normal Colon Tissue. 91

6-26. Renormalized Fluorescence Spectra for the Inter-patient Comparison of Cancerous Colon Tissue. 91

EQUATIONS

Equations		Page
2-1.	Law of Reflection.	4
2-2.	Reflectance.	4
2-3.	Snell's Law.	4
2-4.	Index of Refraction.	5
2-5.	Beer-Lambert Law.	6
2-6.	Change in Energy of a Molecule.	8
2-7.	Quantum Yield of Fluorescence.	11
2-8.	Numerical Aperture.	22
3-1.	Dispersion.	38
3-2.	Optical Resolution.	39
4-1.	Volume of EtBr.	46
6-1.	Spectral Area.	57
6-2.	Normalization of Spectral Data.	58
6-3.	Renormalized Spectra.	59
6-4.	Spectral Difference.	62
6-5.	Inter-patient Spectral Difference.	67
6-6.	Spectral Difference for Living Cells.	82

1. INTRODUCTION

In Canada, it is estimated that 145500 new cases of cancer will be diagnosed this year (Canadian Cancer Society 2004). In 2003, approximately 21000 women and men would have been diagnosed with breast cancer and 18000 men and women would have been diagnosed with colorectal cancer (Canadian Cancer Society 2003a, Canadian Cancer Society 2003b). As a result it is estimated that about 5300 breast cancer patients and 8300 colorectal cancer patients will die. To improve chances of survival, early detection and screening is essential. Optical spectroscopy could aid in such techniques. Optical spectroscopy has been an active area of research for noninvasive diagnostic techniques because of its potential to provide biochemical and morphological properties of cells and tissue (Ramanujam 2000). The work presented in this thesis investigated the potential for optical spectroscopy techniques and instrumentation to form the basis of tools used to characterize normal and cancerous tissue. In particular, a breast cancer cell line and colon tissues were examined. The thesis is divided into a theoretical discussion of techniques studied, instrumentation used for optical spectroscopy, the experiments carried out to characterize normal and cancerous colon tissue and breast cancer cells, the effects of radiation on these cells, discussion, and conclusions.

2. THEORY

Spectroscopic techniques take advantage of the interactions of electromagnetic radiation or light with matter. In general, such techniques have three aspects: excitation from electromagnetic radiation, measurement of the light-tissue interaction, and analysis and interpretation of the spectra (Ramanujam 2000). Clearly for optimal application of

optical spectroscopy it is important to have an understanding of light-tissue interactions, and the complex structure of tissue. The principles of fluorescence spectroscopy will be discussed, with a brief historical overview, including a description of the fluorescence process and an introduction to fluorophores and their key role. Fluorescence imaging for localization will also be discussed with an overview of fluorescence microscopy and CCD cameras. Current diagnostic techniques for breast cancer and colon cancer detection will be discussed to illustrate the need to investigate new techniques. Finally, an introduction to radiobiology will be presented to show effects of radiation on cells.

2.1. LIGHT – TISSUE INTERACTIONS

Upon interaction with tissue, light or electromagnetic radiation can undergo various interactions that are highly wavelength dependent. Figure 2-1, adapted from Beiser (1995), shows the spectrum of electromagnetic (EM) radiation.

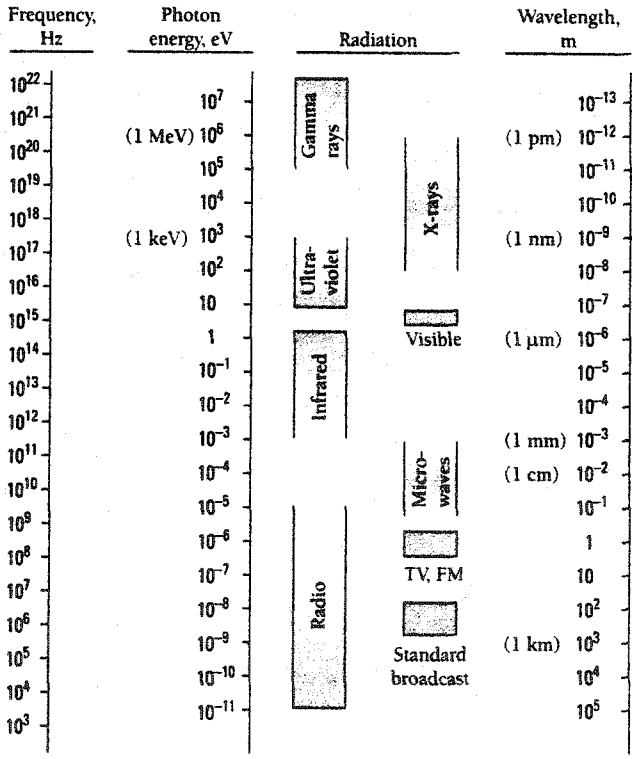

Figure 2-1. EM Radiation Spectrum (Beiser 1995)

For optical spectroscopy the region of interest extends through the ultraviolet (UV), visible (VIS), and the near-infrared (NIR) regions making up only a small portion of the electromagnetic spectrum. Wilson (2002) states that the optical range is useful in giving biochemical information of tissue for two fundamental reasons: the molecular energy level difference in tissue corresponds to the optical photon energies and the size of macromolecules in cells and tissues correspond to the optical wavelength range. The optical photon energies are on the order of 10^{-2} eV to 10^{2} eV, and the optical wavelength range is on the order of micrometers (μm) as seen in figure 2-1.

A typical situation of light incident on tissue with indices of refraction n_1 and n_2 is depicted in figure 2-2 modified from Niemz (1996). The light incident on tissue has the ability to interact through reflection, refraction, absorption, and scattering.

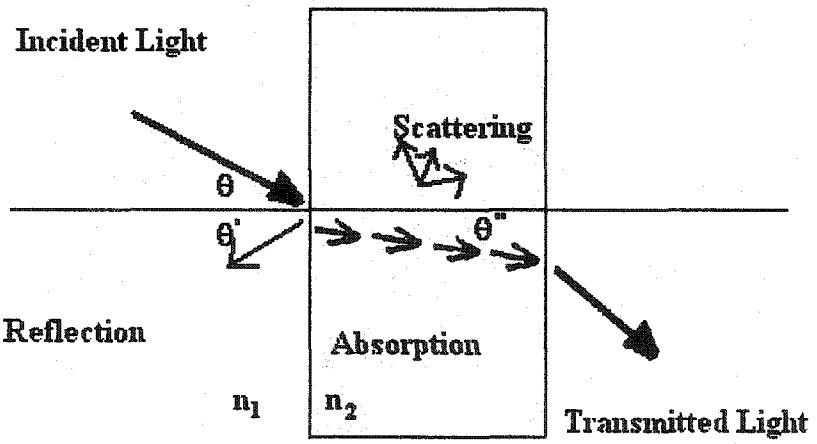

Figure 2-2. Interactions of Light with Tissue (Niemz 1996).

2.1.1. Reflection

Reflection occurs when light incident on an interface such as a tissue surface is deflected without a change in the wavelength. In general, the incident angle θ has to equal the reflected angle θ' in the plane of incidence as illustrated in figure 2-2 and expressed in equation 2-1.

Equation 2-1. Law of Reflection.

$$\theta = \theta'$$

There are two forms of reflection, specular and diffuse, that are highly dependent on the surface of the interface. For specular reflection to dominate, the interface surface must be relatively smooth so that the irregularities are small compared to the wavelength of light allowing the reflection to occur in the plane of incidence. In comparison, diffuse reflection occurs at rough surfaces where irregularities are equal to or greater than the wavelength of light. In general, diffuse reflectance occurs in all tissues where the reflected light does not necessarily lie in the plane of incidence (Niemz 1996). Reflectance is a function of wavelength and is evaluated as a fraction of the emitted intensity over the incident intensity as given by equation 2-2.

Equation 2-2. Reflectance.

$$R = \frac{I}{I_o}$$

Reflectance, incident intensity, and emitted intensity are denoted by R, I_o, and I respectively. In general, a reflection spectrum is a plot of the percent reflectance (%R) versus wavelength.

2.1.2. Refraction

When light passes from one medium to another, such as air to tissue at an oblique angle, the change in direction of propagation is called refraction. Refraction can be explained by Snell's Law that relates the refractive index of the medium to the angle of propagation in that medium (Pedrotti and Pedrotti 1993) as expressed in equation 2-3.

Equation 2-3. Snell's Law.

$$n_1 \sin\theta = n_2 \sin\theta'$$

θ is the angle of the incident light on the medium, and θ'' is the angle of refraction in the medium that depends on the indices of refraction n_1 and n_2 of the two media. The index of refraction is the ratio of the speed of light in a vacuum to the speed of light in the medium as expressed in equation 2-4.

Equation 2-4. Index of Refraction

$$n = \frac{c}{v}$$

The speed of light (c) in a vacuum is 2.998×10^8 m/s, and v is the speed of light in the media in which it is traveling through.

2.1.3. Absorption

If a photon interacting with a molecule has an energy corresponding to the molecules electronic state energy difference, absorption can occur. Figure 2-3, is an electronic energy level (Jablonski) diagram illustrating the absorption process.

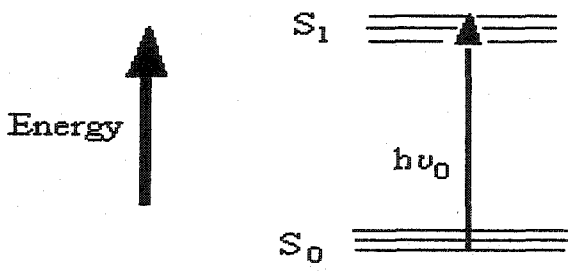

Figure 2-3. Jablonski Diagram of Absorption.

The molecule absorbs a photon of energy $h\nu_0$, raising the molecule to a higher singlet electronic energy level (S_1) from the ground energy level (S_0). Each electronic energy level contains vibrational energy levels (v_n). Absorbance can be defined using the Beer-Lambert law stated in equation 2-5 as a function of wavelength relating the incident intensity to the emitted intensity:

Equation 2-5. Beer-Lambert Law.

$$A = -\log\left(\frac{I}{I_o}\right)$$

A is the absorbance, I_o is the incident intensity, and I is the emitted intensity. The Beer-Lambert law is derived with the assumption that the absorbing material is homogeneous. The Beer-Lambert law fails in four cases because this assumption does not hold: different forms of absorbing molecules are in equilibrium; solute and solvents form association complexes; thermal equilibrium; or for the presence fluorescent compounds or compounds changed by irradiation (Pavia *et al.* 1996). An absorption spectrum is a plot of the absorbance versus the wavelength. Absorption plays a key role in several processes including the excitation stage of fluorescence, phosphorescence, and Raman scattering. Absorption in tissue is caused mainly by oxyhemoglobin, melanin, deoxyhemoglobin, myoglobin, water, and proteins (Richards-Kortem and Sevick-Muraca 1996). The absorption wavelengths of the tissue components adapted from af Klinteberg (2000) and Wilson (2002) are summarized in table 2-1.

Table 2-1. Absorption Wavelengths of Tissue Components (af Klinteberg 2000 and Wilson 2002).

Molecule	Absorption
Oxyhemoglobin	418 nm, 542 nm, and 577 nm
Deoxyhemoglobin	430 nm, 450 nm, and 750 nm
Water	Below 200 nm, and above 1300 nm
Proteins, Amino Acids	100 nm to 400 nm
Melanin	VIS

The visible to near-infrared region of the spectrum (400 nm to 1300 nm) is primarily where these molecules absorb with the notable exception of proteins that absorb in the ultraviolet region.

2.1.4. Scattering

Scattering processes, unlike the absorption process do not correspond to resonant frequencies of a molecule. Scattering can be divided into two categories: elastic and inelastic. Elastically scattered photons have the same energy as the incident photons but have a different direction. Photons scattered inelastically have a lower energy compared to the incident photons (af Klinteberg 2000). In general, tissues are forward scattering for the photon energy range of 0.56 eV to 3.55 eV (Niemz 1996, Richards-Kortum and Sevick-Muraca 1996).

Rayleigh scattering and Mie scattering are forms of elastic scattering. For Rayleigh scattering, particles must be much smaller in size relative to the incident wavelength; Mie scattering particles are closer to the size of the incident wavelength. Rayleigh scattering occurs when a molecule is moved to an excited state through absorption of a photon. The excited state is unstable so the molecule loses energy, returning to the ground state a short time later with the emission of a photon of the same energy as the incident photon. Figure 2-4 shows a Jablonski diagram of Rayleigh scattering.

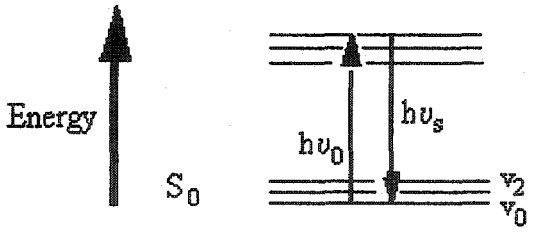

Figure 2-4. Jablonski Diagram of Rayleigh Scattering.

The excited molecule relaxes to the same vibrational level as the original state (i.e. from v_0 excited state and back to v_0). Rayleigh scattering has a radial direction and has a

wavelength dependence of λ^{-4}. Mie scattering has a forward direction and has a weaker dependence on wavelength $\lambda^{-(0.4 \text{ to } 0.5)}$ (Niemz 1996). Biological tissues have been observed to scatter in the forward direction but the wavelength dependence was greater than Mie scattering predicted (Niemz 1996 and Richards-Kortem and Sevick-Muraca 1996).

A form of inelastic scattering is Raman. When an incident photon collides with a molecule, a change in vibrational or rotational energy (ΔE_m) occurs resulting in Raman scattering (Colthup *et al.*1990). Figure 2-5, adapted from Lin-Vien *et al.* (1991), illustrates a Jablonski diagram of the Raman scattering process.

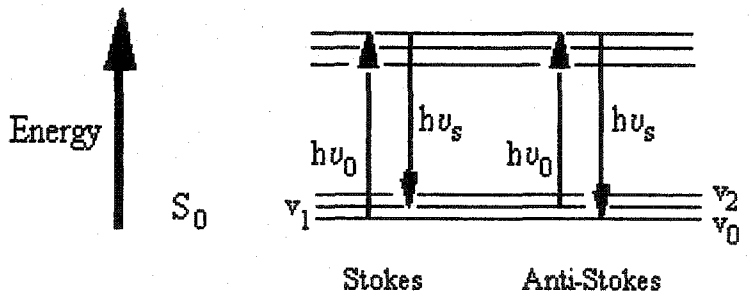

Figure 2-5. Jablonski Diagram of Raman Scattering (Lin-Vien *et al.* 1991).

The excited molecule relaxes to an elevated vibrational level v_1 compared to the original state v_0 resulting in Stokes lines. Anti-Stokes lines result when the excited molecule relaxes to a lower vibrational level compared to the original state (i.e. v_1 to v_0). To conserve energy the scattering photon ($h\nu_s$) must differ from the incident photon ($h\nu_0$) shown in equation 2-6.

Equation 2-6. Change in Energy of a Molecule.

$$\Delta E_m = h\nu_0 - h\nu_s$$

Stokes lines are present in the Raman spectra for positive ΔE_m, anti-Stokes lines are present in the Raman spectra for negative ΔE_m. Stokes lines are red shifted relative to

the excitation energy whereas anti-Stokes lines are blue shifted. The change in energy between the incident and scattered photon is unique to molecular vibration and can be used to determine chemical structure. A Raman signal is approximately 10^{-3} times weaker than a fluorescence signal, so, as a result, imaging is not practicable (Wilson 2002).

Absorption and elastic scattering techniques have been used as diagnostic tools for ophthalmology and white light endoscopy (Wilson 2002). Raman spectroscopy has been used for disease detection and tissue characterization (Hanlon *et al.* 2000 and Wilson 2002). Current diagnostic and therapeutic applications tend to operate in the 600 nm to 1000 nm region where tissue absorption is low compared to tissue scattering, a desirable condition for fluorescence spectroscopy (Richards-Kortem and Sevick-Muraca 1996).

2.2. FLUORESCENCE SPECTROSCOPY

2.2.1. Historical Background

The fluorescence phenomenon has been documented in Chinese literature as far back as the 1500's (Shannon Luminous Materials, Inc. 2001). Centuries later, in 1852, Sir George Stokes observed that the energy of fluorescence emission is lower than the energy of excitation. This observation led to the formulation of Stokes law and the introduction of the term fluorescence. Lakowicz (1999) states Stokes law as fluorescence occurring at longer wavelengths than the excited light. Policard first investigated fluorescence spectroscopy for cancer detection in 1924 using a UV/VIS (ultra-violet and visible) light source for the detection of autofluorescence of porphyrins (Wagnières *et al.* 1998). Over the past 20 years, fluorescence spectroscopy has been

further investigated as a potential diagnostic technique. The research group headed by Robert Alfano has pioneered these investigations (Alfano *et al.* 1984, Alfano *et al.* 1987, Lui *et al.* 1992, Katz and Alfano 1996, Zhandin *et al.* 1997, and Gayen and Alfano 1999). Remarkable progress has been made with fluorescence spectroscopy for medical applications including cancer detection (Yang *et al.* 1997).

2.2.2. Fluorescence Theory

Fluorescence is a three-stage process where a photon from an external excitation source is absorbed by a fluorescent molecule, resulting in a subsequent spontaneous emission by the molecule of a longer wavelength photon. Lakowicz (1999), Ramanujam (2000), and Molecular Probes, Inc. (2002) describe the three-stage fluorescence process as excitation, excited lifetime, and fluorescence emission. As already described excitation occurs when a molecule absorbs a photon of a given energy $h\nu_0$ from an external light source causing the molecule to excite to a higher energy level (S_2). The light absorption occurs almost immediately (roughly 10^{-15} seconds). During the excited lifetime the fluorescent molecule is subject to various interactions. Partial energy dissipation by means of internal conversion occurs with a rapid relaxation of 10^{-12} seconds or less from a higher vibrational level (v_n) of S_2 or S_1 to v_0 of S_1 (Lakowicz 1999). Once excited, molecules can return to the ground state through non-radiative or radiative processes. Fluorescence emission is the radiative process where the ground state is achieved through the emission of a photon of energy $h\nu$ corresponding to the energy difference between S_0 and S_1. The emitted photon has a lower energy than the excitation photon due to energy dissipation such as internal conversion, a non-radiative

process. Figure 2-6 shows a simplified electronic energy level (Jablonski) diagram illustrating the three-stage process.

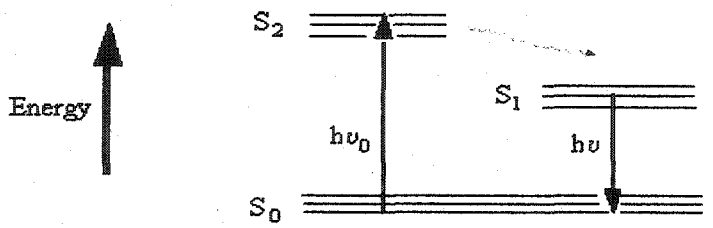

Figure 2-6. Jablonski Diagram of Fluorescence (Molecular Probes, Inc. 2002).

Singlet electronic energy levels have electron spin quantum numbers with a sum of zero therefore the electron in the excited orbital has an opposite spin orientation relative to the ground state electron (Lakowicz 1999). In general, the ground states of most molecules, with the notable exception of the oxygen molecule (O_2), have singlet ground states (S_0). The energy level differences between two energy levels is roughly 6.21 eV to 1.24 eV, corresponds to light with wavelength within the range of 200 nm to 1000 nm.

Fluorescent molecules are characterized by their quantum yield (φ) and lifetime (τ) (Ramanujam 2000). Quantum yield represents the efficiency with which a fluorescent molecule converts absorbed light to emitted light and, as shown in equation 2-7, is the ratio of the number of photons emitted to the number absorbed.

Equation 2-7. Quantum Yield of Fluorescence.

$$\varphi = \frac{N_{em}}{N_{ab}}$$

In this equation, N_{em} is the number of photons emitted and N_{ab} is the number of photons absorbed in the sample and φ is the quantum yield. The quantum yield ranges from 0 for non-fluorescent molecules to 1 for fluorescent molecules with 100% efficiency. Due to

Stokes losses, the quantum yield of fluorescence is always less than 1. The higher the quantum yield for fluorescent molecules the better they can be observed. Fluorescence lifetime (τ) is the average time the fluorescent molecules spends in the excited state before returning to the ground state (Lakowicz 1999). Fluorescent molecules have lifetimes on the order of 10^{-9} seconds.

Data from fluorescence spectroscopy can be analyzed as excitation spectra or emission spectra. In a fluorescence excitation spectrum the emission wavelength is fixed and the fluorescence intensities are plotted over a range of excitation wavelengths. A fluorescence emission spectrum is a plot of the fluorescence intensities over a range of emission wavelengths for a fixed excitation wavelength (Gillenwater 1998). In general, excitation spectra are similar to corresponding absorption spectra, showing the relative emission of the fluorescent molecules at each excitation wavelength (Lakowicz 1999). Emission spectra show the photon emission rate at each wavelength and are highly dependent on the chemical structure of fluorescent molecules present.

2.2.3. Fluorophores

Certain molecules known as fluorophores have the ability to fluoresce at a longer wavelength than the excited light. There are two classifications of fluorophores: exogenous or endogenous. Exogenous fluorophores need to be introduced into a sample while endogenous fluorophores are naturally occurring in a sample. Fluorescence spectroscopy techniques using fluorophores have been investigated for molecular biology and medical applications. In particular, exogenous fluorophores such as δ-aminolevulinic acid (5-ALA), induced protoporphyrin IX (PpIX), and hematoporphyrin derivative (HpD) have been studied as photosensitive agents in photodynamic therapy

(PDT) (Ramanujam 2000 and Wagnières *et al.* 1998). Green fluorescent protein (GFP) is important in biological research for *in situ* investigations of distribution and interaction of cell and tissue components. Green fluorescence protein originates from Jellyfish *Aequorea Victoria* (Knight and Billinton 2001). Ethidium Bromide (EtBr) is another exogenous fluorophore commonly used to stain nucleic acid. Figure 2-7, from Molecular Probes (2003), shows the complex structure of EtBr.

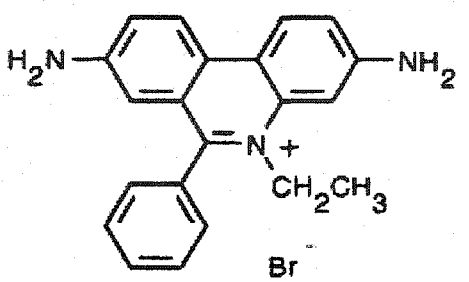

Figure 2-7. Molecular Structure of EtBr (Molecular Probes 2003).

EtBr alone has an absorption (or excitation) peak near 480 nm and an emission peak maximum near 620 nm. Upon binding to DNA the excitation peak shifts to 530 nm and the emission peak to 600 nm (Sigma-Aldrich Co. 2003). Endogenous fluorophores have been studied as potential diagnostic tools through attempts to use them to differentiate normal and diseased tissues such as breast, colon, lung, brain, stomach and cervical tissue. Biological tissues are comprised of a complex combination of molecules such as endogenous absorbers and endogenous fluorophores. Table 2-2 from Ramanujam (2000) summarized endogenous fluorophores found in tissue including the wavelengths corresponding to the peak maxima for the excitation and fluorescence emission.

Table 2-2. Biological Endogenous Fluorophores (Ramanujam 2000).

Endogenous fluorophores	Excitation Maxima (nm)	Emission Maxima (nm)
Amino Acids:		
Tryptophan	280	350
Tyrosine	275	300
Phenylalanine	260	280
Structural Proteins:		
Collagen	325	400,405
Elastin	290,325	340,400
Enzymes and coenzymes:		
FAD, flavins	450	535
NADH	290,351	440,460
NADPH	336	464
Vitamins:		
Vitamin A	327	510
Vitamin K	335	480
Vitamin D	390	480
Vitamin B6 Compounds:		
Pyridoxine	332,340	400
Pyridoxamine	335	400
Pyridoxal	330	385
Pyridoxic Acid	315	425
Pyridoxal 5'-phosphate	330	400
Vitamin B12	275	305
Lipids:		
Phospholipids	436	540,560
Lipofuscin	340-395	540,430-460
Ceriod	340-395	430-460,540
Porphyrins:		
Porphyrins	400-450	630,690

The excitation wavelengths of these fluorophores range from approximately 260 nm to 450 nm and a fluorescence emission wavelength range from approximately 280 nm to 700 nm. Aromatic amino acids, structural proteins, enzymes and coenzymes are some of the endogenous fluorophores that are believed to play significant roles in normal tissues and cancerous tissues.

Amino acids are the basic building block of proteins. Tryptophan, tyrosine, and phenylalanine are amino acids with aromatic side chains that fluoresce. Figure 2-8 modified from Alberts *et al.* (2002) depicts the chemical structures of these three amino acids.

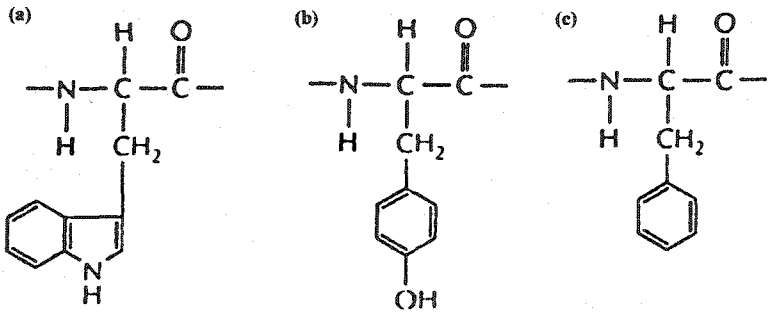

Figure 2-8. Aromatic Amino Acids; (a) tryptophan, (b) tyrosine, (c) phenylalanine (Alberts *et al.* 2002).

The excitation for these amino acids occurs in the 260 nm to 280 nm range with the emission in the 280 nm to 350 nm range. Tryptophan has a broader fluorescence emission range while the range for phenylalanine is narrower. The quantum yield and fluorescence lifetime of the three amino acids are given in table 2-3.

Table 2-3. Quantum Yield and Lifetimes for Aromatic Amino Acids (Lakowicz 1999).

Fluorophore	Quantum Yield	Fluorescence Lifetime (ns)
Tryptophan	0.13	3.1
Tyrosine	0.14	3.6
Phenylalanine	0.02	6.8

Tryptophan and tyrosine have similar quantum yields, while phenylalanine has a much lower quantum yield. Tryptophan is more dominant, with higher fluorescence intensities than tyrosine and phenylalanine. Fluorescence intensity in this context refers to the number of emitted photons of a given energy per unit area. The fluorescence intensity is dependent on the absorption, concentration, quantum yield, excitation source and the efficiency of the instrumentation. Phenylalanine has the lowest fluorescence intensity due to the low quantum yield; its fluorescence emission is rarely observed (Lakowicz 1999).

Ganesan *et al.* (1998) investigated the fluorescence emission spectra for normal and malignant human oral epithelial cells at an emission of 340 nm. These spectra

showed differences that were attributed to tryptophan, tyrosine, and phenylalanine. The normalized fluorescence excitation spectra were greater for normal cells in the 250 nm to 290 nm range and greater for the malignant cells in the 290 nm to 320 nm range. The peak near 290 nm for the malignant cells was red shifted relative to the normal cells.

Structural proteins such as collagen and elastin are major components in the extracellular matrix. Collagen is comprised of fibrous proteins that give connective tissue its tensile strength. Elastin is loose and unstructured covalently linked netting giving skin and other tissue elastic properties (Alberts *et al.* 2002). Figure 2-9 from Alberts *et al.* (2002) illustrates (A) collagen and (B) elastin.

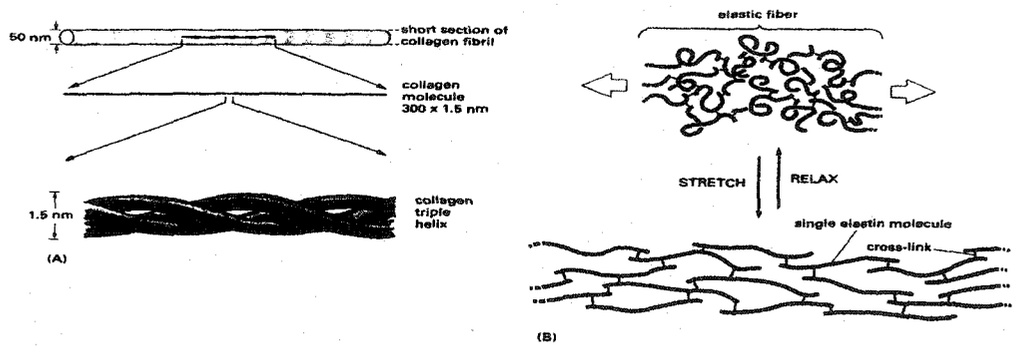

Figure 2-9. Structural Proteins (Alberts *et al.* 2002).

Structural proteins are common components in skin and bone. From table 2-2, the excitation maximum for collagen is 325 nm and for elastin are 290 nm and 325 nm. These structural proteins have an emission maxima range from 340 nm to 405 nm.

Nicotinamide adenine dinucleotide (NADH) and flavins play an important role in cellular energy metabolism. NADH in the reduced form and flavins in the oxidized form in figure 2-10 are electron carriers.

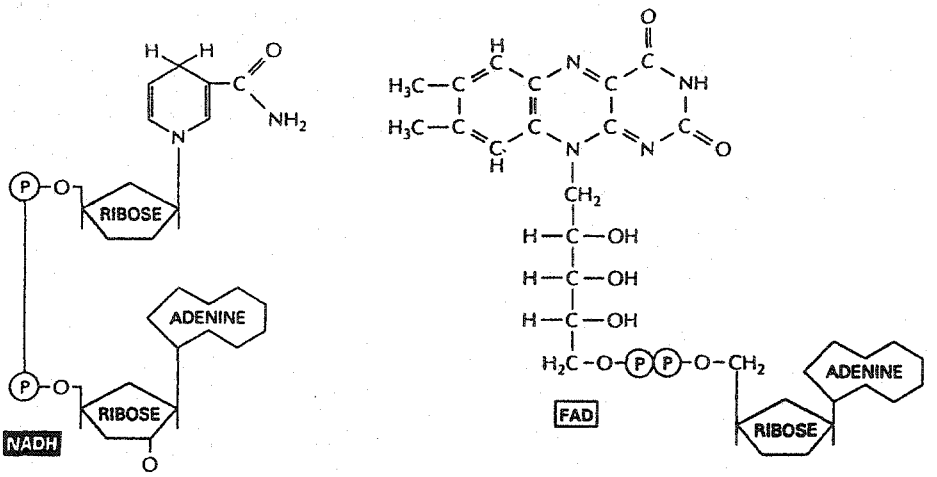

Figure 2-10. NADH and Flavin (Alberts *et al.* 2002).

The reduced nicotinamide ring of NADH and the oxidized form of FAD can fluoresce at wavelengths of approximately 440 nm and 535 nm respectively.

Main peaks near 520 nm to 530 nm in the fluorescence spectra for normal and malignant breast tissues at 488 nm, 514.4 nm, and 457.9 nm excitations with an argon ion laser have been attributed to flavins (FAD). In this study the spectra of malignant tissue had a smoother profile and a greater intensity in the wavelength range of 460 nm to 700 nm compared to the spectra of normal breast tissue (Alfano *et al.* 1987 and Alfano *et al.* 1989).

Fluorescence spectroscopy of breast tissue has shown differences in normal and cancerous tissues that have been attributed to structural proteins, NADH, and flavins (Majumber *et al.* 1996, Gupta *et al.* 1997, Jain *et al.* 1998, and Majumber *et al.* 1999). Jain *et al.* (1998) found that for 310 nm excitation the fluorescence spectra of malignant breast tissue were approximately 2.8 times higher in intensity than the normal breast tissue in the 325 nm to 575 nm range. Results suggest that the concentration of collagen, elastin, NADH, and flavins are greater in cancerous tissue than in normal tissue. Majumber *et al.* (1999) found that at 337 nm excitation the fluorescence emission

spectra of cancerous breast tissue were higher in intensity compared to normal or benign breast tissue. Further investigations using fluorescence excitation spectra determined that NADH has a higher concentration in cancerous tissues.

Liu *et al.* (1992) investigated fluorescence spectroscopy of breast tissue and breast cells with excitation at 300 nm and 353 nm respectively. The ratio of the emissions at 340 nm to those at 440 nm was calculated for the normal, benign, and cancerous breast tissue. The ratio for the cancerous tissue was significantly greater compared to the normal and benign. The differences were likely due to the concentration of tryptophan, tyrosine, NADH, and the structural proteins. Fluorescence measurements of cultured cells were investigated to provide more insight into tissue fluorescence. As a result the cancerous cell lines had a relatively stronger emission from NADH relative to that of normal tissue. The ratio of the emissions at 450 nm to those at 525 nm was greater for the cancerous cell lines compared to the normal cell line.

Fluorescence spectroscopy of colon tissue has shown differences in normal and malignant tissues that have been attributed to collagen, NADH, and flavins (Schomacker 1992a, and Schomacker 1992b). With ultraviolet excitation, the fluorescence spectra changed significantly between normal and malignant colon tissue. Using a multivariable linear regression analysis, the intensity of normal colon tissue was greater than malignant tissue at a wavelength of 390 nm. Major bands attributed to emission from fluorophores were centered at 390 nm and 460 nm, with minor bands at 630 nm to 680 nm.

Huang *et al.* (1998) studied fluorescence spectroscopy of normal and cancerous colon tissue using wavelengths from a continuous wave mixed-gas (Ar/Kr) laser. The fluorescence emission spectra in the 520 nm to 620 nm range were similar for both

normal and cancerous. Peaks in the 635 nm, 675 nm, and 703 nm range were observed in the cancerous colon tissue and can be attributed to porphyrins.

As shown in various studies, differences in fluorescence emission spectra of normal, benign, and cancerous tissues can be attributed to endogenous fluorophores. Therefore fluorescence spectroscopy has the potential to be a useful tool in differentiating biochemical and morphological changes in tissues. Although significant progress has been made, further investigations are required to improve on existing technique.

2.3. FLUORESCENCE IMAGING

2.3.1. Historical Background

In general, microscopy has been used primarily for investigations in biological and biomedical fields. Fluorescence microscopy was first developed in the early 1900's with excitation of samples using transmitted light. A significant improvement to the fluorescence microscope was realized in 1929 when reflected illumination was introduced for sample excitation. The use of reflected light to illuminate a sample is referred to as epi-fluorescence. In order to retain the images observed through the microscope, imaging capabilities needed to be combined with the system. Initially imaging was achieved with photographic techniques that subsequently led to replacement with digital imaging detectors such as charged-coupled devices (Wang and Herman 1996). Although charged-coupled devices (CCDs) were not commercially available until the mid 1980's for imaging applications (Mason 1999), they were first invented in 1970 at Bell Laboratories by Willard Boyle and George Smith (Taylor 1998).

2.3.2. Epi-fluorescence Microscopy

A fluorescence microscope is designed to deliver light to excite the sample and then to separate the emitted light from this excitation light. (Herman 2001). Key components of a typical epi-fluorescence microscope are shown schematically in figure 2-11. Excitation light passes from the light source, consisting of the lamp and collector lens, through an excitation filter where it is reflected onto an objective to the sample by a dichroic beam splitter. The emitted light from the sample is transmitted back through the objective, passing through the beam splitter and an emission filter to the eyepiece or detector. The fluorescence filter cube is comprised of an excitation filter, dichroic beam-splitter, and emission filter (re. Figure 2-12). The excitation light is of a shorter wavelength than the emitted light due to losses as discussed in the fluorescence theory (re. 2.2.2).

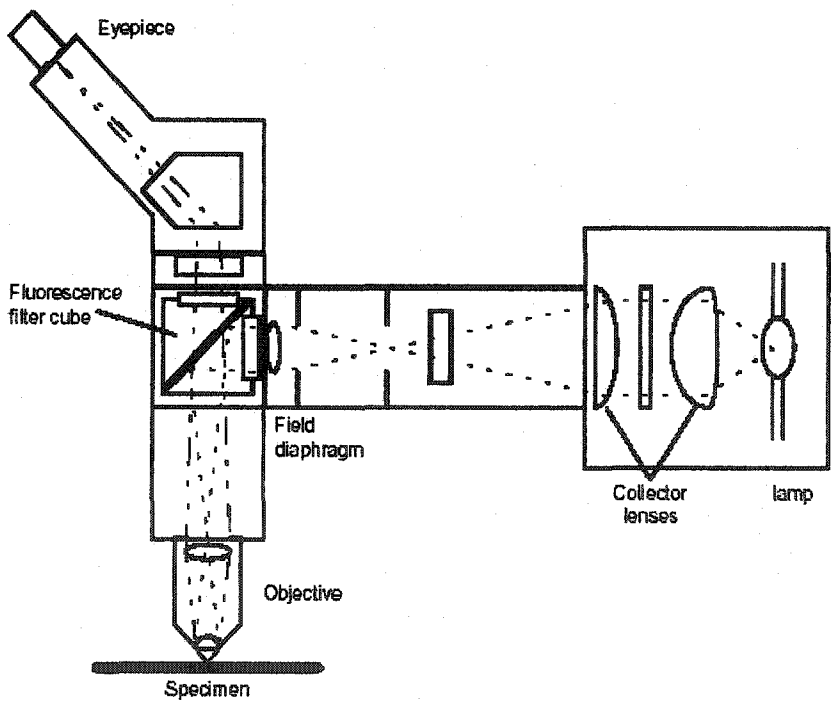

Figure 2-11. Schematic of an Epi-fluorescence Microscope (Reichman 2000).

The light source required in epi-fluorescence microscopy is selected to excite the sample at specific wavelengths, the particular wavelengths depending on the types of fluorophores present in a sample. Halogen, mercury and xenon high pressure arc lamps are a few of the common light sources used. Halogen and xenon lamps have roughly a continuous emission over a broad wavelength range (UV/VIS/NIR). Mercury arc lamps produce line spectra with strong emission peaks at specific wavelengths (i.e. 366 nm, 405 nm, 436 nm, 546 nm, and 578 nm).

The filter cube, as illustrated in figure 2-12, is the primary filter element in the epi-fluorescence microscope and is comprised of three main elements: an excitation filter, a dichroic beam splitter, and an emission (or barrier) filter. The excitation filter is a wide band pass filter that transmits a certain wavelength range of incident light. The coated dichroic beam splitter is aligned at an angle of 45 degrees to separate the excitation and emission light by 90 degrees. The coating on the beam splitter is designed to selectively reflect the excitation wavelengths filtered by the excitation filter and transmits the emitted fluorescence (Reichman 2000). The emission (or barrier) filter is a long pass filter that attenuates the excitation light and transmits longer wavelengths emitted from the sample for a given spectral range.

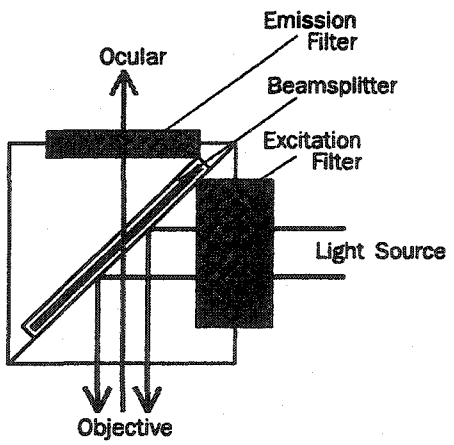

Figure 2-12. Filter Cube (Reichman 2000).

In an epi-fluorescence microscope the objective is used to focus and collect light. Excitation light is reflected into the back aperture of the objective and focused onto the sample. The emitted light is also collected using the objective (Herman 2001). The amount of light focused on or collected from the sample depends on the numerical aperture and magnification of the objective. Numerical aperture (NA) as given in equation 2-8 (Herman 2001) is defined as the light gathering efficiency of the objective lens and provides a measure of detail resolution at a fixed object distance.

Equation 2-8. Numerical Aperture.

$$NA = n \sin \alpha$$

n is the refractive index (re. Equation 2-4) of medium lying between the objective and the sample, and α is the half cone angle of the emitted light relative to the incident light. The larger the numerical aperture value, the greater the brightness of the image. The magnification of the objective is also related to the numerical aperture, resulting in a trade-off situation where, when magnification is increased, image brightness decreases.

2.3.3. CCD Camera

Charged coupled devices (CCDs) are based on physical principles similar to metal oxide semiconductors (MOS). Charged coupled devices are manufactured using a silicon substrate (Mason 1999). In general, CCDs are comprised of light sensitive cells (called pixels) where the charge is generated as a result of the photoelectric effect in the energy range of 1.1 eV to 4.1 eV (Buil 1991 and Mason 1999). Pixels are typically arranged in linear or area (two-dimensional) arrays. Pixel binning represents the area of a single charge of all individual pixels. A pixel binning of one (1 pixel x 1 pixel) refers to an individual pixel, whereas a pixel binning of 2 (2 pixels x 2 pixels) refers to an area of four adjacent pixels which increases the sensitivity by four but decreases the

resolution by half. As for fluorescence, the quantum efficiency for the CCD camera is also important relating the number of electrons collected by a given pixel to the number of photons incident on that pixel.

Typical charged coupled devices are built on p-type silicon with an n-type substrate layer on the surface upon which a silicon dioxide (SiO_2) layer is deposited and metal electrodes attached. Figure 2-13 shows a schematic of a CCD pixel (Taylor 1998). Reverse biasing the p-n junction by applying a positive voltage (V_a) to the electrode creates potential wells in the n-type substrate below the electrode. Photons with energies greater than 1 eV penetrating the silicon have sufficient energy to break covalent bonds, generating electron - hole pairs in the depletion region. Due to the electric field arising from the applied voltage (V_a), the electrons migrate towards the SiO_2 layer, and become trapped in the potential wells.

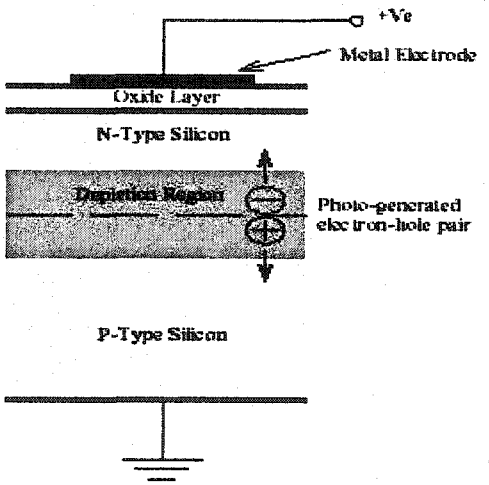

Figure 2-13. CCD Pixel.

The number of electrons is proportional to the number of incident photons (Buil 1991 and Taylor 1998). The electrical charge is transferred across the array surface to read-out registers through charge transfer. The transfer of charge within the detector can be

done through a number of techniques including: four-phase, three-phase, two-phase, or one-phase. Three-phase transfer is a common technique where each pixel has three distinct areas (or phases) arranged vertically. During the exposure time phases 1 and 2 collect and hold charge while phase 3 blocks charge. After the exposure the charge from phase 1 is transferred into phase 2 while phase 3 continues to block charge. Once all the charge from phase 1 is transferred into phase 2, phase 1 begins to blocks charge. Next, phase 3 collects and holds charge from phase 2 dispersing evenly through out the two phases (2 and 3), while phase 1 continues to block charge. The charge is then forced into phase 3 by blocking charge to phase 2. This process is repeated until the charge moves to the adjacent pixel, and completed once reaching the read-out register (Taylor 1998 and Mason 1999). The electrical charge in the read-out registers are converted into a digital signal by an A/D converter.

There are four different architectural types of two-dimensional (area) array CCDs: full frame, frame transfer, split frame transfer, and interline transfer. They differ in the way in which the light sensitive regions and read-out registers are oriented.

2.4. TISSUE DIAGNOSTICS

Optical spectroscopy has been investigated for its potential as a diagnostic tool for many types of tissue including brain (Lin *et al.* 2001), breast (Pradhan *et al.* 2000), lung (Hung *et al.* 1991), upper and lower gastrointestinal tract (Mayinger *et al.* 2000 and Prosst and Gahlen 2002), and gynecological (Glassman *et al.* 1994). A brief discussion of breast and colon tissue and current diagnostic techniques will be discussed. Breast and colon were chosen due to available resources, and the prevalence of these types of cancers.

2.4.1. Breast Tissue

The breast covers an area above the chest wall extending from the armpit to the sternum and up to the collarbone (Canadian Cancer Society 2002a). The female breast is more developed than the male breast. The main function of the breast in women is to produce and secrete milk to nourish newborns. Breast tissue is composed of many structures that can be divided into two categories: glandular and adipose. The glandular tissue includes lobes, lobules, and ducts. Adipose tissue is mainly fat. Figure 2-14 shows the basic structure of the breast adapted from the National Cancer Institute (2003).

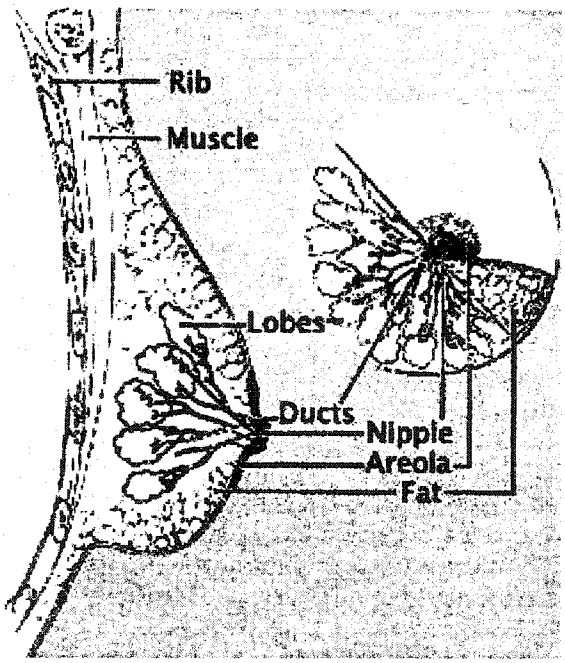

Figure 2-14. Structure of the Breast (National Cancer Institute 2003).

There are about 20 lobes in a breast which are distributed about the nipple in a radial fashion. The lobes consist of lobules (or milk glands) with secreting cells embedded in connective tissue. The milk that is produced in the lobules is carried out to the nipple through ducts. Adipose (fatty) tissue surrounds the lobules and ducts for protection. Lymph nodes act as a defense system and are located in the armpit, collarbone, and

sternum regions filtering blood and removing impurities. Ligaments have an elastic property and act to support and shape the breast. Breast cancers are almost all adenocarcinomas derived from glandular epithelial tissue of the breast. (Canadian Cancer Society 2002a, National Cancer Institute 2003). The subtypes of breast cancer are generally classified by the site of origin. Ductal carcinomas originate in the ducts and are the most common type of breast cancer.

2.4.2. Breast Cancer Screening and Early Detection

It is estimated that one in nine women will develop breast cancer in their lifetime (Canadian Cancer Society 2003a). Canadian Cancer Society (2003a) and Tierney et al. (2003) state that the common diagnostic techniques used for breast cancer detection are clinical breast examinations (CBE), breast-self examinations (BSE), and mammography. The aim of screening mammography is to detect malignant tumours in the breast at an early stage when no signs or symptoms are apparent (Paquette *et al.* 2000). About 40% of early breast cancers can be detected by palpation alone and 35 %-50% can be detected by mammography alone (Tierney *et al.* 2003). Currently clinical breast and breast-self examinations and mammography together are the most reliable screening tools available for early detection.

Both clinical breast examinations and breast-self examinations use palpation of the breast to detect changes such as lumps. Clinical breast examinations are conducted by a doctor or trained health professional during regularly scheduled physical examinations, whereas monthly BSE can be done on one's own breast.

Mammography uses low-dose x-rays of less than 0.4 cGy per view to the mid breast (Tierney *et al.* 2003). The image is produced as a result of x-rays being

attenuated through absorption while they pass through the breast to the image receptor (usually film). The benefits of mammography include the ability to detect small tumours, and an increased detection of ductal carcinoma *in situ* (DCIS) for which it is the only proven reliable method for detection (RadiobiologyInfo 2002). Interpretation of mammograms can be difficult due to variability of the structure and density of the breast tissue. With age, the breast tissue composition changes from mostly glandular to mostly adipose tissue (Canadian Cancer Society 2002a). A mammogram from a younger woman with very dense breast tissue may not reveal the presence of a clinical cancer. As with other detection techniques; mammography can result in false-positives (findings that may turn out to be non-cancerous), or false-negatives (be missed).

Other techniques used for breast cancer detection include thermography, and ultrasound (Basset and Gold 1982). The working principle of thermography is detecting temperature variation due to metabolic changes by collecting the infrared radiation that is emitted. An increase in temperature results from the increase metabolism in tumour. Ultrasound uses high frequency sound waves (greater than 20000 Hz), detecting acoustic impedance changes between tissues.

Optical spectroscopy and imaging modalities are emerging in the diagnostic field as promising techniques (Gayen and Alfano 1999, and Chaudhury *et al.* 2001). Optical spectroscopy techniques avoid the use of ionizing radiation, which is cancer inducing, while providing high spatial resolution that could potentially detect small tumours that are undetectable by pathology (Bigio and Mourant 1997 and Katz *et al.* 1996).

2.4.3. Colon Tissue

The colon is part of the large intestine spanning between the small intestine and the rectum. The basic structure of the lower gastrointestinal tract, including the stomach, small intestine, colon, and rectum is shown in figure 2-15 adapted from National Cancer Institute (2002). The gastrointestinal tract forms part of the digestive tract, functioning to remove nutrients from food and move waste through the body. The colon removes water from the completely digested food (Canadian Cancer Society 2002b).

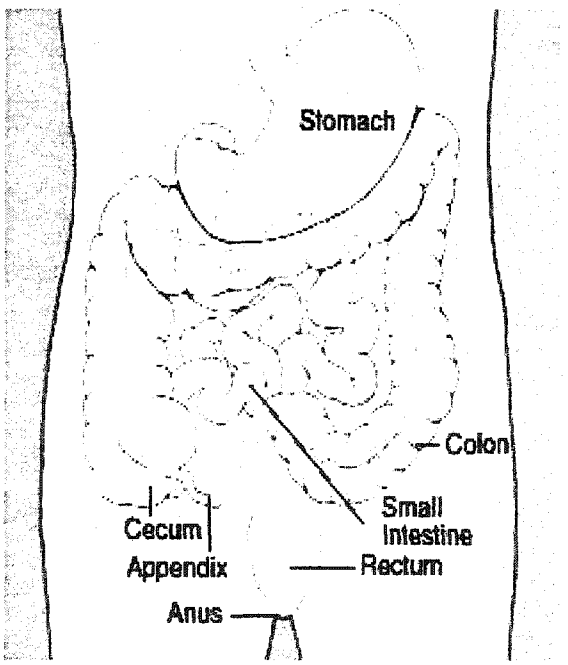

Figure 2-15. Structure of Gastrointestinal Tract (National Cancer Institute 2002).

The colon has four sections starting with the ascending colon, extending between the cecum upwards to the transverse colon. The ascending colon extends upward from the cecum, bends and crosses the abdominal cavity to form the transverse colon. The transverse colon leads to the descending colon and onto the sigmoid colon that curves to a mid-plane connection to the rectum. The colon is composed of many different tissue

types enclosed in four layers. The four layers include the mucous membrane, submucosa, muscular layer, and serous layer. The mucous membrane has an inner lining (epithelium), connective tissue, and muscle; the submucosa contains connective tissue, glands, blood vessels, lymphatic vessels and nerves; the muscular layer contains connective tissue and muscle; and the serous layer is an outer lining of epithelium and connective tissue. Many of the colon cancers begin in the glandular cells lining the inside layer (mucosa membrane) of the colon (Canadian Cancer Society 2002b). Polyps are clusters of cells that grow, divide, and reproduce abnormally on the lining of the colon. Although not all polyps become cancerous, most colon cancers originate with development of benign polyps. Approximately ninety-five percent of all colorectal cancers are adenocarcinomas (Holowaty *et al.* 1998).

2.4.4. Colon Cancer Screening and Early Detection

In Canada, colorectal cancer is the second leading cause of cancer deaths, after lung cancer (Holowaty *et al.* 1998). Statistics from the Canadian Cancer Society estimate that one in sixteen women and one in fifteen men will develop colon cancer in their lifetime (Canadian Cancer Society 2003b). Fecal occult blood test (FOBT), colonoscopy, sigmoidoscopy, and double contrast barium enema are common diagnostic techniques available for colorectal cancer detection. The benefits of early detection and screening for colorectal cancer is currently controversial; however, the FOBT is endorsed by Cancer Care Ontario, the National Committee on Colorectal Cancer Screening, the Canadian Task Force on Preventive Health Care, Quebec and the National Health Technology Assessment Agencies, and the Canadian Cancer Society for colorectal cancer screening (Schabas 2003).

The fecal occult blood test (FOBT) is used to detect traces of blood in the stool that may result from pre-cancerous polyps (National Cancer Institute 2002). The FOBT procedure can be conducted at home or in a doctor's office and consists of acquiring three small stool samples onto chemically treated test strips. The test strips containing the samples are then analyzed at a laboratory. If traces of blood are detected (positive result), further diagnostic techniques are employed to determine the cause. The benefits of FOBT are that it is easy, noninvasive, and cost-effective. Although shown to be effective in the prevention of cancer, it is not an ideal screening tool since almost the same amount of cancers are missed as detected (Schabas 2003).

Both colonoscopy and sigmoidoscopy use a white light instrument to view the colon and rectum, and both require that the bowels are empty and pumped with air to improve the imaging of the organs. Colonoscopy also typically requires that the patient be sedated. A long flexible tubular instrument attached to a camera is used in a colonoscopy to view the entire length of the colon and rectum. A sigmoidoscope is similar but extends only long enough to view the rectum and sigmoid (lower) colon. The principle benefit of these techniques is that biopsy samples of suspicious areas can be targeted and acquired while disadvantages include the duration, invasiveness, and discomfort of the procedures (Screening for Colon Cancer. 2003).

Double contrast barium enema (DCBE) and computer tomography (CT) with DCBE are both x-ray imaging procedures used to provide details of the colon and rectum. The barium outlines the colon and rectal line so that abnormalities can be more readily identified. Typically several x-ray images are obtained in a given study. The advantage of the CT with DCBE is that a 3-dimensional image is obtained.

2.5. RADIOBIOLOGY

Radiobiology is defined as the study of ionizing radiation interactions with biological systems such as biological molecules, cell components, cells, tissues, organs, and whole bodies (Hall 1988). Radiobiological experiments were not conducted until the late 1800's after the production of x-rays by Wilhelm Roentgen in 1895, the discovery of radioactivity by Antoine Henri Becquerel in 1896, and the isolation of radium by Pierre and Marie Curie in 1898 (Badash 2003 and Hall 1988).

The energy from the radiation can be absorbed in a volume of a biological system resulting in an ionization or excitation. Ionizing radiation with energies on the order of 4 to 25 eV are needed to excite and eject orbital electrons from atoms or molecules (Attix 1986 and Hall 1988). Ionizing radiation can be divided into two categories: charged and uncharged. Uncharged ionizing radiation includes x-rays, γ-rays, and neutrons, and charged ionizing radiation includes electrons, protons, α-particles, negative π-mesons and heavy charged particles. Further discussion of ionizing radiation will focus primarily on x-rays and γ-rays which are classified as indirectly ionizing radiation along with neutrons.

As illustrated in the EM radiation spectrum in figure 2-1, γ-rays and x-rays are electromagnetic radiation with energies on the order of 10^2 eV to 10^8 eV which, for the most part, is significantly higher than for photons in the optical range.

X-rays and γ-rays have the same nature and properties but differ in the way they are produced (Attix 1986 and Hall 1988). Gamma-rays are emitted from excited and unstable nuclei whereas x-rays originate from energy transitions of electrons in atoms or by accelerating or decelerating charged particles. For example, in x-ray tubes, electrons

are accelerated to high energies and then decelerate when striking a target such as tungsten or gold. The deceleration results in an emission of x-ray (bremstrahlung radiation). In radiotherapy, γ-rays, x-rays and electrons are commonly used to deliver treatments to cancer patients. γ -rays are produced by Cobalt-60 (^{60}Co) for external beam therapy and radioactive isotopes Cesium-137, Irridium-198, and Iodine-125 (^{137}Cs, ^{198}Ir, and ^{125}I) for brachytherapy. X-rays are typically generated with linear accelerators for external beam therapy.

Indirect ionization is a two-stage process. First, as the radiation is absorbed in the biological material its energy is transferred to charged particles (e.g. electrons), an exchange that takes place on the order of 10^{-5} seconds. In turn, the charged particles then deliver the energy along their path of travel through coloumb interactions, resulting in chemical or biological damage (Attix 1986 and Hall 1988). The indirectly ionizing radiation can interact with matter through three major processes: photoelectric, Compton, and pair-production. Which process is used is dependent upon the energy of the radiation and the chemical composition of the biological material. For typical radiation therapy energies within the range of 100 keV to 30 MeV, the Compton process dominates. The Compton process occurs when an incident photon of a given energy hν collides with an unbound or loosely bound electron as in figure 2-16 (Hall 1988).

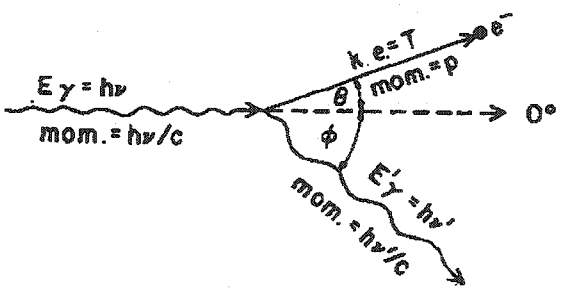

Figure 2-16. Compton Interaction (Hall 1988).

The collision imparts some of incident photon's energy to the free electron. As a result, the electron is set in motion (momentum p and energy T) at some angle θ and the photon with a lower energy (hν) is scattered at some angle ϕ.

Biological changes from x- and γ-rays can be caused by direct action or indirect action (Hall 1988). Figure 2-17, illustrates the effects of direct and indirect action.

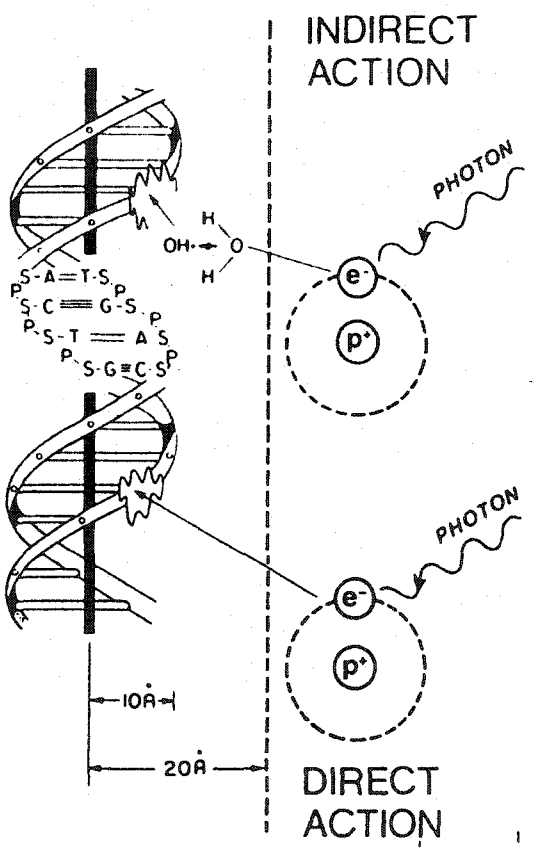

Figure 2-17. Direct and Indirect Action (Attix 1986).

With direct action, the δ-rays, or secondary electrons arising from photon absorption interact directly with the DNA. The process is referred to as indirect action when a δ-ray interacts with a molecule such as water and produces a free radical that subsequently interacts with the DNA to cause damage. Damage is inflicted by either single or double strand breaks to the sugar phosphate backbone. Indirect action is primarily responsible

for approximately two thirds of biological damage (Hall 1988). Chemical changes such as breakage of bonds or biological damage in cells may not be evident until attempts are made by the cell to divide. The cell can either effect repair (i.e. only a single strand break of the DNA) or lose its reproductive integrity (cell death). Cellular death may not be evident during the first division but may occur after several divisions. The phase of the cell cycle when radiation exposure occurs also plays a significant role in the extent of the biological damage. The cells are most sensitive during the G2 phase when the DNA have been replicated and the M phase when the nuclei divide (mitosis) and cells split (cytokinesis). The G1 phase, the interval between M and S, and the S phase when the DNA are replicating are the least sensitive. In general, chemical and biological damage may take days, years, or even generations to manifest. For example, mutations to the DNA as a result of radiation exposure may be suppressed for several generations before being expressed.

3. INSTRUMENTATION

The basic components necessary for optical spectroscopic measurements include a light source, illumination and collection optics, and a computer controlled spectrometer. A spectroscopic measurement system is used for absorption, whereas a combined spectroscopic measurement and imaging system is used for fluorescence.

3.1. ABSORPTION SPECTROSCOPY

Absorption spectroscopy was investigated using a measurement system that samples a tissue area of approximately 1.6 cm^2. A "point" measurement system as defined by Wagnières *et al.* (1998) is one that samples a tissue area typically having a

diameter range of 50 μm to 1000 μm. So our system used for absorption spectroscopy can not be considered a point measurement system. A typical system from Ocean Optics, Inc. (2000a) shown schematically in figure 3-1, is a computer controlled spectrometer connected to a light source, flexible illumination and collection fibres, and a sample holder. The instrumentation used to perform absorption spectroscopy containing these components is illustrated in figure 3-2.

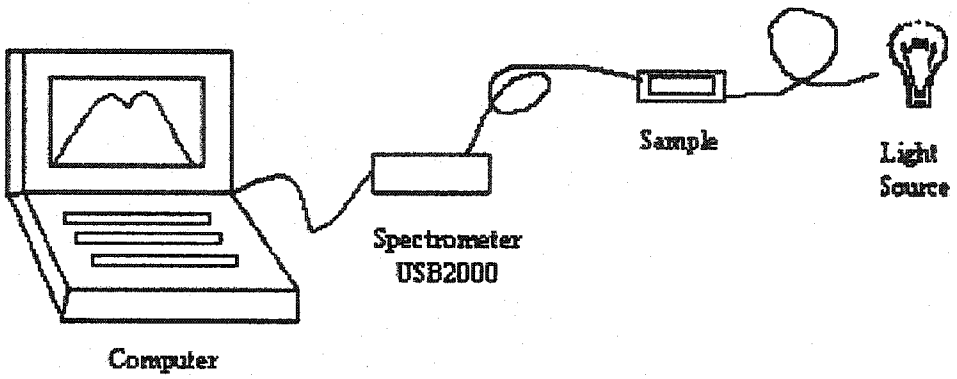

Figure 3-1. Basic Components for Absorption Spectroscopy (Ocean Optics, Inc. 2000a).

Figure 3-2. Components for Absorption Spectroscopy.

3.1.1. Light Source

The excitation light source used for the absorption measurements is a tungsten halogen light source (LS-1) with a wavelength range of 360 nm to 2000 nm and a power output of 6.5 W (Ocean Optics, Inc. 2000b). The light source has an associated color temperature of 3100 K. The white light source offers a built in filter slot to accommodate attenuation or colour filters up to 3mm thick allowing for a measure of tuning of the excitation wavelength. A collimating lens (74-VIS) is attached to the light source to couple the light into an optical fibre for illumination. The 74-VIS collimating lens accommodates a spectral wavelength range of 350 nm to 2000 nm and is composed of borosilicate crown (BK-7) glass.

3.1.2. Illumination and Collection

The incident light is guided through a 400 μm diameter fibre optic patch cord and focused onto the sample by a collimating lens (74-UV). The collimating lens and the sample are separated by approximately 6 cm. Subsequent to interaction with the tissue, the light is recollected by a second collimating lens (74-UV) attached to a 400 μm diameter fibre optic patch cord that directs light into the spectrometer. The 74-UV collimating lenses transmit a spectral wavelength range of 200 nm to 2000 nm and are composed of fused silica. The 400 μm diameter patch cords, also composed of silica, are single stranded with a numerical aperture (NA) of 0.22. Their optimal transmission wavelengths range from 200 nm to 750 nm, but good for transmission to 1100 nm.

For absorbance measurements the illumination and collection fibres were aligned at 180 degrees as shown in figures 3-2 and 3-3. This experimental set-up for absorption spectroscopy shows the mounts holding the 74– UV collimating lenses and fibres for the

illumination and collection of light from the sample. This sample holder was designed to accommodate a sample on a microscope slide.

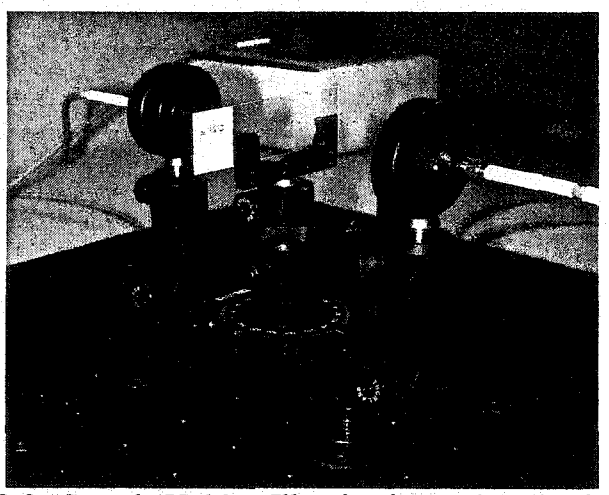

Figure 3-3. Sample Holder, Illumination and Collection Fibre.

3.1.3. Spectrometer

A USB2000 miniature fibre optical spectrometer from Ocean Optics, Inc. is used for the absorbance measurements. The spectrometer has a unique built-in optical bench design to detect the collected light.

The components of the spectrometer optical bench include an entrance slit, collimating mirror, grating, focusing mirror, detector collection lens, and filters aligned in an asymmetric crossed Czerny-Turner geometry and coupled to a CCD detector, as illustrated in figure 3-4.

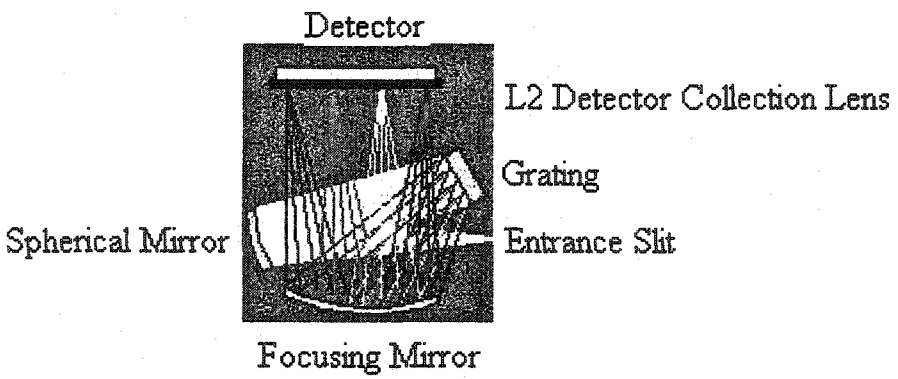

Figure 3-4. Asymmetric Crossed Czerny Turner Design (Ocean Optics, Inc. 2002).

The entrance slit built into the spectrometer acts as an aperture controlling the amount of light entering the optical bench. The entrance slit in this system has a height of 1 mm and a width of 25 μm. The light passing through the slit is collimated by a spherical mirror that directs the light into the grating for wavelength selection. The fixed grating has the best efficiency in the spectral range of 350 nm to 800 nm, with maximum efficiency at 500 nm. The light from the grating is projected onto a second spherical mirror that focuses the wavelengths onto a collection detector lens (L2) in front of the detector. L2 is a cylindrical lens that focuses the light, after it passes through a variable long pass order sorting filter, onto the detector elements. The variable long pass order sorting filter (OFLV) eliminates the second and third order effects to the detector signal (Ocean Optics, Inc. 2002). The detector is a 2048 element SONY ILX511 linear CCD array. The electronic data collected by the detector is reconstructed into an image by the software OOIBase 32.

Dispersion, resolution, and optical resolution are properties important for characterization of system performance. Linear dispersion is associated with the instrument's ability to resolve fine spectral detail. Equation 3-1 from Ocean Optics, Inc. (2000b) expresses dispersion as:

Equation 3-1. Dispersion.

$$\text{Dispersion} = \frac{\text{GSR}}{\text{2048 elements}}$$

Dispersion is therefore dependent on the spectral range of the grating (GSR) and the array size of the CCD detector. Resolution is defined as the minimum difference in wavelength between two wavelengths that can be distinguished. The optical resolution is

the separation between cut-on and cut-off wavelength at 50% of peak transmission (FWHM) in equation 3-2 (Ocean Optics, 200b).

Equation 3-2. Optical Resolution.

$$\text{Optical Resolution} = \text{Dispersion} \times \text{Resolution}$$

Optical resolution is dependent on the groove density of the grating (600 lines/nm) and the dimensions of entrance slit.

With the spectrometer configuration previously described, the dispersion is 0.3174 nm/pixel, the resolution is 4.2 pixels for the 25 μm slit (Ocean Optics, Inc. 2000b), and the optical resolution is 1.333 nm.

3.2. FLUORESCENCE SPECTROSCOPY AND IMAGING

The combined spectroscopic measurement-imaging system is used for fluorescence spectra acquisition. The imaging component facilitates identification and selection of particular areas of interest of a tissue sample. In particular, such localization of the source from which a spectrum is obtained can clearly be beneficial when interpreting the acquired data. Figure 3-5 shows the system for fluorescence spectroscopy and imaging. The basic components of the system are labeled **A** through **F**. The light source (**A**) is connected to an epi-fluorescence microscope (**B**). Emitted light from the sample is collected through an adapter (**C**) and collection fibre (**D**) and directed to both a spectrometer (**E**), and the CCD camera (**F**).

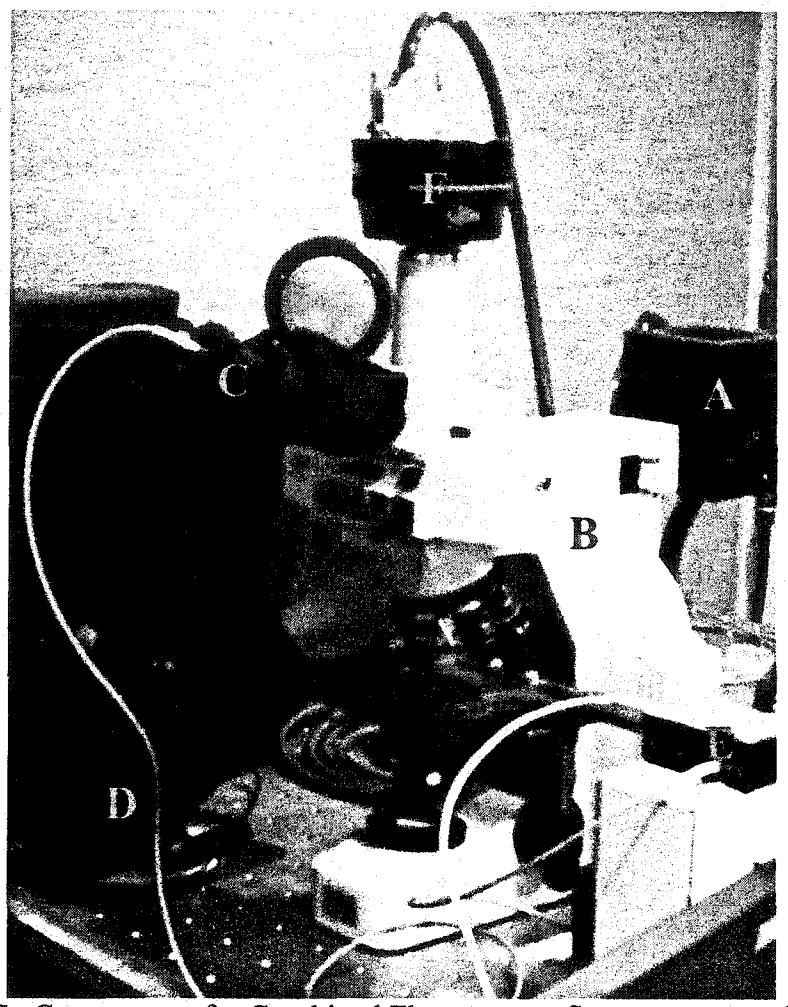

Figure 3-5. Components for Combined Fluorescence Spectroscopy and Imaging.

3.2.1. Light Source

For fluorescence measurements, the excitation light source is a 100 W halogen lamp with a brightness control. The brightness control can be adjusted from 0% to 100% of the maximum intensity. The halogen lamp and a collector lens that focuses the light onto the filter cube are mounted in the lamp housing.

3.2.2. Illumination and Collection

The illumination and collection optics for fluorescence measurements are more complex than the tabletop optics for absorbance measurements. An epi-fluorescence

Eclipse E400 microscope† with an adapter between the eyepiece and fibre are the key components used to illuminate and collect fluorescence signals from the sample.

The B-3A filter cube† is used for all measurements with the epi-fluorescence microscope. The filter cube contains an excitation filter, dichroic beam splitter, and emission filter. The excitation filter is a wide band-pass filter with a wavelength range of 420 nm to 490 nm permitting excitation wavelengths within this range to pass through the excitation filter and reflect onto the objective to the sample via the dichroic beam splitter. The dichroic beam splitter has a transmission cut-off wavelength of 505 nm; light of wavelengths shorter than 505 nm is reflected onto the objective while that of longer wavelengths is transmitted through to the emission filter. The emission filter is long pass with a wavelength cut-on at 520 nm i.e., light from the sample with wavelength equal to or above the cut-on are collected. The epi-fluorescence microscope has mounts to accommodate up to four filter cubes. Depending on the desired application, different filter cubes can be readily selected.

For living cells, an incubator was designed to hold the sample and maintain an environment that would sustain the cells.** The incubator was manufactured using aluminum. Two 20 Ω resistors in parallel were mounted in the aluminum on either side of the sample chamber insert. A constant current was then applied to the resistors to establish a constant temperature. Figure 3-6, shows the microscope incubator. The dimensions of the incubator surface are 7.61 cm x 3.32 cm with a thickness of 0.6 cm.

---

† Refer to Appendix III for Product Information.

** The incubator was a collaborative effort between the Medical Physics Department at the Northwestern Ontario Regional Cancer Centre and the Physics Department at Lakehead University.

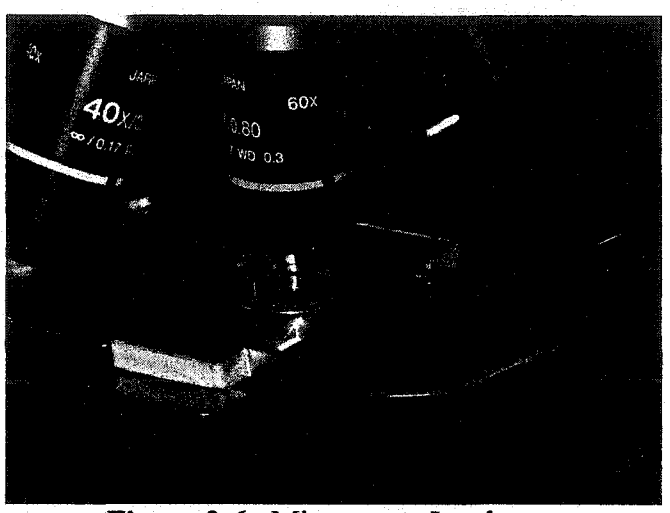

Figure 3-6. Microscope Incubator.

The insert slot has a diameter of 2.75 cm with a nylon screw to tighten the chamber into place. The dimensions of the incubator surface are 7.61 cm x 3.32 cm with a thickness of 0.6 cm. The insert slot has a diameter of 2.75 cm with a nylon screw to tighten the chamber into place. The removable sample chamber has an outer diameter of 2.71 cm. When the chamber is sealed with cover glasses, a 400 μm thick chamber is created. The top of the sample chamber has an inner diameter of 1.91 cm and the bottom has an inner diameter of 2.31 cm. The insert has an overall thickness of 0.5 cm.

An adapter was designed to connect fibre optic cable to the eyepiece of the microscope.*** Figure 3-7, show two viewing angles of the eyepiece/fibre adapter.

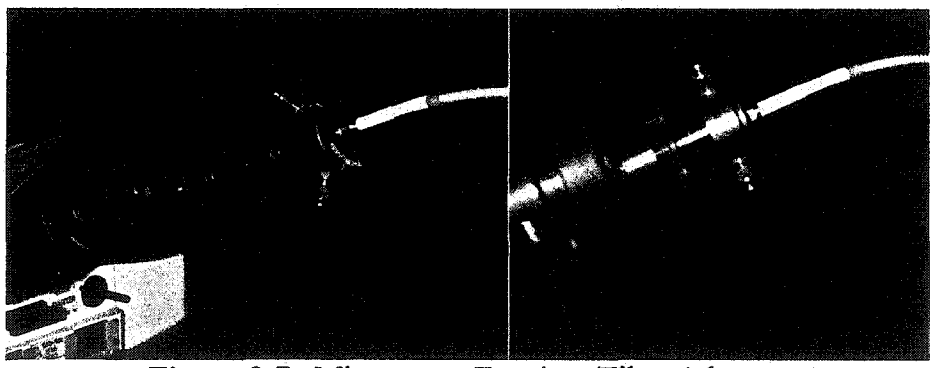

Figure 3-7. Microscope Eyepiece/Fibre Adapter.

*** The adapter design was a collaborative effort between the Medical Physics Department at the Northwestern Ontario Regional Cancer Centre and the Physics Department at Lakehead University.

The eyepiece/fibre adapter fits over a PVC collar with a diameter of roughly 4.4 cm that, in turn, is mounted onto the microscope eyepiece. Figure 3-8, shows the adapter and PVC collar detached from the microscope eyepiece.

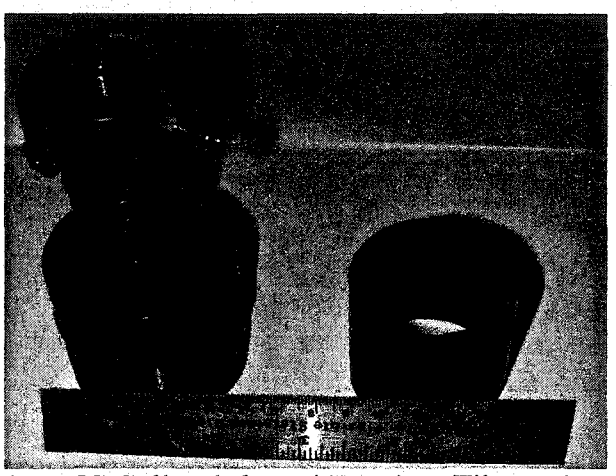

Figure 3-8. PVC Collar (left) and Eyepiece/Fibre Adapter (right).

The adapter consists of a 20 x Newport objective with a numerical aperture (NA) of 0.4 and a series of tubes, a fibre adapter, and an X - Y translating lens mount. Table 3-1, summarizes the components of the adapter, listing the components from the fibre

Table 3-1. Adapter Components.

ThorLabs Inc. Parts	Description
SM1SMA	SMA Fibre Adapter
LM1XY	X and Y Translating Lens Mount (+/- 1 mm)
SM1L05	1" Tube 1/2" Deep
SM1V05	1" Tube Rotating Adjustment Focus 1/2" Travel
SM1L03	1" Tube 1/3" Deep
SM1A3	Microscope Objective to 1" Tube Adapter
SM1A2	1" Tube to 2" Tube Adapter
SM2V10	2" Tube Rotation Adjustment Focus 1" Travel
SM2L05	2" Tube Lens Tube 1/2" Deep

connection to the eyepiece. The 400 μm fibre from Ocean Optics fastens into the SM1SMA fibre adapter and the SM2L05 tube lens slides tightly over the PVC collar. The objective is mounted inside the tubing so that the back aperture is at a minimum distance from the exit pupil of the eyepiece. The minimum distance is limited by the

tubing. The X and Y translation mount connecting the fibre to the adapter to align the fiber with the objective is critical for optimization of the spectral signal.

3.2.3. Spectrometer

The Ocean Optics, Inc. USB2000 miniature fibre optic spectrometer discussed above for absorption spectroscopy (re. 3.1.3.) is also used for fluorescence spectroscopy analysis. The spectrometer is shown in figure 3-5 (E) as a component of the fluorescence instrumentation. In figure 3-9, the spectrometer is shown with the USB connection on the left-hand side of the image and the SMA connector and fibre optic patch cord connection shown towards the bottom of the image.

Figure 3-9. Miniature Fibre Optic Spectrometer.

3.2.4. CCD Camera

Imaging of the sample is achieved using a cooled CCD camera. Cooling of the CCD camera is achieved with forced air from a thermoelectric cooler. The array size is 2184 pixels × 1472 pixels, where a pixel is 6.8 μm × 6.8 μm. The maximum imaging area is 14.9 mm × 10.0 mm. The CCD camera collects the emitted photons generated

from the fluorescence emission of the sample. Approximately 50% of the eyepiece field of view (FOV) in the 1472 pixels direction and 70% of the FOV in the 2184 pixel direction is actually imaged by the CCD array. Figure 3-10, shows the sensitivity of the CCD camera as a plot of absolute quantum efficiency versus wavelength.

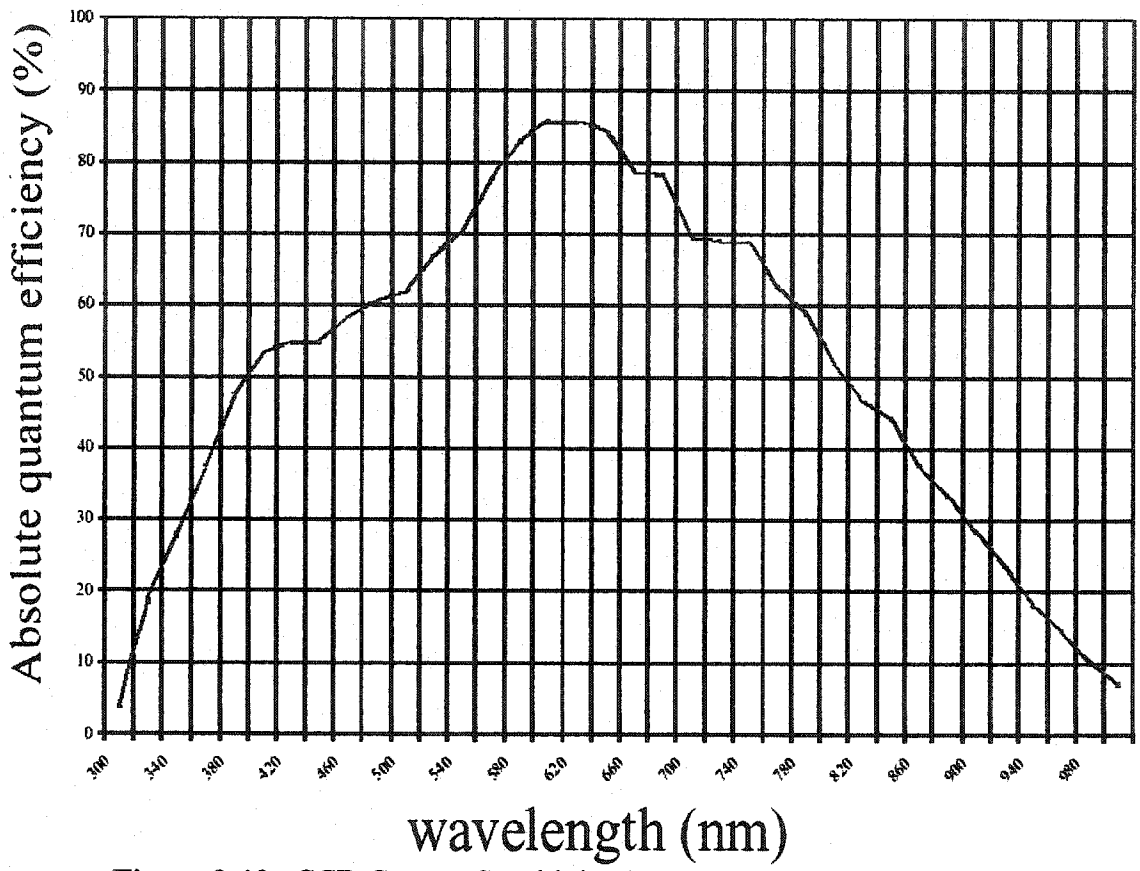

Figure 3-10. CCD Camera Sensitivity (Apogee Instruments Inc.2002).

The quantum efficiency (QE) is the number of electron-hole pairs generated per photon. At 400 nm the QE of the CCD camera is 50% and at the peak (approximately 620 nm) 85% of the electron-hole pairs are generated per photon. †

† Refer to Appendix III for Product Information.

4. SAMPLE PREPARATION

Spectroscopic and imaging data were obtained from a variety of samples using a number of different preparation techniques. Reference samples were established using various concentrations of ethidium bromide (EtBr) and fixed tagged cells. Living cells, prepared with GFP tags in the nucleus (H1) or in the cytoplasm (Actin), were cultured from a breast cancer cell line (MCF-7). Tissue was obtained from biopsy samples of normal and cancerous colon tissue.

4.1. REFERENCE STANDARDS

EtBr was established as a reference standard for spectroscopic purposes because it has a well characterized spectrum, is stable, homogenous, and may be readily diluted. In total, five different concentrations of EtBr were prepared. The main stock of EtBr† had a concentration of 10 mg/ml, with 50 µl available. From the main stock an intermediate concentration is made by pipeting the 50 µl EtBr solution with 9.95 ml of distilled water, yielding a concentration of 50 µg/ml (C^{i}_{EtBr}). To acquire 3 ml of each target concentration (50 µg/ml, 10 µg/ml, 5 µg/ml, 0.5 µg/ml, and 0.1 µg/ml) of EtBr, the volume of EtBr from intermediate concentration is calculated using equation 4-1.

Equation 4-1. Volume of EtBr.

$$V_{EtBr} = \frac{V_T C^{t}_{EtBr}}{C^{i}_{EtBr}}$$

From equation 4-1, V_{EtBr} is the volume of 50 µg/ml intermediate solution to reach a total volume of V_T of 3 ml for a target concentration C^{t}_{EtBr} starting from the intermediate concentration (C^{i}_{EtBr}). Table 4-1, summarizes the volume and concentrations used.

Table 4-1. Volumes and Concentrations of EtBr.

EtBr Target Concentration C^t_{EtBr} (μg/ml)	Volume of Water V_{H20} (ml)	Volume of EtBr V_{EtBr} (from 50 μg/ml EtBr) (ml)	Total Volume V_T ($V_{H20} + V_{EtBr}$) (ml)
50	0	3	3.000
10	2.4	0.6	3.000
5	2.7	0.3	3.000
0.5	2.97	0.03	3.000
0.1	3	0.006	3.006

For spectral analysis the 3 ml concentrations were syringed into Petri dishes. During measurements the Petri dish lids were taken off. After the measurements the Petri dishes were stored at room temperature with their lids on and sealed with paraffin film. The Petri dishes were covered in aluminum foil to protect the solvent from long-term exposure to light. Precautions, such as wearing gloves, were necessary since EtBr can bind to and damage DNA.

4.2. CELL LINES

A total of six Actin GFP tagged MCF-7 cell samples and six H1 GFP tagged MCF-7 cell samples were prepared. MCF-7 is the designation for an established cell line for breast adenocarcinoma cells (ATCC No. HTB-22). These cells were tagged with green fluorescence protein (GFP) in the cytoplasm (actin) and the nucleus (H1).

The actin GFP tagged and the H1 GFP tagged MCF-7 cells are from actively growing stock cultures. The cells are incubated at a humidified 37 °C with 5% CO_2 in 35 mm by 10 mm polystyrene cell culture dishes† containing growth medium for nourishment. The growth medium used is Gibco RPMI medium 1640† plus fetal bovine serum (FBS) and 1% antibiotic-antimycotic†. A 22 mm no. 1 round micro cover glass† is placed in the culture dish for the cells to adhere and grow. For actin GFP tagged MCF-7

† Refer to Appendix III for Product Information.

cells, 1 mM butyrate solution is added the day after the start of incubation. The butyrate enhances the GFP expression in the cells. For MCF-7 cells, approximately two days of incubation is required for a sufficient number to be plated onto the cover glass. As the MCF-7 cells are needed, the growth medium is aspirated out of the culture dish and replaced by new growth medium the day of the sample preparation.

An incubator chamber with a depth of 400 μm is used in fluorescence measurements of the tagged living cells. A cover glass is fitted into the bottom of the chamber and sealed approximately an hour before filling the chamber with growth medium. The plated cover glass is fitted face down and sealed on top of the chamber. Initially sealing of the plated cover glass was accomplished using nail polish. The disadvantages were that the nail polish is toxic to cells if there is leakage into the chamber and the drying time resulted in lengthy preparation times. The nail polish sealing technique was replaced by using thin adhesive spacers[†] for the top cover glass resulting in an improved cell preparation time.

Once the cells are sealed in the chamber, the chamber is placed in the incubator where fluorescence measurements were either performed on the tagged MCF-7 cells directly, or subsequent to exposure to radiation. Although no detectable spectroscopic change was anticipated as an immediate result of exposure, the living tagged cells were irradiated to simply investigate the possibilities. The incubator is connected to a voltage supply set at 5.0 V and left to stabilize for roughly half an hour before acquiring measurements. A dose of 5 Gy was delivered to three Actin GFP tagged and three H1 GFP tagged MCF-7 cell samples of ^{60}Co gamma rays (1.25 MeV) prior to performing

[†] Refer to Appendix III for Product Information.

fluorescence measurements. During irradiation the sample is set at a distance of 80.0 cm from the source, at a depth of 0.5 cm with a radiation field size is 10.0 cm by 10.0 cm, which is a standard geometry in dosimetry. Figure 4-1, illustrates the irradiation geometry for the tagged cell samples sealed in the incubator chamber.

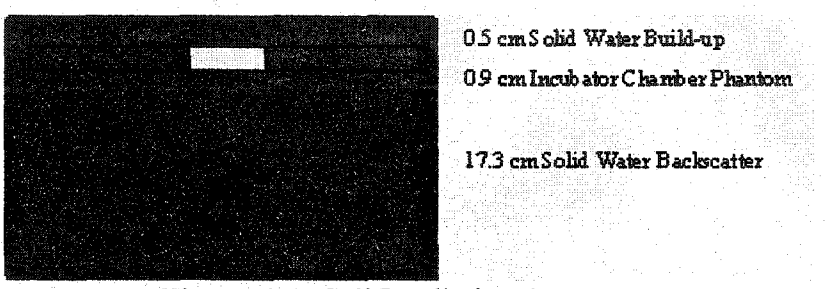

Figure 4-1. Cell Irradiation Geometry.

The time required to deliver 5 Gy (or 500 cGy) to the given sample using this geometry was calculated using Patient Dose Calculation Version 6.4 (McGhee 2003). The calculated times are summarized in Table 4-2. The times vary due to the date of the exposures and the decay of the ^{60}Co source.

Table 4-2. Time to Deliver 500 cGy (with F.S. 10 cm × 10 cm , 80 cm SAD, Depth 0.5 cm) of ^{60}Co gamma rays (See Appendix IV).

Cell Type	Sample Number	Time (min)
Actin GFP tagged MCF-7	6	3.59
Actin GFP tagged MCF-7	9	3.60
Actin GFP tagged MCF-7	10	3.60
H1 GFP tagged MCF-7	3	3.52
H1 GFP tagged MCF-7	5	3.63
H1 GFP tagged MCF-7	7	3.64

4.3. TISSUE

A total of 24 colon tissue samples from two patients (PA and PB) were obtained from biopsy specimens. The samples were provided from the Biochemistry Research Laboratory with six normal and six cancerous samples provided for each patient. The biopsy specimens for Patient PA were surgically removed from the sigmoid colon. The pathology report identified a moderately differentiated adenocarcinoma. The surgically

removed biopsies from Patient PB were taken from the cecum and ascending colon. The pathology examination identified a moderately differentiated invasive adenocarcinoma.

The randomly shaped colon tissue samples were sectioned to a thickness of 10 μm. The samples are first frozen using liquid nitrogen, than sectioned using a Cryostat (Model Lieca CM 1850 from Meyer Instruments Inc.). The sectioned samples are mounted to a microscope slide by contact. After preparation the samples on the microscope slide are stored at room temperature in a microscope slide box. For safe handling of the samples, gloves and a face mask were worn. The images and spectroscopic measurements were acquired at room temperature at varying times after preparation.

5. METHODS

Absorption and fluorescence measurements were the two optical spectroscopic techniques investigated. The experimental methods associated with each of these techniques are described in detail in the following sections (re. 5.1. Absorption Measurements and 5.2. Fluorescence Measurements). With all extraneous illumination sources extinguished, the laboratory room had an adequate dark seal to minimize ambient light during all spectroscopic measurements. In general, spectroscopic measurements were obtained using a "scope" mode, meaning that the measured signal is provided as the raw data generated by the analogue to digital (A/D) converter incorporated into the spectrometer. These raw data include effects arising from the light intensity, grating reflectivity, fibre transmission, and detector response. For absorption and fluorescence measurements, the raw spectral data were acquired for background readings, including dark and/or reference spectra, and a sample reading.

5.1. ABSORPTION MEASUREMENTS

The apparatus used for absorption spectroscopy of colon tissue was discussed previously (re. 3.1. Absorption Spectroscopy). The spectra are acquired in "scope" mode consisting of the raw data from the sample less the dark spectra.

A reference reading is obtained by placing a blank microscope slide in the tabletop sample holder between the two collimating lenses of the 400 μm diameter illumination and collection fibres. The reference reading and the light intensity are significant features influencing selection of an appropriate integration time so that the signal does not saturate. A 3 mm Teflon diffusion disc is added into the path of the excitation light to simply attenuate the light to the sample by approximately 70%. Teflon is used because at these spectral energies all wavelengths are equally attenuated so that the overall spectrum remains in essence unaffected. The integration time employed for the absorbance measurements of the normal and cancerous colon tissue was typically 5 milliseconds. Since the integration time was short, multiple samplings were acquired and averaged to improve the signal to noise ratio (SNR). Signal to noise ratio is defined as the signal measured relative to the background noise. The signal to noise is improved by a factor equivalent to the square root of the number of samplings used to establish an average spectrum. For example, with 5 spectra averaged the signal to noise is improved by a factor of approximately 2.24. The dark spectrum is taken by covering the collection lens/fibre with a lens cap to block the light entering the spectrometer, the dark subtract collects leakage current from the system. To remove the dark spectrum from the reference, a dark subtract is performed (The dark subtract is only applicable in scope mode). Once the background readings have been established with

set integration times, averaged sample spectra can be acquired by replacing the blank microscope slide with the microscope slides containing the 10 μm thick colon tissue samples. A tissue sample thickness of 10 μm was selected as a compromise between a thin section (give very little absorption) and a thick chunk (high absorption). A timeline of the absorption measurements for the colon tissue is provided in the appendices (re. Appendix V).

5.2. FLUORESCENCE MEASUREMENTS

Fluorescence measurements were acquired for various Ethidium Bromide (EtBr) concentrations, fixed reference cells, living cells, and normal and cancerous colon tissue samples using the apparatus described previously (re. 3.2. Fluorescence Spectroscopy and Imaging). Slightly different methods were used for the cells and tissue samples as opposed to the EtBr sample measurements.

For fluorescence measurements of various concentrations of EtBr, reference spectra, dark spectra including dark subtract, and sample spectra were acquired. For each set of measurements the microscope stage was adjusted to 14 cm ± 0.05 cm below the filter cube holder. The reference reading is obtained by placing a Petri dish with 3 ml of distilled water on the microscope stage. A maximum light intensity from the halogen light source was applied and an integration time of 2 s for the spectrometer was selected. The integration time of the spectrometer is the period in which the detector collects the emitted photons. The dark spectrum was then obtained with the shutter on the microscope closed. The dark spectrum correction is then applied to the spectrum from the distilled water reference. Sample spectra are subsequently obtained by opening

the shutter and replacing the distilled water with a Petri dish containing 3ml of a known concentration of EtBr.

To acquire fluorescence measurements of the cells or tissue samples, the CCD camera is first cooled down to -13 °C. A temperature of -13 °C was found to be the optimal temperature for imaging in our lab environment due to airflow and room temperature fluctuations. The fixed reference cells are focused in the field of view with a light intensity of approximately 70% of the maximum intensity. A higher light intensity would photo-bleach the sample causing the fluorophore intensity to decrease. Therefore to minimize photo-bleaching the light intensity was applied depending on the brightness of the sample as observed through the eyepiece. The light intensity of approximately 70% was set by adjusting the brightness control for the halogen light source where a scale ranged from zero (minimum) to ten (maximum) Focusing of the image is achieved through a combination of appearance via the eyepiece directly and observation of CCD images. To ensure that the spectrometer is detecting light from a localized area of the sample, the iris size on the microscope is adjusted to both the minimum and optimum diameters for each of 40 x and 60 x objectives. The minimum iris size ensures the alignment of the eyepiece/fiber adapter and centers a given sample area containing one cell in the field of view. The optimal iris size approximates the collection area of the fiber. For a given sample area, an image and a corresponding spectrum are acquired for these configurations of the two diameter sizes for each of 40 x and 60 x objectives. These measurements were compared to the initial measurements taken at the time of the eyepiece/fibre adapter alignment. These measurements served as a reference reading to ensure that the adapter remained aligned and that the iris size was

kept approximately the same. Once the optimum iris size is established, the system is focused on the living cells or tissue samples of interest and an integration time giving an optimal signal is chosen. Table 5-1, shows the typical integration times and light intensities used in fluorescence measurements of the various samples. The light intensity (% of the maximum intensity) is selected for each sample area based on the observations of the emitted fluorescence intensity as seen through the eyepiece.

Table 5-1. Spectrometer Integration Times and Light Intensities for Fluorescence Measurements.

Sample Type	Light Intensity (% of Maximum Intensity)	Integration Time (s)
Fixed Tagged Reference Cells	70	3 to 5
Actin GFP MCF-7 Cells	50	9
H1 GFP MCF-7 Cells	50	9
Colon Tissue - Patient PA	70	12
Colon Tissue - Patient PB	70	12

To facilitate inter-comparison of data acquired from different samples, the light intensity and integration time were kept constant for each sample type. Using the selected integration time, a dark spectrum is again acquired with the shutter on the microscope closed, blocking light from reaching the spectrometer. Application of the dark subtract has a net effect of decreasing the signal noise. Spectra were then acquired for the area of interest, immediately followed by acquisition of an image of the same area of interest. For living breast cancer cells the acquisition of fluorescence images and fluorescence spectra were obtained at 5 minute intervals over a period of approximately 4 hours. With the colon tissue samples, the fluorescence measurements were repeated twice for two different areas on each sample. To obtain a clear image of the sample area, the cooled CCD cameras exposure time was set to 5 seconds with a binning of 2. The binning averages the four nearest pixels as discussed in Section 2.3.3. A timeline for

the fluorescence measurements of the living cell line and the colon tissue samples are summarized in the appendices (re. Appendix V).

6. ANALYSIS AND RESULTS

The analysis and results are presented in the same sequence as the methods (re. 5. Methods), and is further divided into raw spectra and images, normalized spectra, and spectral differences. The significance of the results acquired for the absorption and fluorescence measurements are presented in the discussion (re. 7. Discussion). In general, for the two distinct measurement techniques used, absorbance and fluorescence, there were different limitations on the spectral range acquired. Absorbance spectra were acquired for normal and cancerous colon using a tungsten halogen lamp with a wavelength range of 360 nm to 2000 nm as the light source. Fluorescence measurements were acquired for five concentrations of EtBr, fixed tagged cells, living Actin and H1 GFP tagged MCF-7 cells, and normal and cancerous colon tissue using excitation wavelengths of 420 nm to 490 nm. Fibre and spectrometer combinations used imposed another limitation as detection response was restricted to the wavelength range of 350 nm to 1000 nm (re. 3.1.3). For both absorbance and fluorescence measurements of the colon tissue samples, the acquired data for each group of six samples for the two patients and two tissue types have been defined as a "spectral set".

6.1. ABSORBANCE SPECTRA

6.1.1. Raw Absorbance Spectra for Colon Tissue

Three spectral sets for absorbance at different locations on each normal and cancerous colon tissue sample were acquired for each of the two patients. Note that the

absorbance spectra are in fact the transmitted intensity through the tissue sample. Three sets of absorbance spectra were acquired in an effort to verify the consistency of absorbance trends. Data corresponding to each patient is distinguished by using the labels PA and PB. A total of 36 spectra from 6 normal and 6 cancerous colon samples were accumulated for each patient. The raw absorbance spectra of colon tissue are illustrated in figures 6-1 for patient PA and figure 6-2 for patient PB.

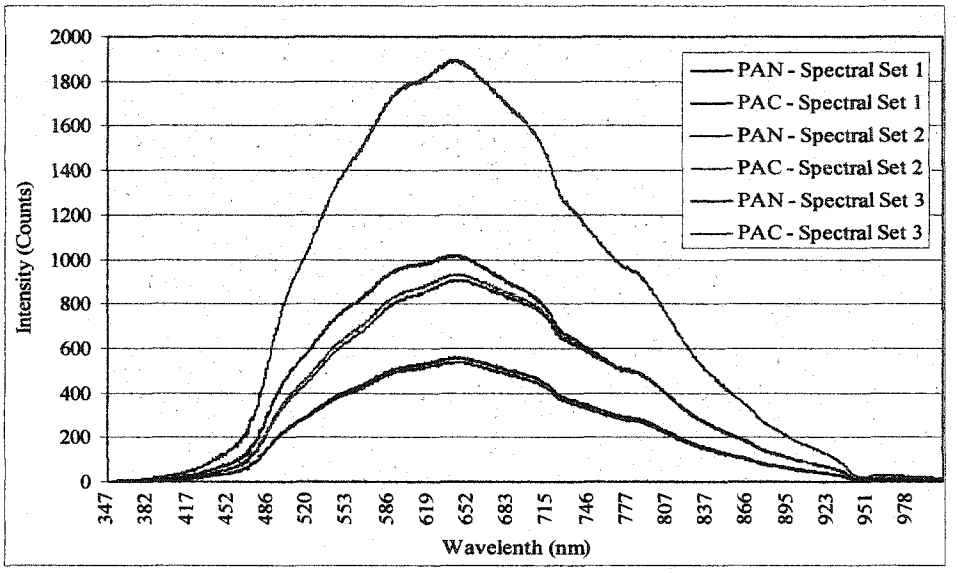

Figure 6-1. Raw Absorbance Spectra for Colon Tissue of Patient PA.

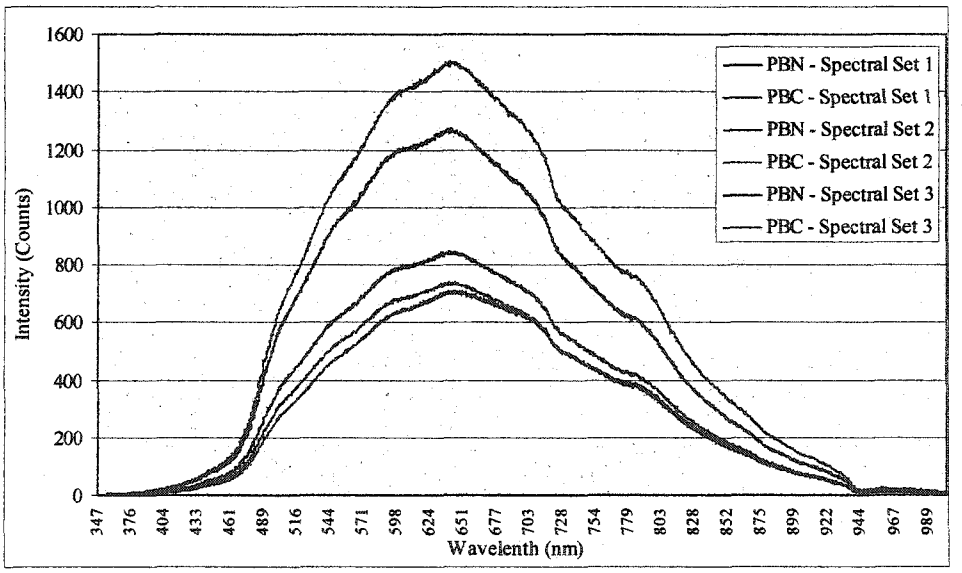

Figure 6-2. Raw Absorbance Spectra for Colon Tissue of Patient PB.

The absorbance spectra for both patients are an average of the 6 sample spectra for each of the three spectral sets. The spectra are comprised of data obtained within a wavelength range of 350 nm to 1000 nm. The maximum intensities vary from spectral set to spectral set. For normal colon tissue spectra, the PAN data have a maximum intensity ranging from approximately 550 counts to 1000 counts (re. Figure 6-1) while that of the PBN data ranges from 700 counts to 1300 counts (re. Figure 6-2). For cancerous colon tissue spectra, the PAC data has a range of approximately 900 counts to 1900 counts (re. Figure 6-1) while the PBC data ranges from 700 counts to 1500 counts (re. Figure 6-2). These variances can be attributed to dependencies on the area of the sample, variations in the sample set-up, and the time that elapsed after sample preparation (re. 7.1. Absorption Spectroscopy for further discussion). The spectral data were then normalized in an attempt to minimize the effects of some of these undesirable contributions.

The areas of the spectra were calculated by summing the spectral intensities (S) using equation 6-1.

Equation 6-1. Spectral Area.

$$\text{Spectral Area} = \sum_{\lambda} S(\lambda)$$

The variable $S(\lambda)$ is the intensity for the given wavelength range of 350 nm to 1000 nm. The spectral intensities were acquired at 0.36 nm increments for the 2048 element linear CCD array in the spectrometer. Table 6-1, expresses the spectral area of a spectral set as a ratio to the average area of all spectral sets and tissue types for each patient. As can be readily observed, spectral characteristics also vary. One measure of this variation is the ratio of spectral areas acquired for each spectral set (re. Equation 6-1) over the average

area of the three spectral sets of both normal and cancerous tissue samples for each patient.

Table 6-1. Ratio of the Spectral Area for Absorbance of Colon Tissue.

Spectral Set	Sample	Ratio of Area to Average (all six) per Patient	Sample	Ratio of Area to Average (all six) per Patient
1		1.04		1.31
2	PAN	0.55	PBN	0.77
3		0.57		0.88
1		1.94		1.56
2	PAC	0.96	PBC	0.74
3		0.93		0.74

For patient PA, the ratio of the spectra areas for the normal and cancerous colon tissues were shown to vary from a minimum of - 45% to a maximum of + 94%. For patient PB, the ratio of the spectral areas for the normal and cancerous colon tissue samples varied from a minimum of – 26% to a maximum of + 56%. For both patients the ratio of spectral areas was found to be greater for spectral set 1 compared to spectral set 2 and spectral set 3. For a discussion of these results refer to 7.1. Absorption Spectroscopy.

6.1.2. Normalized Absorbance Spectra for Colon Tissue

The individual raw absorbance spectra of colon tissue were normalized to remove less desirable experimental considerations (i.e. sample thickness). The spectral data were normalized using a normalization ratio of the average area to the spectral area. The normalized intensities (NI) were calculated using equation 6-2.

Equation 6-2. Normalization of Spectral Data.

$$NI = S(\lambda) \times \left(\frac{\text{Average Area}}{\text{Spectral Area}} \right)$$

Again S(λ) is the raw spectral reading for a given wavelength, the spectral area is calculated using equation 6-1, and the average area is calculated from the spectral areas

obtained from each spectrum in a given spectral set. For both patients 6 normal and 6 cancerous colon tissue spectra were acquired for each spectral set. This normalization method yields the same area under the curve for a given patient.

The normalized spectra data is re-analyzed to facilitate comparison between cancerous to normal colon tissues for the same patient as well as an inter-patient comparison for the same colon tissue types (i.e. normal to normal and cancerous to cancerous).

For the same patient comparison the averages of the normalized spectral areas for each of the normal and cancerous spectral sets were calculated (Average NI), and the average area was recalculated to determine the renormalized intensities using equation 6-3.

Equation 6-3. Renormalized Spectra.

$$\text{RenormalizedNI} = \text{AverageNI} \times \left(\frac{\text{Average Area}}{\text{Average Normormalized Area}} \right)$$

The term in the brackets of equation 6-3 is the renormalization ratio used to acquire the same spectral areas between spectral sets for comparison between cancerous and normal colon tissues from the same patient. Table 6-2 shows the renormalization ratio (the average area to the average normalized area) for each spectral set for both normal and cancerous colon tissue in the third column, and the ratio of the renormalized areas to the average area for each patient in the fourth column for the three spectral sets of patients PA and PB.

Table 6-2. Summary of Renormalized Absorbance Parameters for the Same Patient Comparison of Colon Tissue Samples.

Spectral Set	Sample	Renormalization Ratio Per Spectral Set (re. Equation 6-3)	Ratio of Renormalized Area to Average Area (All Spectral Sets) per Patient (re. Equation 6-1)
1	PAN	1.43	1.49
	PAC	0.77	
2	PAN	1.37	0.76
	PAC	0.79	
3	PAN	1.32	0.75
	PAC	0.81	
1	PBN	1.09	1.44
	PBC	0.92	
2	PBN	0.98	0.75
	PBC	1.02	
3	PBN	0.92	0.81
	PBC	1.09	

For patients PA and PB the renormalization ratios (column 3) were used to calculate the renormalized data (re. Equation 6-3). The renormalization ratio for PAN was consistently higher compared to PAC, whereas for patient PB the renormalization ratios were similar for both the normal and cancerous colon tissue. For patient PA the ratio of the renormalized areas (column 4) vary from a minimum of – 25% to a maximum of + 49% where as for patient PB the ratio of the average normalized areas vary from a minimum of – 25% to a maximum of + 44%. As observed for the raw absorbance, the ratios of the areas were found to be greater for the first spectral set compared to the second and third spectral sets. The importance of these ratios are discussed further in the discussion (re. 7.1 Absorption Spectroscopy).

Figures 6-3 and 6-4 show the renormalized spectra for patient PA and for patient PB respectively, to facilitate comparison between the cancerous and normal colon tissue (same patient comparison).

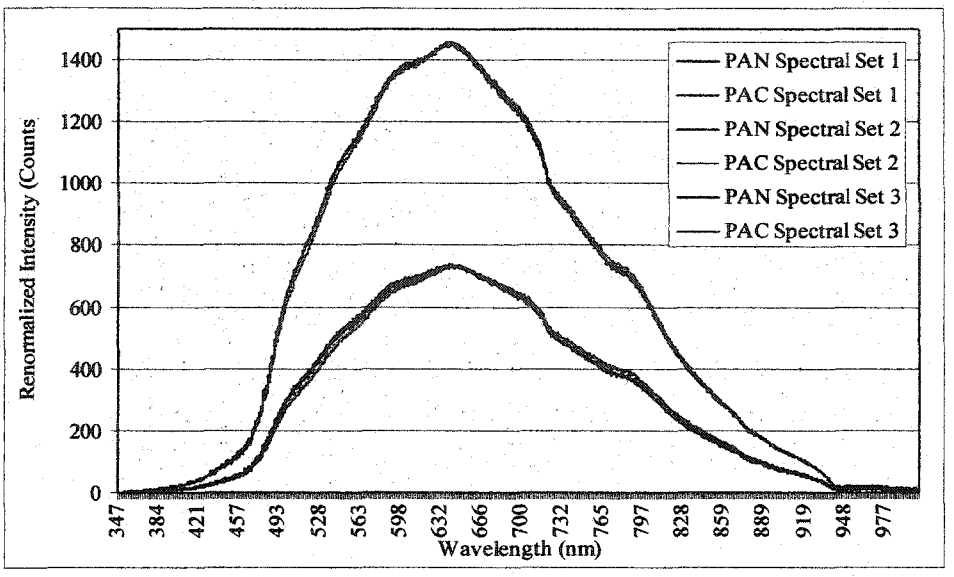

Figure 6-3. Renormalized Spectra of Colon Tissue (N and C) from Patient PA.

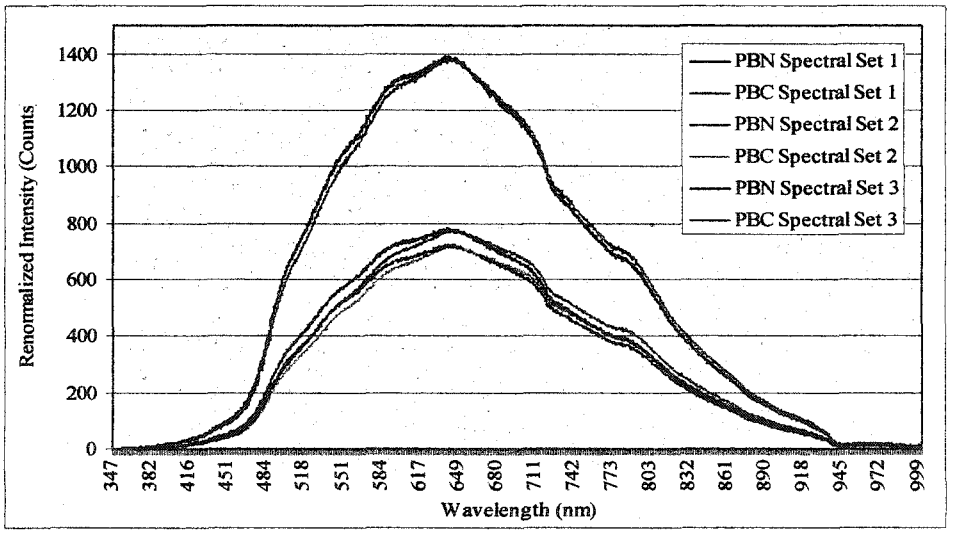

Figure 6-4. Renormalized Spectra of Colon Tissue (N and C) from Patient PB.

From figure 6-3, the renormalized spectra for the normal and cancerous colon tissue from patient PA had maximum intensities ranging from approximately 700 counts to 1450 counts. For each spectral set the cancerous tissue spectra for patient PA were shifted. For the wavelength range of 450 nm to 550 nm an average shift of 4 nm ± 2 nm was determined. For the wavelength range of 750 nm to 850 nm this average shift was found to be 5 nm ± 3 nm. These shifts were determined by the mean difference over the

given wavelength range and the uncertainty is determined from the standard deviation (re. Appendix IV.i. for the standard deviation equation). Further analysis including the uncertainty is all carried out using this method unless otherwise stated. For PBN and PBC the maximum renormalized intensities range from approximately 700 counts to approximately 1400 counts for the three spectral sets (re. Figure 6.4.). For each spectral set the cancerous tissue spectra for patient PB were shifted. For the wavelength range of 450 nm to 550 nm an average shift of 5 nm ± 3 nm was determined whereas, an average shift of 8 nm ± 4 nm was determined for the wavelength range of 750 nm to 850 nm. Both spectral set 1 from patients PA and PB yielded the higher intensities, whereas spectral sets 2 and 3 yielded similar intensities.

The absolute values of the spectral differences were calculated between the cancerous and normal spectra in equation 6-4 for each spectral set for PA and PB where the sign of the difference is ignored.

Equation 6-4. Spectral Difference.

$$SpectralDifference = |RenormalizedC - RenormalizedN|$$

The absolute values of the spectral differences were plotted with the calculated data from equation 6-4 and a Gaussian fit shown in figure 6-5. A Gaussian fit was chosen due to the general shape of the spectral difference curves. In general, the Gaussian fit conforms well to the data except in the region between the two main peaks. Table 6-3 summarizes the fitting parameters obtained for the Gaussian fit to the spectral data.

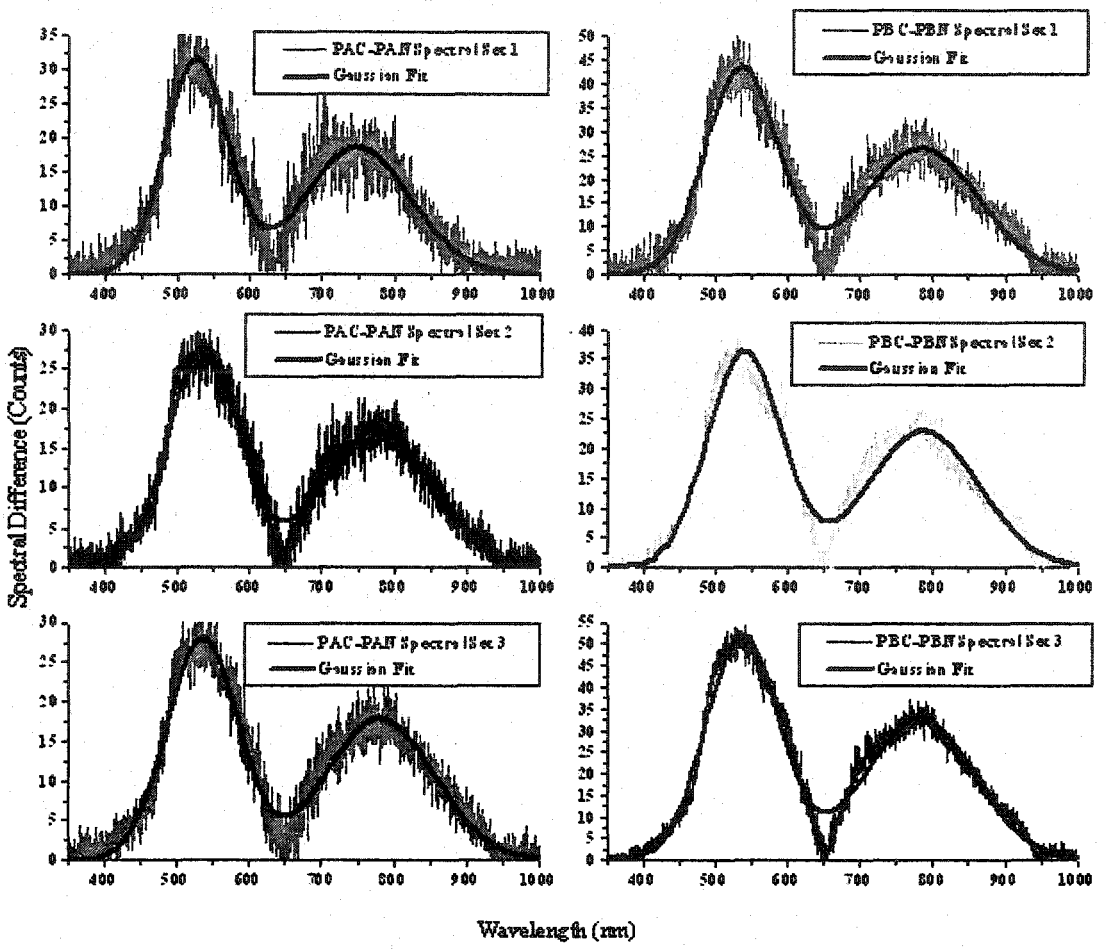

Figure 6-5. Plots of Spectral Difference PAC-PAN (left), and PBC-PBN (right) for Colon Tissue.

Table 6-3. Fitting Parameters of Spectral Difference PAC-PAN, and PBC-PBN for Colon Tissue.

Spectral Set	Sample Difference	Peak Maxima (nm)	Width (nm)	Peak	Average Peak Maxima (nm)	Average Width (nm)
1		524	87			
2	PAC-PAN	536	98	1	532	95
3		535	99			
1		749	147			
2	PAC-PAN	778	149	2	770	149
3		782	150			
1		536	100			
2	PBC-PBN	540	101	1	538	100
3		538	100			
1		784	161			
2	PBC-PBN	788	154	2	785	155
3		783	151			

For PAC-PAN the first peak had a maximum at 532 nm and a full width half maximum of 95 nm, and the second peak had a maximum at 770 nm and a full width half maximum of 149 nm. For PBC-PBN the first peak had a maximum at 538 nm and a full width half maximum of 100 nm, and the second peak had a maximum at 785 nm and a full width half maximum of 155 nm.

The area under the spectral difference curves were calculated by summing the intensity differences for 350 nm to 1000 nm (re. Equation 6-1 and 6-4). The ratios of areas of the spectral difference to the average area for each spectral set are summarized in table 6-4.

Table 6-4. Ratio of Area of Spectral Difference for Colon Tissue.

Sample Difference	Ratio of Area to Average Spectral Difference per Patient Spectral Set 1	Ratio of Area to Average Spectral Difference per Patient Spectral Set 2	Ratio of Area to Average Spectral Difference per Patient Spectral Set 3
PAC - PAN	0.78	0.85	0.70
PBC - PBN	1.22	1.15	1.30

In general, the ratios of spectral differences were found to be greater for patient PB compared to patient PA. The ratios of spectral difference between the cancerous and normal spectra of patient PA had a minimum of – 30% for spectral set 3 and a maximum of – 15% for spectral set 2. The ratios of spectral difference between the cancerous and normal spectra of patient PB for the three spectral sets were found to have a minimum of + 15% for spectral set 2 and a maximum of + 30% for spectral set 3. This approach is applicable to compare more than two data sets, although only two are available, as a result the ratios add up to 2.00 for each spectral set.

For the inter-patient comparison the averages of the normalized spectral areas for the normal tissue spectra for both PA and PB were calculated (Average NI), and the

average area was then recalculated to determine the renormalized intensities using equation 6-3. The term in the brackets of equation 6-3 is the renormalization ratio used to acquire the same spectral areas between spectral sets to compare between the same colon tissue types (i.e normal) from the different patients. Table 6-5 summarizes the renormalization parameters for the inter-patient comparison. For each spectral set, the renormalization ratios shown in the third column are the average areas to the spectral areas, and the ratios of the spectral areas to the average areas for all the normal tissue data were calculated in the fourth column. The same was done separately for the cancerous tissue from the different patients.

Table 6-5. Normalization Parameters for the Inter-patient Comparison.

Spectral Set	Sample	Renormalization Ratio per Spectral Set (re. Equation 6-3)	Ratio of Renormalized Area to Average Area (All Three Spectral Sets) per Tissue Type (re. Equation 6-1)
1	PAN	1.12	1.38
	PBN	0.90	
2	PAN	1.18	0.77
	PBN	0.87	
3	PAN	1.25	0.85
	PBN	0.83	
1	PAC	0.90	1.53
	PBC	1.13	
2	PAC	0.88	0.74
	PBC	1.16	
3	PAC	0.89	0.73
	PBC	1.14	

The renormalization ratios (column 3) were applied to calculate the renormalized data to acquire the same spectral areas between spectral sets to compare between the same tissue types from different patients. For normal tissue the renormalization ratios for patient PA are greater than that for patient PB. In contrast, for cancerous tissue the renormalization ratios for patient PB are greater than that for patient PA. The ratio of renormalized areas for each spectral set to the average renormalized area for all spectral

sets for each tissue type were calculated (column 4). With this ratio a minimum of - 23% and a maximum of + 38% for the normal colon tissue samples and a minimum of - 27% and a maximum of + 53% for the cancerous colon tissue samples were determined. Figure 6-6 illustrates the inter-patient comparison of normal tissue spectra for both patients PA and PB, and the cancerous tissues spectra for both PA and PB are presented in figure 6-7. The importance of the inter-patient comparisons for absorption spectroscopy between patients PA and PB are discussed in the discussion (re. 7.1. Absorption Spectroscopy).

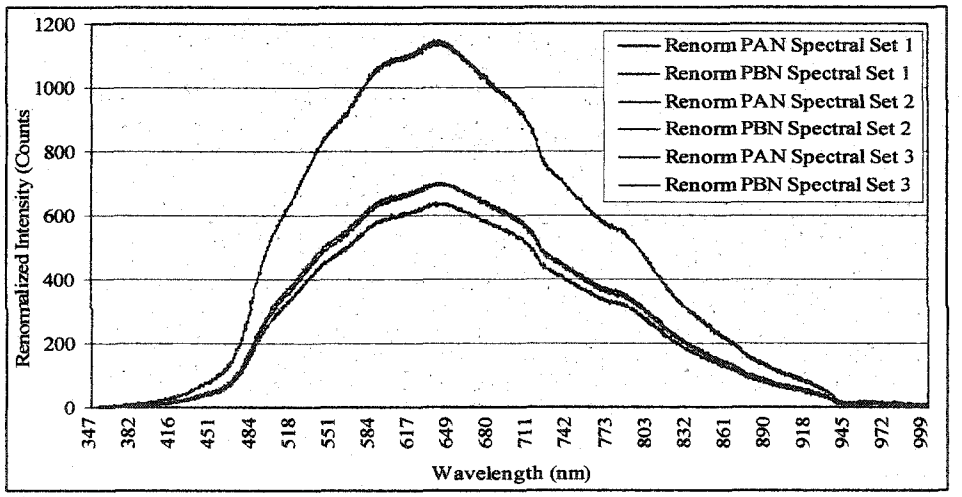

Figure 6-6. Renormalized Spectra for the Inter-patient of Normal Colon Tissue.

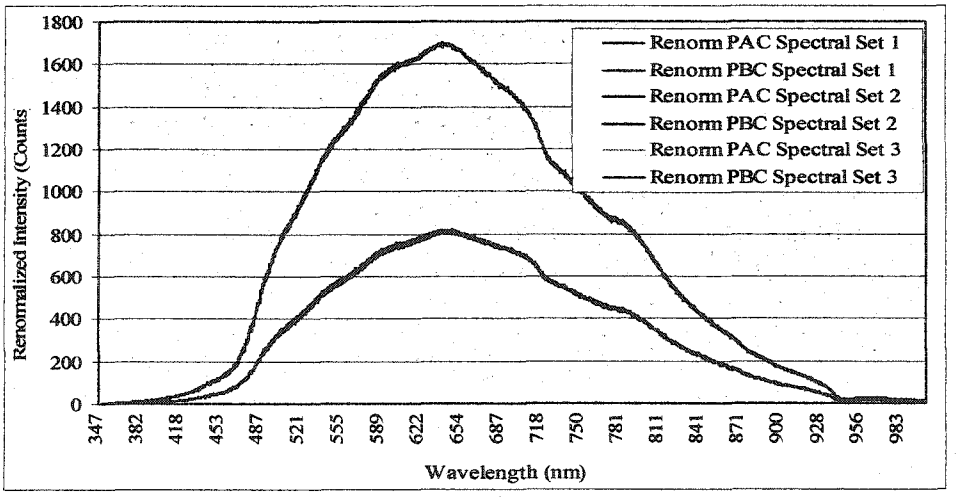

Figure 6-7. Renormalized Spectra for the Inter-patient of Cancerous Colon Tissue.

The normal tissue comparison showed maximum peak intensities from about 650 counts to 1150 counts between the three spectral set. The cancerous tissue comparison had maximum intensity peaks of roughly 800 counts to 1700 counts between the three spectral sets.

From the renormalized data the spectral difference was calculated with equation 6-5 to compare same colon tissue types (i.e. normal to normal and cancerous to cancerous) between patients PA and PB (inter-patient comparison).

Equation 6-5. Inter-patient Spectral Difference.

$$SpectralDifference = |Re\,normalizedPA - Re\,normalizedPB|$$

The absolute values of the inter-patient spectral differences for the three spectral sets were plotted with the calculated data from equation 6-5 and a Gaussian fit shown in figure 6-8. Because of the general shape of the spectral difference curves, a Gaussian line shape was chosen to perform a fit to the data. With the inter-patient spectral difference data for colon tissue, two main peaks are observed. In general, the Gaussian fit conforms well to the inter-patient spectral difference data except in the region between the two main peaks (re. Figure 6.8). Table 6-6 summarizes the fitting parameters (peak maxima and width) obtained for the Gaussian fit to the spectral data.

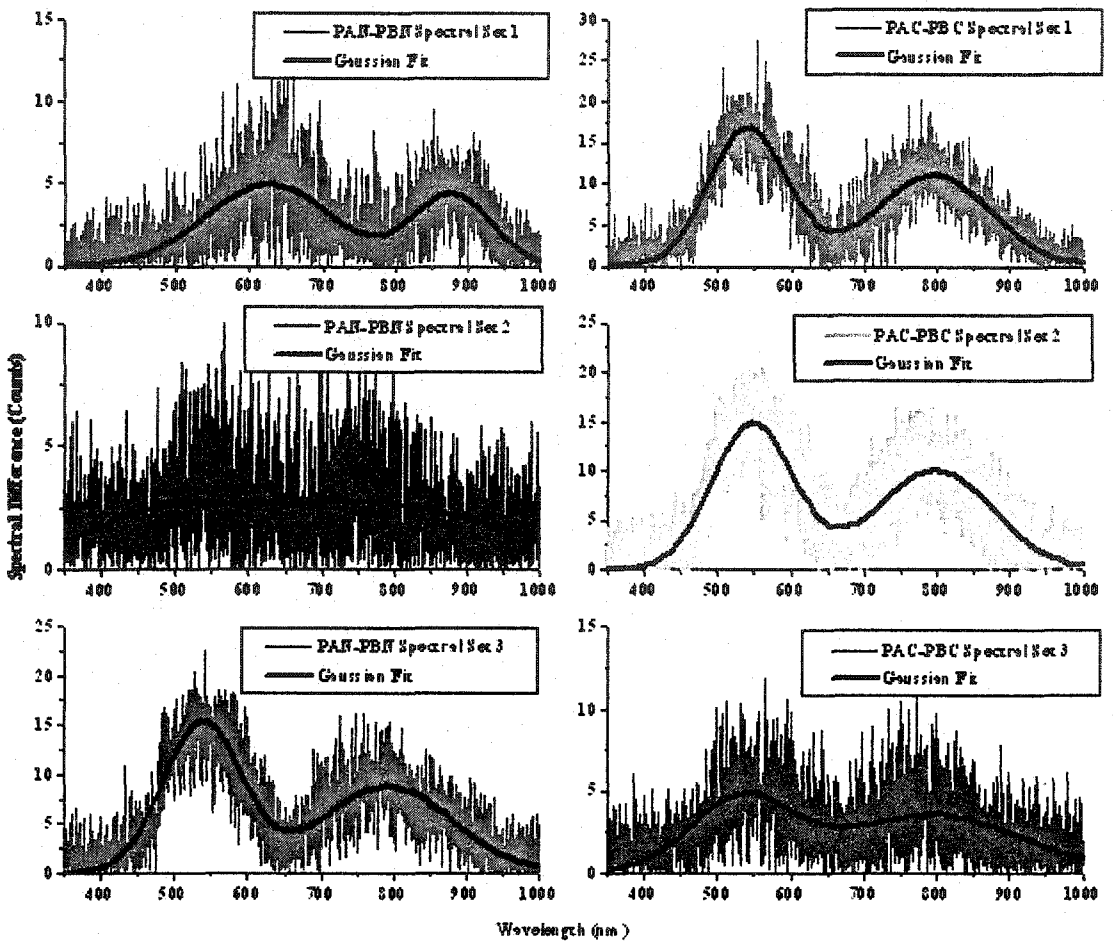

Figure 6-8. Plots of Inter-patient Spectral Differences PAN-PBN (left) and PAC-PBC (right) for Colon Tissue.

Table 6-6. Fitting Parameters of Spectral Difference PAN-PBN, and PAC-PBC for Colon Tissue.

Spectral Set	Sample Difference	Peak Maxima (nm)	Width (nm)	Peak	Average Peak Maxima (nm)	Average Width (nm)
1		626	172			
2	PAN-PBN	462	197	1	542	158
3		537	105			
1		876	108			
2	PAN-PBN	748	399	2	803	229
3		784	179			
1		541	106			
2	PAC-PBC	548	110	1	541	120
3		533	143			
1		793	159			
2	PAC-PBC	796	160	2	795	189
3		795	247			

For PAN-PBN the first peak had an average maximum positioned at 542 nm and an average full width half maximum of 158 nm, and the second peak had an average maximum positioned at 803 nm and an average full width half maximum of 229 nm. For PAC-PBC the first peak had an average maximum positioned at 541 nm and an average full width half maximum of 120 nm, and the second peak had an average maximum positioned at 795 nm and an average full width half maximum of 189 nm (re. 7.1. Absorption Spectroscopy for a discussion of these results).

The areas under the curves were calculated by summing the spectral difference (re. Equation 6-1 and 6-5). The ratios of these areas to the average area for each spectral set are summarized in table 6-7.

Table 6-7. Ratios of Area for Inter-patient Spectral Difference for Colon Tissue.

Sample Difference	Ratio of Area to Average Spectral Difference per Tissue Type Spectral Set 1	Ratio of Area to Average Spectral Difference per Tissue Type Spectral Set 2	Ratio of Area to Average Spectral Difference per Tissue Type Spectral Set 3
PAN - PBN	0.61	0.54	1.37
PAC - PBC	1.39	1.46	0.63

For the normal colon tissue the ratio of areas for the spectral difference vary between a minimum – 46% and a maximum of + 37% for the three spectral sets. The ratio of spectral difference for cancerous colon tissue samples was calculated to be within a minimum of – 39% and a maximum of + 46% for the three spectral sets. Although the intent of the analysis format is to compare more than two data sets, only two are available. The ratios are, therefore, symmetric about the mean since only two separate groups are investigated for a given spectral set.

A summary of the absorbance spectroscopy analysis is given in the appendices (re. Appendix VI.i. Analysis Summary for Absorption Spectroscopy for Colon Tissue).

6.2. FLUORESCENCE SPECTRA AND IMAGES

6.2.1. Raw Fluorescence Spectra for EtBr

The ethidium bromide (EtBr) samples of 50 μg/ml, 10 μg/ml, 5 μg/ml, 0.5 μg/ml, and 0.1 μg/ml were established as reference standards. In total, 12 fluorescence spectra were obtained for each concentration over time. Figure 6-9 presents the raw fluorescence spectra obtained using these EtBr sample concentrations for the emission range of 510 nm to 800 nm. The fluorescence spectra were acquired for the 350 nm to 1000 nm range, although the range of 510 nm to 800 nm was chosen to display the data. This portion of the entire wavelength range was chosen due to the dichroic mirror and emission filter parameter of the filter cube (re. 3.2.2.), and the signal obtained from the samples. As a result there was little to no signal detected between 350 nm and 509 nm. Also, at wavelengths greater than 800 nm again there was little to no signal detected.

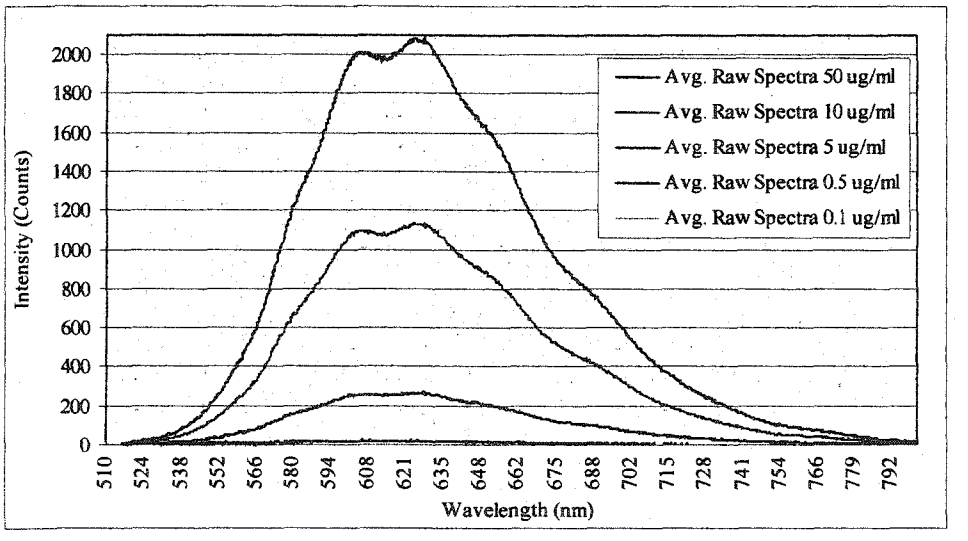

Figure 6-9. Raw Fluorescence Spectra for EtBr.

The fluorescence spectra shown are an average of the 12 spectra for each concentration. The maximum intensity, located at a wavelength of 628 nm ± 5 nm, ranges from approximately 5 counts for an EtBr concentration of 0.1 μg/ml to 2100 counts for an

EtBr concentration of 50 μg/ml. In figure 6-9 the average raw spectra for the 0.5 μg/ml and 0.1 μg/ml concentrations of EtBr are difficult to see since there fluorescence intensities are much lower compared to the higher concentrations of EtBr (5 μg/ml, 10 μg/ml and 50 μg/ml).

The area under the curve was calculated using a summation over the wavelength range of 510 nm to 800 nm (re. Equation 6-1). Table 6-8 summarizes these areas for the average raw spectra and the standard deviation from the mean for the 12 spectra for each concentration.

Table 6-8. Spectral Area for EtBr Concentrations.

Concentration (μg/ml)	Spectral Area (counts)	Standard Deviation (counts)	Spectral Area over Concentration (counts/[μg/ml])	Error of Spectral Area over Concentration (counts/[μg/ml])
50	661000	67000	13220	1340
10	360000	49000	36000	4900
5	85000	12000	17000	2400
0.5	7000	3000	14000	6000
0.1	-1000	2000	-10000	20000

The spectral area (column 2) is shown to decrease from approximately 661000 counts ± 67000 counts to -1000 counts ± 2000 counts (which is essentially 0 counts due to the negative value) as the concentration of EtBr decreases from 50 μg/ml to 0.1 μg/ml. The ratio of the spectral area to the concentration is shown to range from -10000 counts/[mg/ml] ± 20000 counts/[mg/ml] to 36000 counts/[mg/ml] ± 1340 counts/[mg/ml], indicating that there in a nonlinear relationship between the spectral area and the concentration of the EtBr.

A summary of the fluorescence spectroscopy analysis of EtBr has been provided in the appendices (re. Appendix VI.ii. Analysis Summary for Fluorescence Spectroscopy for Ethidium Bromide).

6.2.2. Raw Fluorescence Measurements for Fixed Tagged Reference Cells

Before fluorescence spectra and images of colon tissue or living cells were obtained, measurements of fixed tagged cells were acquired for 40 x and 60 x objective magnifications with a minimal and an optimized iris size. These measurements were performed as previously discussed (re. 5.2. Fluorescence Measurements). Data acquired for the fixed cells were compared to the results obtained during the initial alignment of the eyepiece/fibre adapter to ensure consistency. In total, 13 spectra were acquired for the minimum and optimum iris size for each of the two objective magnifications. Figure 6-10 shows the average raw spectra for the 40 x and 60 x objective magnifications with minimal and optimal iris sizes for the wavelength range of 510 nm to 800 nm.

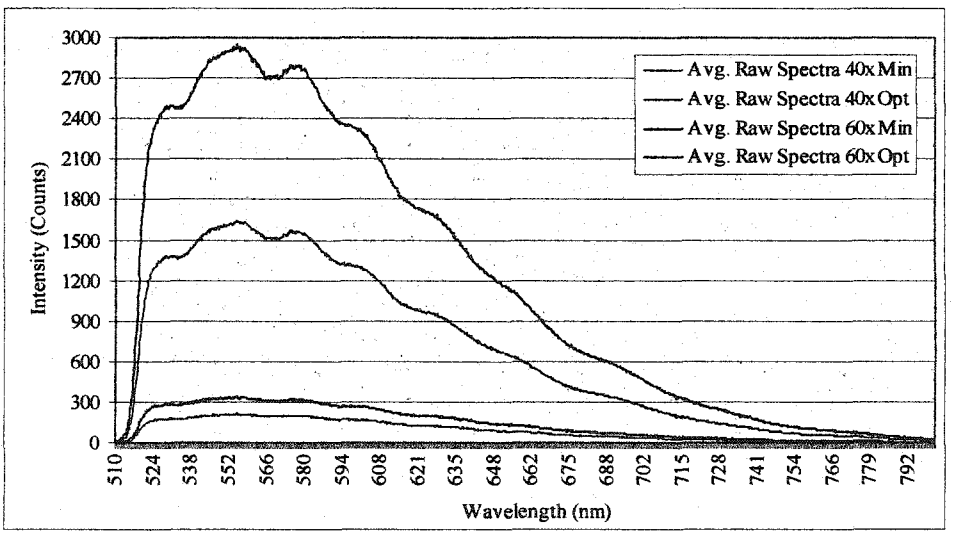

Figure 6-10. Raw Fluorescence Spectra for Fixed Tagged Reference Cells.

The raw fluorescence spectrum for each case was calculated by averaging the 13 spectra obtained. The maximum intensity occurs at approximately 555 nm ± 5 nm for these fixed tagged cells. The minimum iris yields maximum intensities in the range of several hundred counts for the two objective magnifications. On the other hand the optimal iris

size provides maximal intensities on the order of several thousand counts for the two magnifications

Using equation 6-1, the spectral areas were calculated for the average raw spectra of the fixed tagged cells for both objective magnifications with the minimum and optimum iris size. Table 6-9 provides the total number of spectra obtained and the values calculated for the spectral areas of the fixed tagged cells.

Table 6-9. Spectral Areas of Fixed Tagged Reference Cells.

Reference Sample	No. of Spectra	Spectral Area (Counts)
40 x Magnification - Minimum Iris	13	76000
40 x Magnification - Optimum Iris	13	596000
60 x Magnification - Minimum Iris	13	122000
60 x Magnification – Optimum Iris	13	1060000

For the 40 x objective magnification and 60 x objective magnification the spectral areas for the minimum and optimum iris size have an uncertainty of ± 1000 counts. Compared to the 60 x objective magnification the spectral areas are 59 ± 3% greater than the spectral areas for the 40 x objective magnification corresponding for each of the minimum and optimum iris sizes.

Fluorescence images were acquired in conjunction with the fluorescence spectra in order to align the reference sample and set the optimal iris size. Figure 6-11 shows a series of four typical images for the corresponding magnifications and iris sizes for the fixed tagged cells. Images 6-11(a) and 6-11(c) represent the area of the sample that is centred in the overall field of view with minimum iris size to acquire the corresponding spectra for 40 x and 60 x objective magnifications respectively. Images 6-11(b) and 6-11(d) show the optimal iris size that approximates the collection area of the optical fibre through the eyepiece.

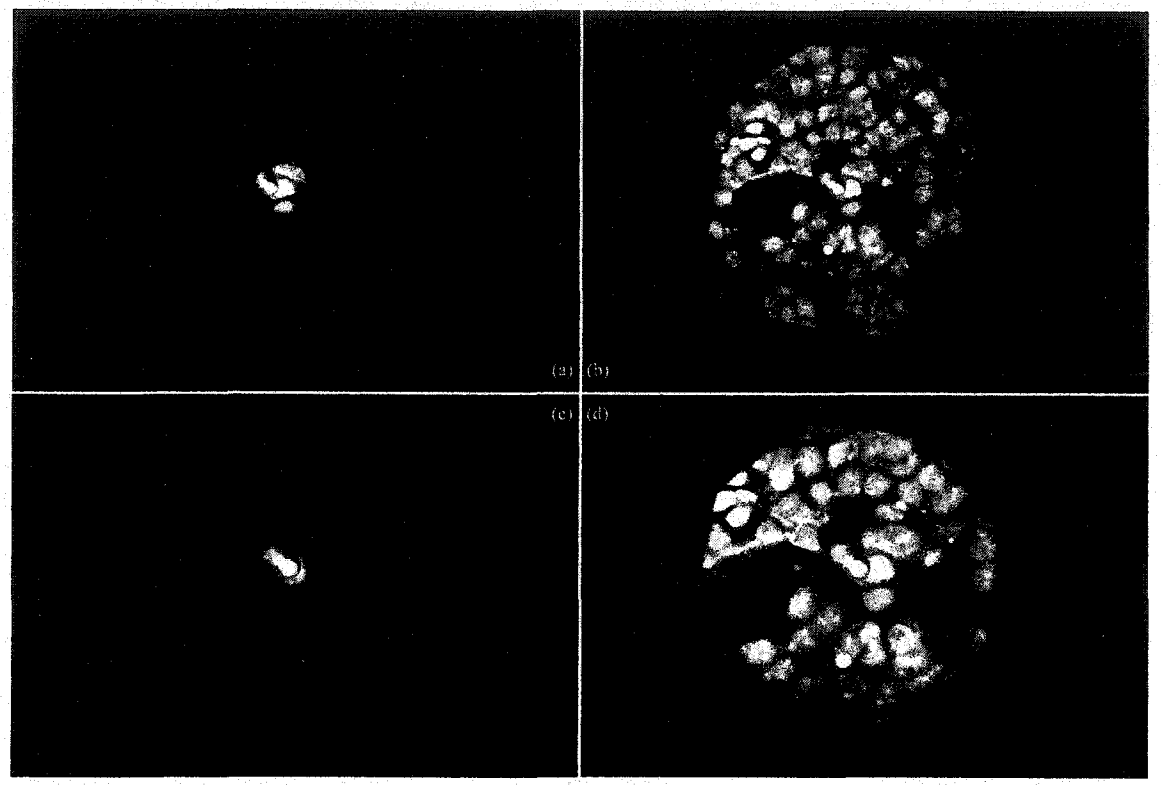

Figure 6-11. Fluorescence Images of Fixed Tagged Reference Cells (a) 40 x Min Iris, (b) 40 x Opt Iris, (c) 60 x Min Iris, and (d) 60 x Opt Iris.

An analysis summary for the fluorescence measurements of the fixed tagged reference cells is given in the appendices (re. Appendix VI.iii. Analysis Summary for Fluorescence Measurements for Fixed Tagged Reference Cells).

6.2.3. Raw Fluorescence Measurements for Actin and H1 GFP Tagged MCF-7 Cells

In total 512 fluorescence images and 512 fluorescence spectra were obtained using living Actin GFP tagged MCF-7 cells and H1 GFP tagged MCF-7 cells. The living GFP tagged MCF-7 cells samples were either non-irradiated or irradiated with 5 Gy of ^{60}Co gamma rays. A dose of 5 Gy is a high dose compared to a more typical fractioned dose of 2 Gy to 2.5 Gy received by a patient on a given day during a treatment. Table 6-10 shows a breakdown of the cell type, sample number, radiation dose delivered and total number of images and spectra. Three samples of each cell type

were irradiated and three samples were not, yielding 128 images and 128 spectra for each radiation dose and cell type.

Table 6-10. Fluorescence Images and Spectra Summary for GFP Tagged MCF-7 Cells.

Cell Type	Sample No.	Radiation Dose (Gy)	No. of Images	No. of Spectra
Actin GFP MCF-7	3	0	49	49
	4	0	49	49
	6	5	49	49
	7	0	30	30
	9	5	49	49
	10	5	30	30
H1 GFP MCF - 7	2	0	49	49
	3	5	49	49
	4	0	49	49
	5	5	49	49
	6	0	30	30
	7	5	30	30

The average raw fluorescence spectra for all the Actin GFP tagged MCF-7 cells and H1 GFP tagged MCF-7 cells are shown in figures 6-12 and 6-13, respectively. The fluorescence spectra for the living Actin GFP tagged MCF-7 cells and the H1 GFP tagged MCF-7 cells were acquired for the 350 nm to 1000 nm range, although the range of 510 nm to 800 nm was chosen to display the data as previous mentioned (re. 6.2.1.)

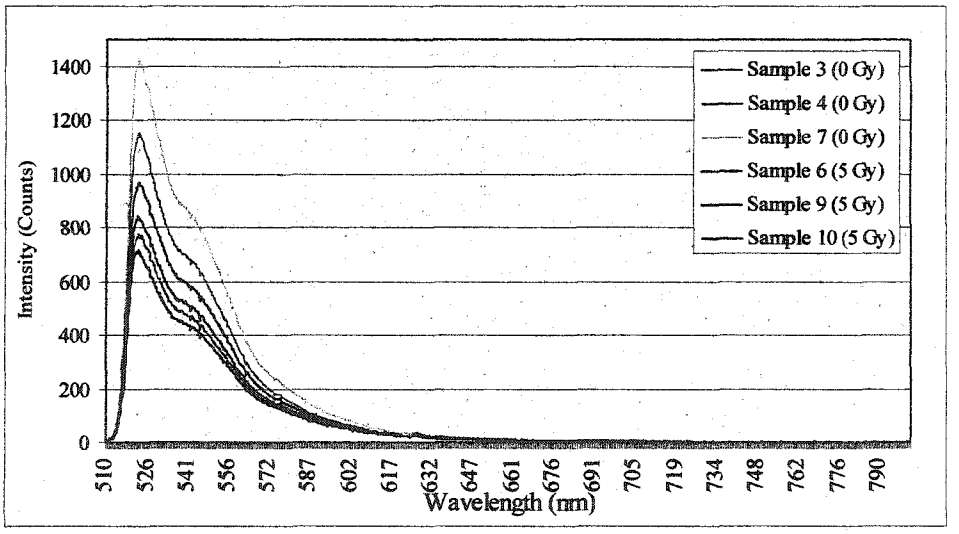

Figure 6-12. Average Raw Fluorescence Spectra of Actin GFP Tagged MCF-7 Cell Samples.

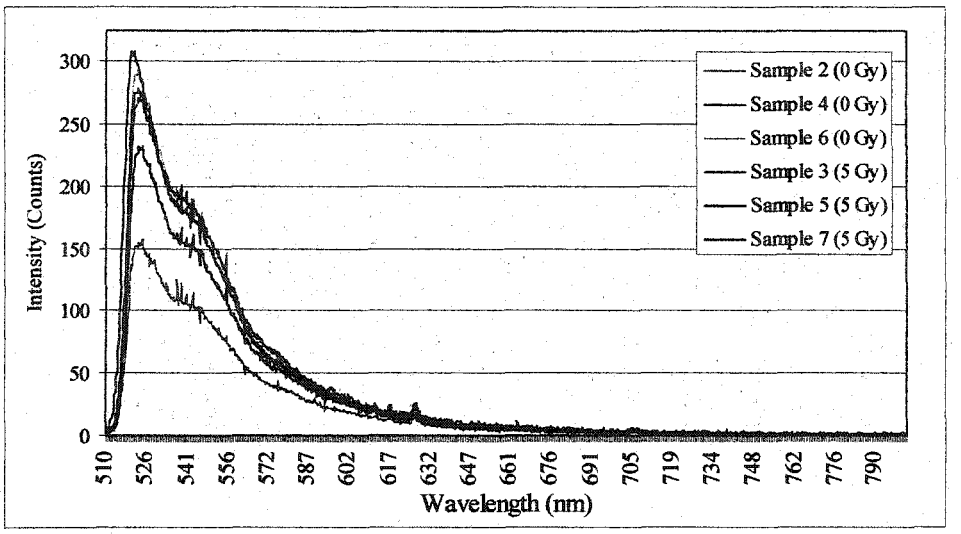

Figure 6-13. Average Raw Fluorescence Spectra of H1 GFP Tagged MCF-7 Cell Samples.

There is no apparent difference between results obtained from the non-irradiated and irradiated cell samples. For the Actin GFP tagged MCF-7 cell samples, the maximum intensity ranges from a minimum of about 700 counts to about 1400 counts at about 526 nm ± 5 nm. For the H1 GFP tagged MCF-7 cell samples the maximum intensity ranges from about 150 counts to 300 counts at 526 nm ± 5 nm. For both the Actin GFP tagged MCF-7 cells and H1 GFP tagged MCF-7 cells there is a slight shoulder after the main peak. For the H1 GFP tagged MCF-7 cell samples there appears to be a slight peak near 626 nm. The spectral areas of each of the average spectra were calculated for Actin GFP tagged MCF-7 and the H1 GFP tagged MCF-7 cell samples. The ratios of the spectral areas relative to the average area for each cell type are summarized in the fourth column of table 6-11.

Table 6-11. Ratio of Spectral Area for Actin and HI GFP tagged MCF-7 Cell Samples.

Cell Type	Sample No.	Radiation Dose (Gy)	Ratio of Area to Average (All Six Samples) per Cell Type
Actin GFP MCF - 7	3	0	1.14
	4		0.81
	7	5	1.44
	6		0.99
	9		0.76
	10		0.87
H1 GFP MCF - 7	2	0	0.65
	4		1.06
	6	5	1.13
	3		1.04
	5		0.94
	7		1.18

For the Actin GFP tagged MCF-7 cells the ratios of spectral area for the non-irradiated and irradiated cells vary from a minimum of – 24% to a maximum of + 44%. The ratios of spectral areas for the non-irradiated and irradiated H1 GFP tagged MCF-7 were within a minimum of – 35% to a maximum of + 18%.

Generally, before acquiring any fluorescence measurements, an area of interest on the sample is chosen to image over a given time period that ranged from 2.5 hours to 4 hours. The criterion for choosing an area of interest was a combination of the view through the microscope, and the number of cells in the field of view. During the measurement time period the image in the field of view changed depending on the activity of the sample. Figure 6-14 shows a sequence of 3 images for Actin GFP tagged MCF-7 sample 3, a non-irradiated sample, taken at times t = 0 h, t = 2 h 05 min., and t = 4 h 10 minutes. The time t = 0 h represents the initial measurement taken after the sample preparation in the incubator, mounting, focussing, and cell incubator temperature stabilization. The images illustrate the activity of the sample in the field of view. The lighter shades represent the fluorescence from the GFP in the cell cytoplasm. One readily observable variation in the time progression of the images is the movement of

cells initially at the centre of the field of view towards the upper left corner. Changes in the shape of the cells can also be observed.

Figure 6-14. Image Sequence of Actin GFP tagged MCF-7 Sample 3.

Figure 6-15 shows a sequence of 3 images for Actin GFP tagged MCF-7 sample 6, irradiated with 5 Gy of ^{60}Co gamma rays. The images were taken at an initial time of measurement (t = 0 h), t = 1 h 55 min., and t = 4 h. This sequence of images shows the activity occurring in the field of view as time elapses. The main difference can be seen in the cells initially in the center of the field of view.

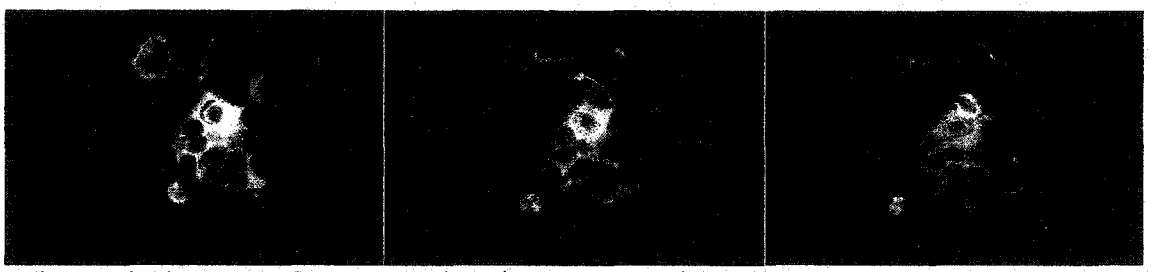

Figure 6-15. Image Sequence of Actin GFP tagged MCF-7 Sample 6 (Irradiated with 5 Gy of ^{60}Co gamma rays).

Figures 6-16 and 6-17 show a set of three images for the H1 GFP tagged MCF-7 samples 4 and 5 respectively. Sample 5 was irradiated while sample 4 was not.

Figure 6-16. Image Sequence of H1 GFP tagged MCF-7 Sample 4.

Figure 6-17. Image Sequence of H1 GFP tagged MCF-7 Sample 5 (Irradiated with 5 Gy of ^{60}Co gamma rays).

In figure 6-16 the images were acquired at times of 0 h, 1 h 55 min, and 4 h. In the first image a brighter nucleus compared to the rest in the field of view is evident. It is in the process of dividing. In the third and final image the cell has divided and the nuclei of the two daughter cells are now approximately the same intensity as the other nuclei visible in the field of view. The images in figure 6-17 were acquired at the same time intervals of figure 6-16. Once again a brighter nucleus is seen in the initial image and divides as time elapses. During the 4 hour period there is also a significant amount of movement observed in the field of view representing a general migration to the lower left.

6.2.4. Normalized Fluorescence Spectra for Actin and H1 GFP Tagged MCF-7 Cells

The individual raw fluorescence spectra of Actin GFP tagged MCF-7 cells and H1 GFP tagged MCF-7 cells were normalized using a ratio of the average area to the spectral area computed using equation 6-2 for each sample. Once normalized, the spectra were averaged for each sample. To compare between the Actin GFP tagged MCF-7 cell samples (and the H1 GFP tagged MCF-7 cell samples separately), the average normalized spectra were renormalized with the same method used for the absorbance measurements (re. 6.1.2.). Table 6-12 summarizes the normalization parameters for the fluorescence spectra of Actin and H1 GFP tagged MCF-7 cell samples. Samples 3, 4, and 7 for Actin GFP tagged MCF-7 cell and samples 2, 4, and 6

for H1 GFP tagged MCF-7 cells were not irradiated. The remaining samples for each were irradiated with 5 Gy of ^{60}Co gamma rays.

Table 6-12. Normalization Parameters for Actin and H1 GFP Tagged MCF-7 Cells.

Cell Type	Sample	Renormalization Ratio (re. Equation 6-3)	Ratio of Area to Average (All Six Samples) per Cell Type (re. Equation 6-1)
Actin GFP MCF - 7	3	0.88	1.00
	4	1.24	
	6	1.01	
	7	0.70	
	9	1.32	
	10	1.15	
H1 GFP MCF - 7	2	1.53	1.00
	3	0.95	
	4	0.95	
	5	1.08	
	6	0.88	
	7	0.85	

The normalization ratios in the third column (re. Equation 6-3) were applied to the average normalized data to acquire the same renormalized areas to compare the Actin GFP tagged MCF-7 cell samples and the H1 GFP tagged MCF-7 cell samples separately. The variations in the renormalization ratios were found to be consistent for all cell samples with no distinction between those non-irradiated and irradiated. The ratios of the spectral area for each cell sample to the average spectral area for each cell type in the fourth column were determined to be identical due to the renormalization; which confirms that the normalization was consistent but was included for consistency with the thesis format.

Figure 6-18 and figure 6-19 show the renormalized spectra for the Actin GFP tagged MCF-7 cell samples and for the H1 GFP tagged MCF-7 cell samples respectively.

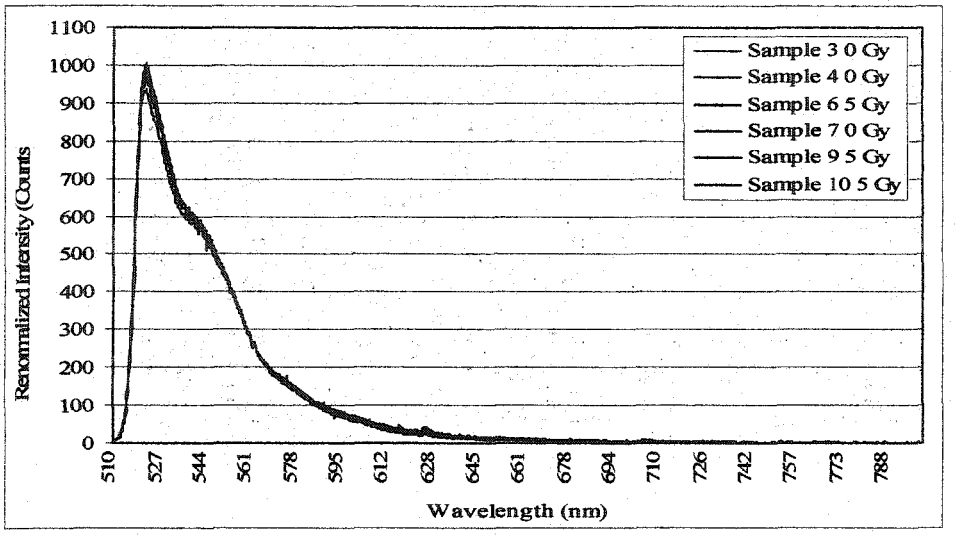

Figure 6-18. Renormalized Spectra of Actin GFP Tagged MCF-7 Cell Samples.

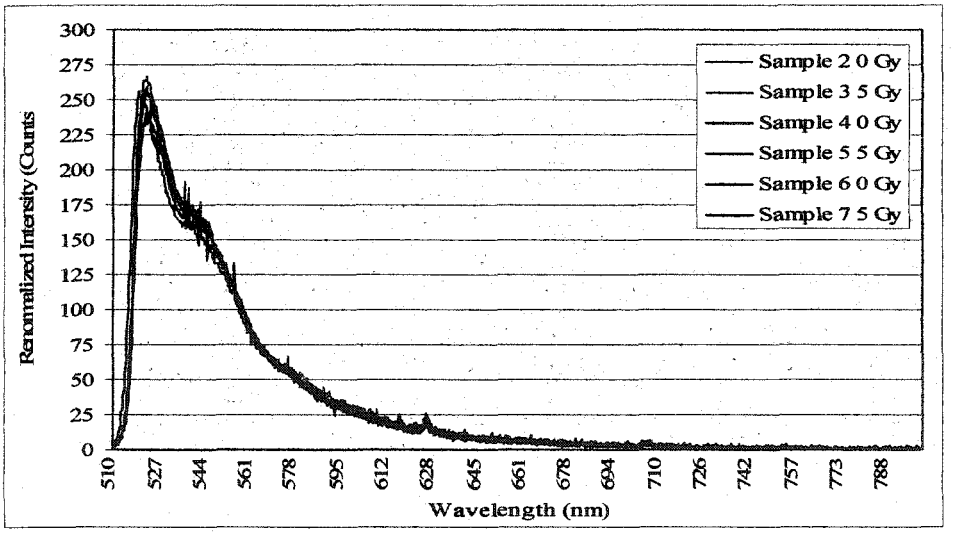

Figure 6-19. Renormalized Spectra of H1 GFP Tagged MCF-7 Cell Samples.

For the Actin GFP tagged MCF-7 cell samples, the renormalized spectra had a maximum intensity of approximately 950 counts ± 50 counts. For the H1 GFP tagged MCF-7 cell samples, the renormalized spectra had a maximum intensity of approximately 250 counts ± 50 counts. The small variation in the fluorescence intensities indicates little change in the renormalized spectra, which have equal areas under curve for each type of tagged cells.

From the renormalized spectra of living Actin GFP tagged MCF-7 cells in figure 6-18 the absolute values of the spectral differences were calculated with equation 6-6. Spectral differences were calculated between samples prepared the same way (i.e. irradiated minus irradiated), and between samples prepared differently (i.e. non-irradiated minus irradiated). The absolute values of the spectral differences were repeated for living H1 GFP tagged MCF-7 cells. The intent of this analysis was to identify changes in spectral shape not evident from previous ratios of areas.

Equation 6-6. Spectral Difference for Living Cells.

$$\text{Spectral Difference} = |\,\text{Renorm } S(\lambda) - \text{Renorm } S(\lambda)\,|$$

The ratios of the areas of spectral differences for the renormalized spectra to the average area were calculated for the wavelength range of 510 nm to 800 nm and are summarized in table 6-13 for Actin GFP tagged MCF-7 cells and in table 6-14 for H1 GFP tagged MCF-7 cells. Where the average areas were calculated separately for the non-irradiated minus non-irradiated (N-N), irradiated minus irradiated (I-I), and non-irradiated minus irradiated (N-I).

Table 6-13. Ratios of the Spectral Difference for Actin GFP Tagged MCF-7 Cells.

	Sample No.'s	Ratio of Area to Average Area of Spectral Difference
N-N	3 – 7	0.48
	4 – 7	1.08
	3 – 4	1.44
I-I	6 – 10	0.59
	9 – 10	0.98
	6 – 9	1.43
N-I	7 – 6	0.41
	4 – 10	0.48
	4 – 6	0.72
	3 – 6	0.74
	7 – 10	0.82
	4 – 9	0.98
	3 – 10	1.06
	7 – 9	1.78
	3 – 9	2.02

Table 6-13 shows the ratio of the spectral area to the average area of Actin GFP tagged MCF-7 cell samples. For N-N the ratios vary from a minimum of – 52% to a maximum of + 44%, for I-I the ratios vary from a minimum of – 41% to a maximum of + 43%, and for N-I the ratios vary from a minimum of – 59% to a maximum of + 102%.

Table 6-14. Ratios of the Spectral Difference for H1 GFP Tagged MCF-7 Cells.

	Sample No.'s	Ratio of Area to Average Area of Spectral Difference
N-I	4 – 6	0.64
	2 – 4	1.17
	2 – 6	1.18
I-I	3 – 5	0.86
	5 – 7	1.02
	3 – 7	1.13
N-N	4 – 3	0.61
	2 – 5	0.61
	6 – 3	0.65
	4 – 5	0.76
	6 – 5	0.78
	6 – 7	1.25
	2 – 3	1.39
	2 – 7	1.44
	4 – 7	1.51

Table 6-14 shows the ratio of the spectral area to the average area of H1 GFP tagged MCF-7 cell samples. For samples prepared in the same way the ratios varied from a minimum of – 36% to a maximum of + 18% (for N-N and I-I), and for samples prepared in different ways (for N-I) the ratios varied from a minimum of – 39% to a maximum of + 51% (re. 7.2. Fluorescence Spectroscopy and Imaging for a discussion of the significance of these results).

Appendix VI.iv. Analysis Summary for Fluorescence Measurements for Living Tagged MCF-7 Cells) contains an overview of the raw and normalized fluorescence measurements of both Actin and HI GFP tagged MCF-7 cells.

6.2.5. Raw Fluorescence Measurements for Colon Tissue

Fluorescence measurements were also acquired with the normal and cancerous colon tissue samples for patients PA and PB. Two sets of fluorescence spectra and images were obtained for each sample, resulting in 48 spectra in total. Raw fluorescence spectra of the colon tissue for patient PA and PB are shown in figures 6-20 and 6-21 respectively, for the established wavelength range of 510 nm to 800 nm.

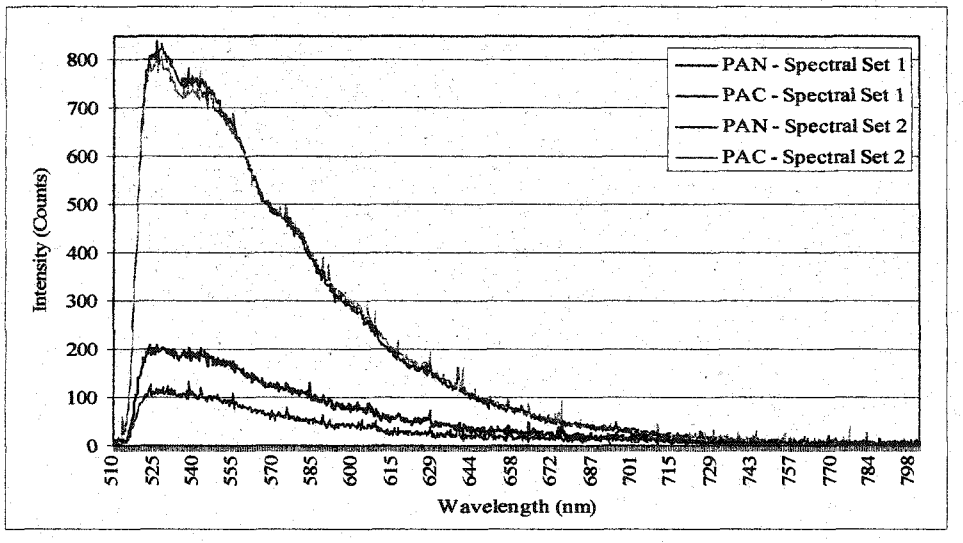

Figure 6-20. Raw Fluorescence Spectra of Colon Tissue from Patient PA (Normal – N and Cancerous – C).

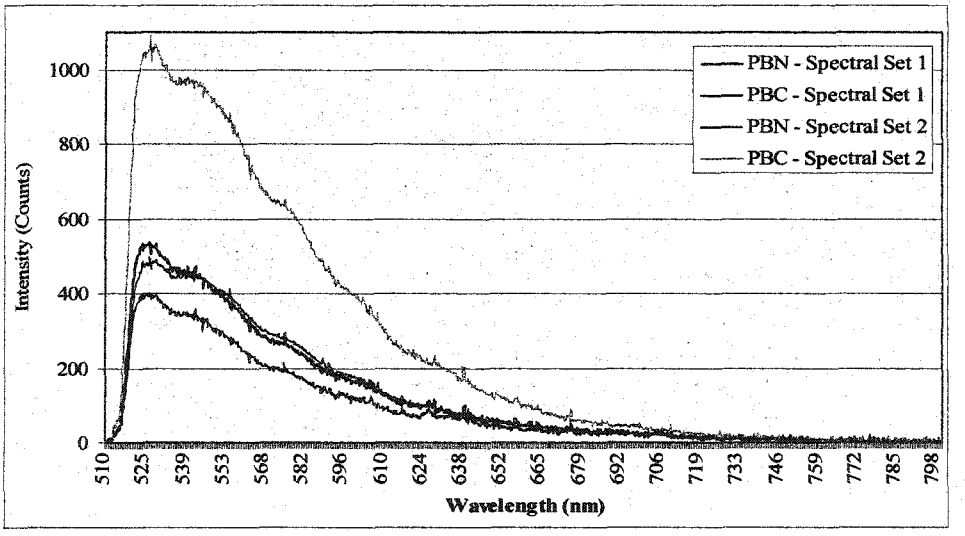

Figure 6-21. Raw Fluorescence Spectra of Colon Tissue from Patient PB (Normal – N and Cancerous – C).

Each spectral set was plotted for the fluorescence spectra of each patient tissue type, where N denotes normal and C denotes cancerous colon tissue samples. The maximum intensities for patient PA from figure 6-20 varied between 200 counts and 900 counts for normal tissue and 100 counts to 800 counts for the cancerous tissue. Similarly the maximum intensities for patient PB in figure 6-21 ranged from 450 counts to 550 counts for normal and 400 counts to 1100 counts for cancerous tissue samples. These variations in the fluorescence spectra are discussed in section 7.2. Fluorescence Spectroscopy and Imaging.

To facilitate analysis of these results, the spectral areas were also calculated by performing a summation of the spectral intensities for the averaged spectra (re. Equation 6-1) for the wavelength range of 510 nm to 800 nm. Table 6-15 shows the ratios of the spectral areas for each spectral set and tissue type relative to the average area of all spectral sets and tissue types for each patient.

Table 6-15. Ratios of Spectral Area for Fluorescence of Colon Tissue.

Spectral Set	Sample	Ratio of Area to Average (both Spectral Sets) per Patient
1	PAN	0.45
2		1.64
1	PAC	0.26
2		1.65
1	PBN	0.81
2		0.81
1	PBC	0.61
2		1.77

The ratios of the spectral areas for each patient were an alternative means of assessing the spectral data. For patient PA this ratio varies between - 74% to + 65%, whereas for patient PB this ratio varies between a minimum of - 39% and a maximum of + 77% for the normal and cancerous colon tissue samples. For spectral set 1 the ratio of the areas

to the average area were less than or equal to those for spectral set 2 for patient PA and PB.

Fluorescence images of the colon tissue samples were obtained in conjunction with each spectrum. Attempts were made to use similar looking areas on each tissue type (normal and cancerous) between patients. Figure 6-22 shows four typical fluorescence images, two from each patient. In the fluorescence images of the normal tissue (6-22a and 6-22c) definite structure can be seen whereas the cancerous tissue (6-22b and 6-22d) structures are not as well defined.

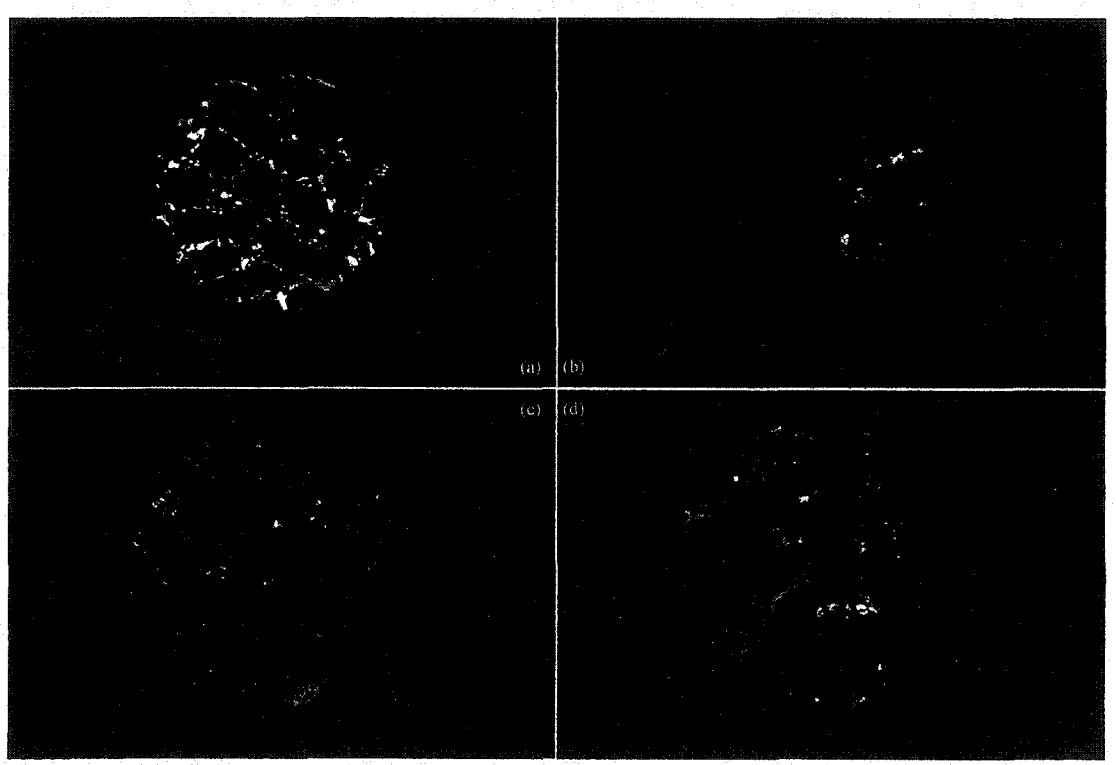

Figure 6-22. Fluorescence Images of (a) PAN, (b) PAC, (c) PBN, and (d) PBC Samples.

6.2.6. Normalized Fluorescence Spectra for Colon Tissue

The individual raw fluorescence spectra of colon tissue were normalized using the ratio method of the average area to the spectral area as in equation 6-2. The normalized fluorescence spectra were calculated for each spectral set. Similar to the

normalized absorbance spectra for colon tissue, the spectral data were interpreted by comparing normal to cancerous tissue of the same patient and by comparing patient to patient the same type of tissue, i.e. PAN to PBN, and PAC to PBC (re. 6.1.2).

For the comparison of cancerous to normal tissue for each patient, the spectral data were renormalized using the same techniques as described for absorbance (re. 6.1.2.). Table 6-16 summarizes the renormalization ratio (re. Equation 6-3) for each spectral set of patients PA and PB in the third column and the ratio of the spectral area to the average area for both spectral sets and tissue types in the fourth column.

Table 6-16. Fluorescence Renormalization Parameters for Colon Tissue.

Spectral Set	Sample	Renormalization Ratio Per Spectral Set (re. Equation 6-3)	Ratio of Renormalized Area to Average (both Spectral Sets) per Patient (re. Equation 6-1)
1	PAN	0.79	0.35
	PAC	1.37	
2	PAN	1.00	1.65
	PAC	1.00	
1	PBN	0.88	0.52
	PBC	1.16	
2	PBN	0.89	1.48
	PBC	1.14	

The renormalization ratios are used so that the same areas are obtained for each spectral set to compare between the cancerous and normal colon tissue. For PAN the renormalization ratios are less than or equal to the normalization ratios for PAC. For PBN the renormalization ratios are less than the normalization ratios for PBC. The ratio of the average renormalized areas for the fluorescence spectra of patient PA varied between - 65%, and + 65% whereas for patient PB the ratios varied between – 48% and + 48%. As observed for the raw fluorescence, the ratios of the areas were found to be less for the first spectral set compared to the second spectral set. The renormalized fluorescence spectra for patient PA are shown in figures 6-23 and for patient PB are

shown figure 6-24 for the wavelength range of 510 nm to 800 nm. From figure 6-23 the renormalized fluorescence spectra for patient PA ranges from a maximum peak intensity of approximately 150 counts to 850 counts. The renormalized fluorescence spectra for patient PB vary between a maximum peak intensity of 450 counts to 1225 counts. The maximum peak appeared at 528 nm ± 2 nm for patient PA and at 527 nm ± 1 nm for patient PB, where the uncertainty is determined from the standard deviation.

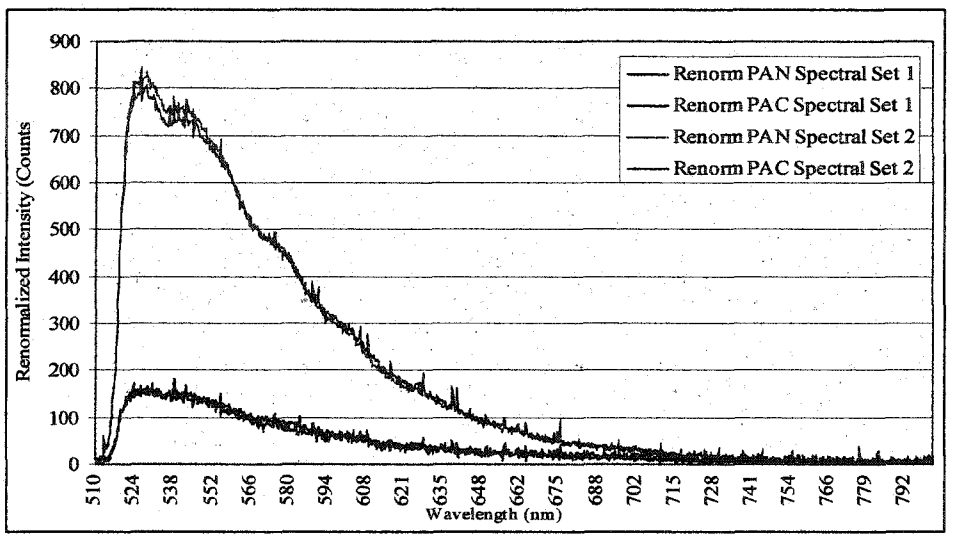

Figure 6-23. Renormalized Fluorescence Spectra to Compare Colon Tissue Samples of Patient PA.

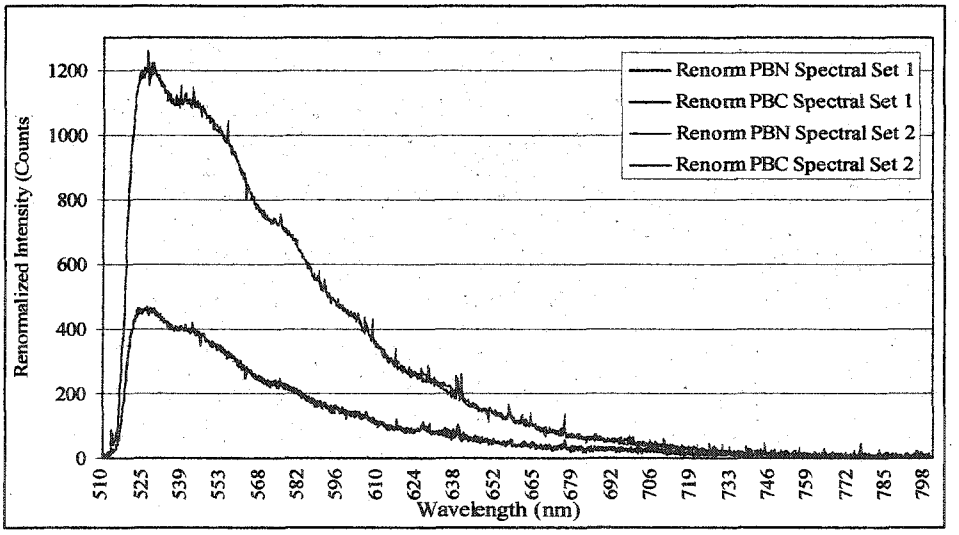

Figure 6-24. Renormalized Fluorescence Spectra to Compare Colon Tissue Samples of Patient PB.

The difference between the cancerous colon tissue and normal colon tissue spectra was calculated for patient PA and for patient PB (re. Equation 6-4). A summation was then performed over the spectral difference for the wavelength range of 510 nm to 800 nm (re. Equation 6-1). Table 6-17 summarizes the ratios of the area of the spectral difference to the average spectral difference for each spectral set.

Table 6-17. Ratios of the Spectral Difference between Fluorescence Spectra of Cancerous and Normal Colon Tissue.

Sample Difference	Ratio of Area to Average Spectral Difference per Patient Spectral Set 1	Ratio of Area to Average Spectral Difference per Patient Spectral Set 2
PAC - PAN	0.74	0.97
PBC - PBN	1.26	1.03

The ratios of the area of spectral differences between the fluorescence spectra of cancerous and normal colon tissue for patient PA varied from - 26% for spectral set 1 to – 3% for spectral set 2. For patient PB the ratios of the areas of spectral differences varied from + 3% for spectral set 2 to + 26% for spectral set 1. The differences are symmetric about the mean due to the limitation of having only two patients. As already mentioned the analysis approach is intended (and more appropriate) for use with numbers of patient samples greater than two.

A renormalization of the spectral data was then performed to again facilitate the inter-patient comparison of patient PA to patient PB. Table 6-18 summarizes the renormalization ratio for each set of spectra for patients PA and PB in the third column (re. Equation 6-3) per spectral set and the ratio of the spectral areas to the average normalized areas for each tissue type for both spectral sets in the fourth column.

Table 6-18. Fluorescence Renormalization Parameters for the Inter-patient Comparison of Colon Tissue.

Spectral Set	Sample	Renormalization Ratio per Spectral Set (re. Equation 6-3)	Ratio of Renormalized Area to Average Area (both Spectral Sets) per Tissue Type
1	PAN	1.61	0.49
	PBN	0.73	
2	PAN	1.35	1.51
	PBN	0.79	
1	PAC	1.96	0.42
	PBC	0.67	
2	PAC	1.16	1.58
	PBC	0.88	

The renormalization ratios for normal and cancerous colon tissue spectra were used to facilitate inter-patient comparison. As a result the renormalized spectral areas were set to be equal for each spectral set and tissue type. The renormalization ratios for both the normal and the cancerous colon tissue from patient PA were greater compared to those for patient PB. The ratios of the renormalized areas for the normal tissues varied by ± 51% and for the cancerous tissues were within ± 58%. The renormalized fluorescence spectra for the inter-patient comparison for normal colon tissues are shown in figures 6-25 while those for cancerous colon tissue are shown figure 6-26. Again the wavelength range was of 510 nm to 800 nm was chosen to display the data. For the interpretation of these results refer to the discussion 7.2. Fluorescence Spectroscopy and Imaging.

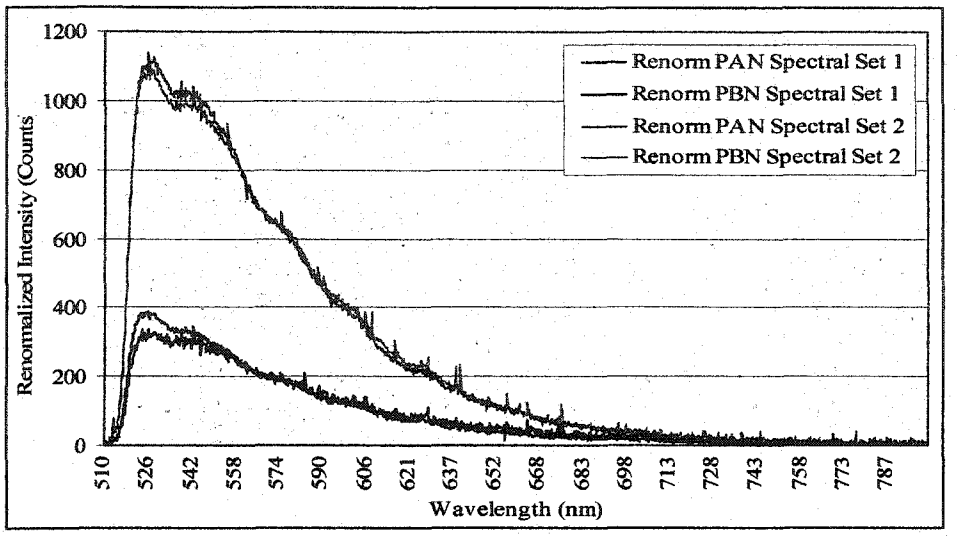

Figure 6-25. Renormalized Fluorescence Spectra for the Inter-patient Comparison of Normal Colon Tissue.

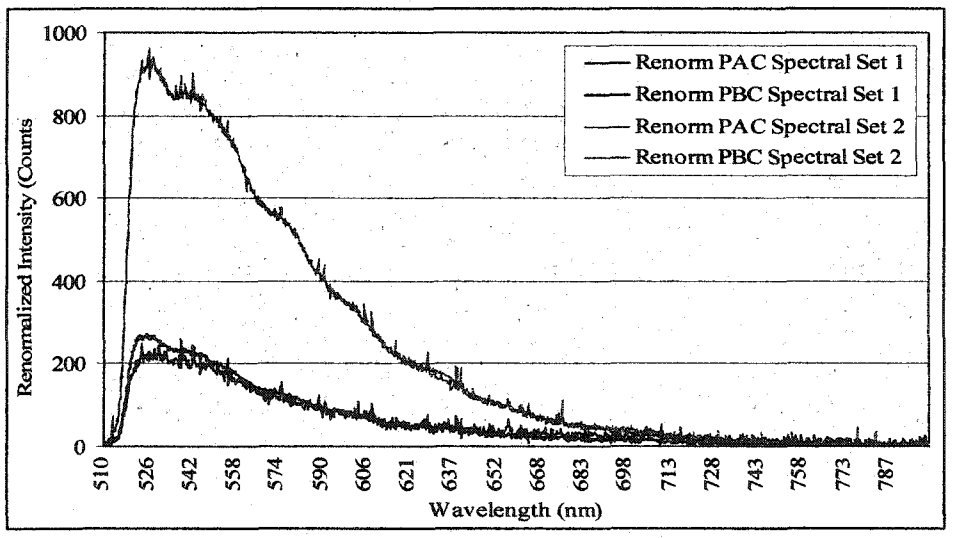

Figure 6-26. Renormalized Fluorescence Spectra for the Inter-patient Comparison of Cancerous Colon Tissue.

For both the renormalized fluorescence spectra for normal and cancerous colon tissue spectral set 2 yielded higher intensities relative to spectral set 1 by 24 ± 3% (re. 7.2. Fluorescence Spectroscopy and Imaging for a discussion of these results).

The absolute value of the spectral difference was also calculated for the inter-patient comparison of normal to normal and cancerous to cancerous colon tissue (re. Equation 6-5). The spectral difference was again summed over the wavelength range of

510 nm to 800 nm (re. Equation 6-1), and the spectral difference for each tissue type relative to the average spectral difference were calculated for each spectral set. Table 6-19 summarizes the ratios of areas between the normal tissue spectra for patients PA and PB and the cancerous spectra for patient PA and PB.

Table 6-19. Ratio of Spectral Differences by Inter-patient Comparison of Fluorescence Spectra of Colon Tissue.

Sample Difference	Ratio of Area to Average Spectral Difference (all six) per Tissue Type Spectral Set 1	Ratio of Area to Average Spectral Difference (all six) per Tissue Type Spectral Set 2
PAN - PBN	1.00	0.75
PAC - PBC	1.00	1.25

The ratio acquired for the absolute value of the spectral difference relative to the average area of normal colon tissue for the fluorescence spectra had a spread of 0% to – 25% for the two spectral sets. For cancerous colon tissue the ratio varied from 0% to + 25% for the two spectral sets.

An analysis summary for raw and normalized fluorescence measurements of colon tissue has been provided in the appendices (re. Appendix VI.v. Analysis Summary for Fluorescence Measurements for Colon Tissue).

7. DISCUSSION

Absorption and fluorescence are the two basic and distinct spectroscopic approaches that were exploited as a practical means of distinguishing between biological samples, in particular cancerous and normal tissue. Due to the inhomogeneous nature of cells and tissues, fluorescence spectroscopy was complemented using imaging techniques that permitted clear delineation of the area from which the spectroscopic information was derived.

7.1. ABSORPTION SPECTROSCOPY

Absorption spectroscopy was investigated using a spectroscopic measurement system to characterize the normal and cancerous colon tissue samples at an area on the sample. The area of this sample is approximately 1.6 cm^2, large in comparison to cellular dimensions, but relatively small in terms of the typical volume of organs and samples. Optical fibres with diameters of 400 μm were used to illuminate and collect light from the samples. The challenges included designing a sample holder to accommodate tissue samples mounted onto microscope slides and adjusting the sample to examine areas of interest. In general, the tabletop sample holder worked well for the preliminary measurements; however there were disadvantages to the design including a poor light seal that allowed stray light from external sources to potentially affect acquired spectra. The mounts holding the illumination and collection optics were difficult to align reproducibly at the same height and proper angle for maximum spectral signal.

For the raw absorbance spectra of normal and cancerous colon tissue for patient PA and PB, the maximum peak intensities varied between 550 counts to 1900 counts (re. Figures 6-1 and 6-2). This variance is attributed to dependencies on the area of the sample, variations in the sample set-up, and the time that elapsed after sample preparation. For each sample type, the areas of interest were chosen in a relatively *ad hoc* manner without a microscope to assist in identifying areas based on similarity of appearance. Consequently, differences in experimental results may also be attributed to variations in morphology, which could be useful, and the thickness of the tissues, which does not offer the type of biological indicator or marker being sought. Tissue samples

were prepared using a nominal thickness of 10 μm in an effort to enhance the contribution of morphology over thickness. The alignment of the tabletop sample holder was verified before each measurement although, as already mentioned, the prototype arrangement had limitations in this regard. Furthermore the time of measurement after sample preparation may have also affected the absorbance spectra. Spectral sets 2 and 3 were measured well after the initial preparation. Absorbance measurements performed days after the initial preparation yielded lower intensities. The quality of these samples deteriorated with time when stored at room temperature. The results may have remained more consistent if the samples had been stored at – 80 °C in a microscope slide box with a desiccant to absorb moisture. Clearly future work should incorporate such strategies or, at least, ensure that there is a consistent time frame used for preparation and subsequent measurements.

As an alternative to using simple peak heights, the ratio of the spectral areas relative to the average area of the raw absorbance corresponding to patients PA and PB (re. Table 6-1) were considered as a means of illustrating the variation in the raw absorbance spectra for the normal and cancerous colon tissue. The average deviations from the mean of these ratios were 33% for patient PA and 29% for patient PB, indicating a consistent spread for the two patients. The ratio method would be more practical for studies with a number of patients greater than two. Regardless this method was chosen as groundwork for future comparison studies involving larger groups of patients.

To facilitate analysis of variations in spectral characteristics between spectra, the raw absorbance spectra were also normalized on the basis of areas. This approach minimized the influence of some of the less desirable experimental considerations (re.

6.1.2). Two separate inter-comparisons were performed on this basis. First, the normalized spectra were renormalized to compare between normal and cancerous colon tissue spectra from the same patient. A second renormalization was performed to compare between the same tissue types from different patients.

When renormalized absorbance spectra obtained from cancerous colon tissue were compared to those obtained for normal colon tissue from the same patient, a spectral shift was observed. The cancerous colon tissue spectra had a shift of 4 nm ± 2 nm for patient PA and a shift of 5 nm ± 3 nm for patient PB in the wavelength range of 450 nm to 550 nm. In the wavelength range of 750 nm to 850 nm the spectral shifts were 5 nm ± 3 nm and 8 nm ± 4 nm for patient PA and PB respectively (re. Figures 6-3 and 6-4). The ratios of the renormalized area to the average area were greater for spectral set 1 compared to spectral sets 2 and 3 (re. Table 6-2), consistent with the raw absorbance spectra. The effect can be attributed to factors already identified. The absolute value of the spectral difference between cancerous and normal colon tissue spectra for all three renormalized spectral sets demonstrated two distinct peaks for both patient PA and patient PB. These peaks arise as a result of the offset between the cancerous and normal colon tissue spectra. The largest spectral differences were observed at two inflection points near 530 nm ± 10 nm and 780 nm ± 10 nm while that near 640 nm showed the smallest differences (re. Figure 6-5). As suggested by the general shape of the spectral differences curves, a multiple peak Gaussian fit was applied. The Gaussian fits conformed well with the spectral differences except in the region between the peaks where the smallest difference existed (near 640 nm ± 10 nm). The Gaussian fit was useful in providing quasi-parameterizations, i.e. the peak maximum and the full width half maximum (FWHM), that facilitate inter-comparison

between cancerous and normal tissue from the same patient (re. Table 6-3). In these spectra there were two prominent peaks. For patient PA the peak maxima were located at 532 nm and 770 nm, with respective FWHM of 95 nm and 149 nm. For patient PB the peak maxima were located at 538 nm and at 785 nm, with respective FWHM of 100 nm and 155 nm. The differences between the peak maxima indicates a spectral shift, whereas differences between the FWHM are indicative of changes in the line shape. The spectral differences as determined by calculating the area under the curves (including the signs) were essentially zero, indicating that the observed differences were simply a result in a shift of the spectrum rather than an actual change in the characteristics or shape. For the spectral difference between normal and cancerous colon tissue, the spread of the spectral areas relative to the average area was 22% for both patients PA and PB (re. Table 6-4). The Gaussian fit parameters and the ratio (area of spectral difference to average area) suggests a potential means for distinguishing between cancerous and normal tissue types, and warrants further investigation.

The comparison of the same tissue types from different patients yielded renormalized spectra with a similar shape but without a spectral shift (re. Figures 6-6 and 6-7). The ratios of the renormalized area relative to the average area for the inter-patient comparison (re. Table 6-5) were greater for the first spectral set compared to the later two spectral sets, and again this difference is attributed to reasons previously mentioned. The spectral difference between patients PA and PB resulted in a curve similar to the comparison of tissue from the same patient, but with less than half the intensity (re. Figure 6-8). The Gaussian fits conformed well to the spectral differences showing the general shape excluding the noise. Two main peaks were observed, with the maximum peak positions and the full width half maximum (FWHM) values obtained

for the Gaussian fit (re. Table 6-6). The average peak maximum for normal colon tissue had the first peak at 542 nm and the second peak at 803 nm, with respective FWHM of 158 nm and 229 nm. The average peak maxima of the two peaks were 541 nm and 795 nm respectively with widths of 120 nm and 189 nm for cancerous colon tissue. The maximum peak positions were similar for both the normal and cancerous colon tissue whereas the FWHM values for the two peaks were greater for cancerous compared to normal colon tissue. For the spectral difference between normal and cancerous colon tissue, the spread of the spectral areas relative to the average area was 41% for both patients PA and PB (re. Table 6-7). These variations in the average deviation from the mean being essentially the same make it difficult to use these data to reliably differentiate between the tissue types. Although, the full width half maximum values obtained from the Gaussian fit could potentially be an indicator to differentiate between tissue types.

For the comparison of the different tissue types from the same patient, a spectral shift was observed in contrast to no apparent shift for the comparison of the same tissue types from different patients. The ratios of the spectral differences relative to the average spectral difference for the same patient comparison of colon tissue had a lower average deviation compared to those derived from the comparison of the colon tissue for the inter-patient. The spectral shift, the ratios of the spectral differences and the maximum peak position from the Gaussian fit suggest that, using absorbance spectroscopy, the same patient comparison can be a potential method to distinguish between normal and cancerous colon tissue. However, the full width half maximum from the Gaussian fit which were similar for different tissue types from the same patient, varied for the same

tissue type from different patients, suggesting that, the inter-patient comparison can be a potential means of distinguishing between tissue types.

7.2. FLUORESCENCE SPECTROSCOPY AND IMAGING

After examining several possible arrangements, the final fluorescence system included a combined imaging and spectroscopic measurement system that allowed for subjective localization of the area of interest to be examined. Fluorescence measurements were conducted with normal and cancerous colon tissue, ethidium bromide, fixed tagged cells, and living tagged breast cancer cells. The spectroscopic measurement system for fluorescence incorporated illumination through an epi-fluorescence microscope, and collection through an adapter designed to couple the emitted light from the eyepiece into a 400 μm diameter fibre connected to the spectrometer. The disadvantage was that only a portion of the fluorescence emission could be collected by the spectrometer due to limitations of the adapter and fibre.

As expected, the raw fluorescence spectra of EtBr decreased in intensity as the concentration of EtBr was decreased. With an emission wavelength range of 510 nm to 800 nm, EtBr was used as the reference standard (re. 4.1. Reference Standards). The spectral area under the curve also shows a decrease with concentration (re. Figure 6-9). The spectral areas of the EtBr concentrations (0.1 μg/ml to 50 μg/ml) to the wavelength had a non-linear response. For the 0.1 μg/ml concentration of EtBr, the spectra were essentially noise fluctuations with spectral areas of -1000 counts ± 2000 counts (re. Table 6-8). This last result indicates the lower limit on concentration that is detectable with this system and the associated measurement parameters. If system refinements

were introduced to reduce the signal to noise ratio it is most likely that the lower limit of detection could be extended.

Fluorescence measurements of the fixed tagged reference cells were used to align the eyepiece/fibre adapter and to set the microscopes iris size to collimate the area from which the optical fibre could actually collect light. The disadvantage was that the iris size was established based on centering the fixed tagged cells in the field of view for each measurement, introducing the likelihood of deviations from set-up to set-up. In an effort to ensure consistencies in the iris size, both the spectra and the images acquired during the initial alignment of the adapter were compared to the spectra and images of reference cell sample before acquiring measurements for each sample. The raw fluorescence spectra for the fixed tagged cells taken with both the 40 x and 60 x objective magnifications for the minimum and optimum iris sizes had maximum peak intensities at approximately 555 nm ± 5 nm (re. Figure 6-10). The average spectral areas from the 13 spectra of the fixed tagged cells for each configuration had an uncertainty of ± 1000 counts (re. Table 6-9). Using the details that could be seen in the fluorescence images of the cells, the iris size and center the area of interest in the field of view were both adjusted (re. Figure 6-11).

For the irradiated and non-irradiated Actin GFP tagged MCF-7 cell samples, the raw fluorescence spectra showed a variation in the maximum peak intensities (re. Figure 6-12). The variations in the peak intensities may be due to both the sampling area and the instrumentation set-up. The sampling areas for each may have had a varying number of cells present in the field of view yielding different fluorescence intensities. The eyepiece/fibre adapter and iris size were verified using the fixed tagged cells before each measurement as previously discussed, but clearly this approach introduces some

uncertainties. For the irradiated living cells it would be unlikely to see immediate changes due to radiation damage (re. 2.5.). The DNA would be the critical target and the damage to the backbone would not be evident until after a single cell division or more. As expected, the general shape and the maximum peak intensity about 536 nm ± 5 nm were consistent for both the irradiated and non-irradiated cells. The ratio of the spectral area relative to the average area had an average deviation of 19% (re. Table 6-11) indicating consistencies in the spectra. The bright cytoplasm from the Actin GFP tagging surrounding the dark nuclei was observed in the fluorescence images (re. Figures 6-14 and 6-15). The cells focused in the field of view were observed to change and move with time. Similar activity was observed with both irradiated and non-irradiated cell samples.

As with the Actin GFP tagged MCF-7 cells samples, the average raw fluorescence spectra of the H1 GFP tagged MCF-7 cell samples vary in maximum intensity from sample to sample for both the non-irradiated and irradiated samples (re. Figure 6-13). A peak not apparent with the Actin GFP tagged MCF-7 cells appeared near 626 nm ± 5 nm for the H1 GFP tagged MCF-7 cells. It is possible that this peak may be a result of the presence of porphyrins (re. Table 2-2). The average deviation from the mean of 14% was determined for the spectral areas relative to the average area (re. Table 6-11) showing consistencies in the spectra. Images acquired using H1 GFP tagged MCF-7 cells clearly show fluorescence from the GFP tagging of the cells' nuclei (re. Figures 6-16 and 6-17). Over time some of the nuclei were observed passing through mitosis regardless of whether the cells were irradiated and non-irradiated. The nuclei undergoing mitosis appear to have increased fluorescence intensity in the early stages (prophase and metaphase). In prophase the chromosomes have replicated and in

metaphase the chromosomes are aligned at the mid-plane of the cell. During anaphase and telephase, the replicated chromosomes separated and are pulled to the poles as the nuclear membrane redevelops. No affect attributable to the radiation exposure was observed during the four hour period when measurements were performed.

For renormalized fluorescence spectra, the ratio of the area of spectral difference of Actin GFP tagged MCF-7 cell samples had an average deviation from the mean of 35% for N-N, 29% for I-I and 41% for N-I (re. Table 6-13). The ratio of areas of spectral differences of H1 GFP tagged MCF-7 cell samples had an average deviation from the mean of 24% for N-N, 10% for I-I and 35% for N-I (re. Table 6-14), indicating some similarities between non-irradiated and irradiated cells.

The raw fluorescence spectra for the colon tissue samples for the two patients (re. Figures 6-20 and 6-21) varied due to the time delay between spectral set measurements, alignment of the eyepiece/fibre adapter, and tissue morphology of the area of interest (re. 7.1). The areas of interest were based upon subjective similarity of appearance as observed through the microscope. The spread in the spectral areas relative to the average area had average deviations about the mean from the combination of both available spectral sets of 65% and 39% for the colon tissue for patients PA and PB respectively (re. Table 6-15). The ratios of the spectral areas were an alternative means of illustrating the variation in the raw fluorescence spectra. Fluorescence images were shown for a small area of interest on four samples (re. Figure 6-22). The brighter regions show the auto-fluorescence from the fluorophores present in the tissues. A large number of fluorophores have excitation maxima in the UV and emission in the UV/VIS. As a consequence it is difficult to identify components of tissue that are fluorescing with the filter cube used in the system with an excitation of 420 nm to 490 nm and emission

greater than 520 nm. The fluorescence detected is probably a combination of fluorophores. An improvement could potentially be observed by using a better matching filter cube such as alternative filter cube a UV-2A filter from Nikon Instruments Inc. with an excitation in the 330 nm to 380 nm and an emission above 420 nm. Such an alternative filter should enhance detection of fluorophores such as NADH, NADPH, certain vitamins and lipids (re. to Table 2-2 for excitation and emission maxima).

The fluorescence spectra for colon tissue were renormalized (a) to compare normal to cancerous colon tissue from the same patient, and (b) to compare the same tissue type (i.e. normal to normal, and cancerous to cancerous) from different patients.

The fluorescence spectra comparing different tissue types from the same patient had a maximum peak intensities positioned at approximately 528 nm ± 2 nm for patient PA and 527 nm ± 1 nm for patient PB. The ratios of the spectral differences for each spectral set had an average deviation from the mean of 15% for both patient PA and PB (re. Table 6-17). In general, the sample differences were found to be greater for patient PB compared to patient PA.

The inter-patient comparison revealed large discrepancies between the renormalized areas for both the normal and cancerous colon tissue. Spectral set 2 was 24 ± 3% higher than spectral set 1, which may be attributed to the time elapse between measurements (re. Figures 6-25 and 6-26). The ratios of the spectral differences had an average deviation of 13% for both normal and cancerous tissues (re. Table 6-19). In general, the sample differences for cancerous colon tissues were found to be greater than or equal to that for normal colon tissue.

In contrast to the absorption spectroscopy of colon tissue (22% for same patient and 41% for inter-patient comparison), the ratio of the spectral differences relative to the

average spectral difference for the fluorescence spectra of the same patient comparison and the inter-patient comparison were both low (15% and 13% respectively). The difference in the results obtained for the same patient comparison may be attributed to the fact that the cancerous colon tissue from patient PA is a moderately differentiated adenocarcinoma while that for patient PB is moderately differentiated invasive adenocarcinoma. The same-patient comparison and the inter-patient comparison may be potential methods to distinguish tissues; however, further investigations are required.

8. CONCLUSION

The instrumentation and measurements for absorbance and fluorescence presented offer a preliminary groundwork for further investigation into the potential of optical spectroscopy to provide non-invasive diagnostic techniques for cancer detection.

The tabletop microscope slide holder for absorption spectroscopy worked well for the preliminary measurements. An ideal system for absorption would be a combined imaging - spectroscopic measurement system such that an area of interest could be more readily localized. The microscope, eyepiece/fibre adapter, and CCD camera used for the fluorescence measurements could potentially be modified so that excitation could originate from underneath the microscope stage (i.e. from an optical fibre coupled to a light source). Alignment of the fibre with the objective, matching the excitation and collection areas, and the use of filters are a few of the challenges that would have to be addressed.

The normalization of the absorbance spectra to compare cancerous to normal colon tissue from the same patient for the wavelength range of 450 nm to 550 nm showed a spectral shift of 4 nm ± 2 nm and 5 nm ± 3 nm for patient PA and PB

respectively; and for the wavelength range of 750 nm to 850 nm showed a spectral shift of 5 nm ± 3 nm and 8 nm ± 4 nm for patient PA and PB respectively. The spectral shift suggests differences in the morphology and absorption properties of the colon tissues. The spectral difference relative to the average spectral difference for the same patient comparison had a lower average deviation from the mean compared to the inter-patient comparison indicating a potential method in identifying between normal and cancerous tissues. The Gaussian fit to the spectral difference curves provided fitting parameters that could be useful. For the same patient comparison the maximum peak and full width half maximum (FWHM) were found to be similar between the two patients, although for the inter-patient comparison there was a significant difference in the FWHM. The differences in the FWHM may indicate a potential method to identify different tissue types. For absorption spectroscopy, the framework of analysis for same patient and the inter-patient comparisons have been established. However, more samples from a number of patients are needed to verify whether or not these observations are consistent.

The EtBr concentrations served as fluorescence reference standards for the fluorescence system, where the 0.1 μg/ml concentration of EtBr was determined to be a limiting concentration for the system. The fluorescence instrumentation, including the microscope, eyepiece/fibre adapter, and CCD camera, allowed for the acquisition of spectra and the corresponding image of the sample for use in localizing the areas of interest. The fixed reference cells were used with moderate success to set the iris size for the adapter with the 20 x magnification objective and the 400 μm diameter fibre. Development of a more systematic approach to adjusting the iris size and adapter geometry would be advantageous.

The GFP tagged living cell samples were used to investigate a known fluorescence signal with a high intensity before moving onto less intense untagged cell samples. Untagged samples permit the study of endogenous rather than exogenous fluorophores. The fluorescence imaging with the H1 GFP tagged MCF-7 cell samples illustrated various stages of cell division (mitosis) and cellular movement regardless of whether the or not cells were irradiated. Although mitosis was not observed with Actin tagged MCF-7 cell samples, cellular movement was evident. The normalization of irradiated cell sample spectra investigation revealed, for the time frame of the measurements, no affects which could be attributed to radiation exposure. The spectra from the H1 GFP tagged MCF-7 cell samples had a small peak centered at 626 nm ± 5 nm which was not apparent in the spectra from the Actin GFP tagged MCF-7 cell samples. That peak could potentially be attributed to the presence of porphyrins. Future work with the living cell samples could be done by acquiring spectra at different times after irradiation (i.e. days) or by comparing non-irradiated, irradiated, and dead cells to investigate apoptosis. These measurements could be performed with either tagged or untagged living cells. The problem with untagged cells is that the fluorescence intensity is lower in comparison to tagged cells, and the fluorescence intensity decreases (photo-bleaches) at a faster rate than tagged cells.

Fluorescence measurements of colon tissue yielded similar average deviations of the spectral differences for (a) same patient (cancerous to normal) comparisons and (b) inter-patient (normal to normal and cancerous to cancerous). More samples and other excitation wavelength ranges would be required to establish whether or not any significant clinical information can be reliably obtained. To examine endogenous fluorophores, it would be more practical to excite in the UV wavelength range for

spectral characteristics of known fluorophores as shown by Alfano *et al.* (1987), Schomacker (1992a, 1992b), and Majumber *et al.*(1999).

The cancerous and normal colon tissue, Actin and H1 GFP tagged MCF-7 cells, five EtBr concentrations, and fixed reference cells, were used to study optical spectroscopy techniques. Further spectroscopic investigations of normal and cancerous tissues and cell samples are needed to draw any definitive conclusions regarding the potential for developing non-invasive diagnostic techniques; however, the present work clearly establishes the potential for ultimate development of such techniques and the groundwork that will enable these future investigations.

LITERATURE CITED

LITERATURE CITED

af Klinteberg, C. 2000. On the use of Light for Characterization and Treatment of Malignant Tumours. Ph.D dissertation, Lund Institute of Technology. 121pp.

Alberts, B., A. Johnson, J. Lewis, M. Raff, K. Roberts, and P. Walter. 2002. Molecular Biology of the Cell 4th Edition. Garland Science, New York. 1463pp.

Alfano, R.R., D.B. Tata, J. Cordero, P. Tomashefsky, F.W. Longo, and M.A. Alfano. 1984. Laser Induced Fluorescence Spectroscopy from Native Cancerous and Normal Tissue. IEEE J. Quantum Electionics 20(12): 1507-1511.

Alfano, R.R., G.C. Tang, A. Pradhan, W. Lam, D.S.J. Choy, and E.Oper. 1987. Fluorescence Spectra from Cancerous and Normal Human Breast and Lung Tissue. IEEE J. Quantum Electronics 23(10): 1806-1811.

Alfano, R.R., A. Pradhan, G.C. Tang, and S.J. Wahl. 1989. Optical Spectroscopic Diagnosis of Cancer and Normal Breast Tissue. J. Opt. Soc. Am. B. 6(5): 1015-1023.

Attix, F.H. 1986. Introduction to Radiological Physics and Radiation Dosimetry. John Wiley and Sons, Inc. Toronto. 607pp.

Badash, L. 2003. Marie Curie: In the Laboratory and on the Battlefield. Physics Today. July 2003: 37-43.

Bassett, L. W., and R.H. Gold. 1982. Mammography, Thermography, and Ultrasound in Breast Cancer Detection. Grune and Statton, Inc, New York. 172pp.

Beiser, A. 1995. Concepts of Modern Physics Fifth Edition. McGraw-Hill, Inc. Toronto. 534pp.

Bigio, I.J., and J.R. Mourant. 1997. Ultraviolet and visible spectroscopies for tissue diagnostics: fluorescence spectroscopy and elastic-scattering spectroscopy. Physics in Medicine and Biology 42: 803-814.

Buil, C. 1991. CCD Astronomy Cunstruction and Use of an Astronomical CCD Camera. Willmann-Bell Inc. Virginia. 321pp.

Canadian Cancer Society. 2002a. Breast Cancer What you need to know. Canadian Cancer Society. Canada 8pp.

Canadian Cancer Society. 2002b. Colorectal Cancer What you need to know. Canadian Cancer Society. Canada 8pp.

Canadian Cancer Society. 2003a. Stats at a Glance – Breast Cancer Stats. Canadian Cancer Society. http://www.cancer.ca/ccs/internet/standard/0,2939,3172_14435__langId-en,00.html. August 26, 2003.

Canadian Cancer Society. 2003b. Stats at a Glance – Colorectal Cancer Stats. Canadian Cancer Society. http://www.cancer.ca/ccs/internet/standard/0,3182,3172_14447__langId-en,00.html. August 26, 2003.

Canadian Cancer Society. 2004. Media backgrounder: Canadian Cancer Statistics 2004. http://www.cancer.ca/ccs/internet/mediareleaselist/0,,3172_15232_194634558_langId-en.html. May 27, 2004.

Chaudhury, N.K., S. Chandra, and T.L. Mathew. 2001. Oncologic Applications of Biophotonics. Applied Biochemistry and Biotechnology 96: 183-204.

Colthup, N.B., L.H. Daly, and S.E. Wiberley. 1990. Introduction to Infrared and Raman Spectroscopy 3rd Edition. Academic Press, Inc. Toronto. 547pp.

Diffraction Limited. 2002. MaxIm DL and MaxIm CCD Software Version 3.0.6.

Ganesan, S., P.G. Sacks, Y. Yang, A. Katz, M. Al-Rawi, H.E. Savage, S.P. Schantz, and R.R. Alfano. 1998. Native Fluorescence Spectroscopy of Normal and Malignant Epithelial Cells. Cancer Biochem. Biophys. 16: 365-373.

Gayen, S.K., and R.R. Alfano. 1999. Sensing lesions in tissue with light. Optics Express 4 (11): 475-480.

Gillenwater, A., R. Jacob, and R. Richards-Kortem. 1998. Fluorescence Spectroscopy: A Technique with Potential to Improve the Early Detection of Aerodigestive Tract Neoplasia. Head and Neck 20: 556-562.

Glassman, W., C-H. Liu, S. Lubicz, and R.R. Alfano. 1994. Excitation Spectroscopy of Malignant and Non-malignant Gynecological Tissues. Laser in the Life Sciences 6(2): 99-106.

Gupta, P.K., S.K. Majumber, and A. Uppal. 1997. Breast Cancer Diagnosis using N2 Laser Excited Autofluorescence Spectroscopy. Lasers in Surgery and Medicine. 21: 417-422.

Hall, E.J. 1988. Radiobiology for the Radiologist 3rd Edition. J.B. Lippincotte Company, Philadelphia. 535 pp.

Hanlon, E.B., R. Manoharan, T-W. Koo, K.E. Shafer, J.T. Motz, M. Fitzmaurice, J.R. Kramer, I. Itzkan, R.R. Dasari, and M.S. Feld. 2000. Prospects for in vivo Raman Spectroscopy. Physics in Medicine and Biology. 45: R1-R59.

Herman, B. 2001. Fluorescence Microscopy. ßIOS Scientific Publishers – Springer-Verlag. New York. 170 pp.

Holowaty, E.J., L.D. Marrett, R. Parkes, and G. Fehringer. 1998. Colorectal Cancer in Ontario 1971-1996. Preface/Introduction. Surveillance Unit Division of Preventive Oncology Cancer Care Ontario. 5pp.

Huang, Z.W., T.C. Chia, C.H. Diong, S. Lee, and C. Seow. 1998. Laser-induced autofluorescence of human colonic tissues. Proceedings of SPIE 3250: 88-93.

Hung, J., S. Lam, J.C. LeRiche, and B. Palcic. 1991. Autofluorescence of Normal and Malignant Broncial Tissue. Lasers Surg. Med. 11: 99-105.

Jain, B., S.K. Majumber, and P.K. Gupta. 1998. Time Resolved and Steady State Autofluorescence Spectroscopy of Normal and Malignant Human Breast Tissue. Lasers in the Life Sciences. 8: 163-173.

Katz, A. and R.R. Alfano. 1996. Optical Biopsy – Detecting Cancer with Light. OSA TOPS on Biomedical Optical Spectroscopy and Diagnosis 3: 132-135.

Katz, A., S. Ganesan, Y. Yang, G.C. Tang, Y. Budansky, E. Celmer, H.E. Savage, S.P. Schantz, and R.R. Alfano. 1996. Optical biopsy fiber based fluorescence spectroscopy instrumentation. Proceedings of SPIE 2679: 118-123.

Knight, A.W., and N. Billinton. 2001. Distinguishing GFP from Cellular Autofluorescence. Biophotonics International. 42-50.

Lakowicz, J.R. 1999. Principles of Fluorescence Spectroscopy 2nd Edition. Kluwer Academic/Plenum Publishers, New York. 698 pp.

Lin, W-C, S.A. Toms, M. Johnson, E.D. Jansen, and A. Mahadevan-Jansen. 2001. In Vivo Brain Tumor Demarcation using Optical Spectroscopy. Photochemistry and Photobiology 73(4): 396-402.

Lin-Vien, D., N.B. Colthup, W.G. Fateley, and J.G. Grasselli. 1991. The Handbook of Infrared and Raman Characteristic Frequencies of Organic Molecules. Academic Press, Inc. Toronto. 503pp.

Liu, C.-H., B.B. Das, W.L.S. Glassman, G.C. Tang, K.M. Yoo, H.R. Zhu, D.L. Akins, S.S. Lubicz, J. Cleary, R. Prudente, E. Celmer, A. Caron, and R.R. Alfano. 1992. Raman, fluorescence, and time-resolved light scattering as optical diagnostic techniques to separate diseased and normal biomedical media. J. Photochem. Photobiol. B. Biology 16: 187-209.

Majumber, S.K., A. Uppal, and P.K. Gupta. 1996. Nitrogen Laser Excited Autofluorescence Spectroscopy for Discrimination of Human Breast Malignancy. OSA TOPS on Biomedical Optical Spectroscopy and Diagnosis 3: 142-146.

Majumder, S.K., P.K. Gupta, B. Jain, and A. Uppal. 1999. UV Excited Autofluorescence Spectroscopy of Human Breast Tissues for Discriminating Cancerous Tissue from Benign Tumor and Normal Tissue. Lasers in the Life Sciences. 8: 249-264.

Mason, W.T. 1999. Fluorescent and Luminescent Probes for Biological Activity 2nd Edition. Academic Press. Toronto. 647 pp.

Mayinger, B., P. Horner, M. Jordan, C. Gerlach, T. Horbach, W. Hohenberger, and E.G. Hahn. 2000. Light-induced Autofluorescence Spectroscopy for Tissue Diagnosis of GI Lesions. Gastrointestinal Endoscopy 52(3): 395-400.

McGhee, P. 2003. Patient Dose Calculation Version 6.4. NWORCC Department of Medical Physics.

Molecular Probes, Inc. 2002. Introduction to Fluorescence Techniques. Molecular Probes, Inc. Oregon. 7pp.

Molecular Probes, Inc. 2003. Structure for E-1305. http://www.probes.com/servlets/structure?item+1305. October 10, 2003.

National Cancer Institute. 2002. What You Need To Know About™ Cancer Of The Colon and Rectum. NIH Pub. No. 99-1552. 18 pp.

National Cancer Institute. 2003. What You Need To Know About™ Breast Cancer. NIH Pub. No. 03-1556. 47 pp.

Niemz, M.H. 1996. Laser-Tissue Interactions Fundamentals and Applications. Springer-Verlag, New York. 297 pp.

Ocean Optics, Inc. 1999. OOIBase32™ Spectrometer Operating Software Version 1.0.1.1. Ocean Optics, Inc. Florida.

Ocean Optics, Inc. 2000a. OOIBase32™ Spectrometer Operating Software Manual Version 1.0. Ocean Optics, Inc. Florida. 48pp.

Ocean Optics, Inc. 2000b. Operating Manual and User's Guide USB2000 Miniature Fiber Optic Spectrometer and Accessories. Ocean Optics, Inc. Florida. 80pp.

Ocean Optics, Inc. 2002. 2002 Product Catolog. Ocean Optics, Inc. Florida. 88pp.

Paquette, D., J. Snider, F. Bouchard, I. Olivotto, H. Bryant, K. Decker, and G. Doyle. 2000. Performance of screening mammography in organized programs in Canada in 1996. Canadian Medical Association Journal 163(9): 1133-1138.

Pavia, D.L., G.M. Lampman, G.S. Kriz. 1996. Introduction to Spectroscopy A Guide for Students of Organic Chemistry 2nd Edition. Saunders College Publishing. Toronto. 511pp.

Pedrotti, F.L., and L.S. Pedrotti. 1993. Introduction to Optics 2nd Edition. Prentice-Hall. New Jersey. 602pp.

Pradhan, A, R.N. Panda, M.S. Nair, B.V. Laxmi, A. Agarwal, and A. Rastogi. 2000. Fluorescence study of normal, benign, and malignant human breast tissue. Proceedings of SPIE 3917: 240-243.

Prosst, R.L., and J. Gahlen. 2002. Fluorescence Diagnosis of Colorectal Neoplasms: A Review of Clinical Applications. Int. J. Colorectal Dis. 17: 1-10.

RadiologyInfo. 2002. Mammography. Radiological Society of North America, Inc. http://www.radiologyinfo.org. 4pp.

Ramanujam, N. 2000. Fluorescence Spectroscopy In Vivo. Encyclopedia of Analytical Chemistry. John Wiley & Sons Ltd. Chichester. 20-59 pp.

Reichman, J. 2000. Handbook of Optical Filters for Fluorescence Microscopy. Chroma Technology Corp. Vermont. 37 pp.

Richards-Kortem, R, Sevick-Muraca, E. 1996. Quantitative Optical Spectroscopy for Tissue Diagnosis. Annual Review of Physical Chemistry 47: 555-606.

Schabas, R. 2003. Colorectal Cancer screening in Canada: It's time to act. Canadian Medical Association Journal 168(2): 178-179.

Schomacker, K, J.K. Frisoli, C.C. Compton, T.J. Flotte, J.M. Richter, T.F. Deutsch, and N.S. Nishioka. 1992a. Ultraviolet Laser-Induced Fluorescence of Colonic Polyps. Gastroenterology 102: 1155-1160.

Schomacker,K, Frisoli, C.C. Compton, T.J. Flotte, J.M. Richter, N.S. Nishioka and T.F. Deutsch 1992b. Ultraviolet Laser-Induced Fluorescence of Colonic Tissue: Basic Biology and Diagnostic Potential. Lasers in Surgery and Medicine 12: 63-78.

Screening for Colon Cancer. 2003. Direct Visualization of the Colon and The Rectum. http://www.screening-for-colon-cancer.com/html/visualization.php3. October 3, 2003.

Shannon Luminous Materials, Inc. 2001. http://www.blacklite.com/Technical/history_of_fluorescence.htm. January 9, 2003.

Sigma-Aldrich Co. 2003. FLUKA-46047 Ethidium Bromide. http://www.sigmaaldrich.com/cgi-bin/hsrun/Distributed/HahtShop/HAHTpage/frmCatalogSearchPost?Brand=FLUKA&ProdNo=46047 . October 23, 2003.

Taylor , S.A. 1998. CCD and CMOS Imaging Array Technologies: Technology Review. Technical Report EPC-1998-106. Xerox Limited. Cambridge, United Kingdom. 14 pp.

Tierney, L.M., S.J. McPhee, and M.A. Papadakis. 2003. Current Medical Diagnosis & Treatment. 42nd Edition. Lange Medical Books – McGraw Hill. Toronto. 1860pp.

Wagnières, G.A., W.M. Star, and B.C. Wilson. 1998. In vivo Fluorescence Spectroscopy and Imaging for Oncological Applications. Photochemistry and Photobiology 68(5): 603-632.

Wang, X.F., and B. Herman. 1996. Fluorescence Imaging Spectroscopy and Microscopy. John Wiley & Sons, Inc. New York, NY. 483pp.

Wilson, B.C. 2002. Biophotonics: A new link between physical and life sciences. Physics in Canada 58(2): 145-155.

Yang, Y., E.J. Celmer, M. Zurawska-Szczepaniak, and R.R. Alfano. 1997. Excitation Spectrum of Malignant and Benign Breast Tissue: A Potential Optical Biopsy Approach. Lasers in the Life Sciences. 7(4): 249-265.

Zhandin, N.N., Y. Yang, N. Ockman, and R.R. Alfano. 1997. Biochemical distinctions between normal and cancerous human breast tissues obtained from fluorescence spectroscopy. Proceedings of SPIE. 2979: 585-588.

APPENDICES

APPENDIX I
ABBREVIATIONS AND ACRONYMS

Abbreviation	Full Name
ΔE_m	Change in Energy of a Molecule
100%R	Percent Reflectance
^{125}I	Iodine - 125
^{137}Cs	Cesium - 137
^{198}Ir	Iridium - 198
5-ALA	δ- aminolevulinic acid
^{60}Co	Cobalt - 60
A	Absorbance Reading
α	Half Cone Angle
A/D	Anolog to Digital
Ar/Kr	Argon/Krypton Mix
BK-7	Borosilicate crown
BSE	Breast Self Examination
c	Speed of Light in Vacuum
C	Cancerous Tissue
CBE	Clinical Breast Examination
CCD	Charged Coupled Device
C^i_{EtBr}	Intermediate Concentration of EtBr
CO_2	Carbon Dioxide
CT	Computer Tomography
C^t_{EtBr}	Target Concentration of EtBr
D	Dark Intensity Reading
DCBE	Double Contrast Barium Enima
DCIS	Ductal Carcinoma *in situ*
DNA	Deoxyribonucleic Acid
E	Energy
e^-	Electron
EM	Electromagnetic
EtBr	Ethidium Bromide
ϕ	Deflection (Scattering) Angle
F.S.	Field Size
FAD	Flavin Adenine Dinucleotide
FBS	Fetal Bovine Serum
FOBT	Fecal Occult Blood Tests
fov	Field of View
FWHM	Full Width Half Maximum
GFP	Green Fluorescent Protein
GSR	Grating Spectral Range
H1	Histone - 1 Protein
H_20	Water
HpD	Hematoporphyrin
hυ	Emission Photon
$h\upsilon_0$	Excitation Photon
$h\upsilon_S$	Energy of a scattering photon

Abbreviation	Full Name
I	Emitted Intensity
I-I	Irradiated Cell Sample Spectrum minus Irradiated Cell Sample Spectrum
I_o	Incident Intensity
φ	Quantum Yield
λ	Wavelength
MOS	Metal Oxide Semiconductor
n	Index of Refraction
N	Normal Tissue
N-I	Non-irradiated Cell Sample Spectrum minus Irradiated Cell Sample Spectrum
N-N	Non-irradiated Cell Sample Spectrum minus Non-irradiated Cell Sample Spectrum
n_1	Index of Refraction of Incident Medium
n_2	Index of Refraction of Tissue
NA	Numerical Aperture
N_{ab}	Number of Photons Absorbed
NADH	Reduced Nicotinamide Adenine Dinucleotide
NADPH	Reduced Nicotinamide Adenine Dinucleotide Phosphate
N_{em}	Number of Photons Emitted
NI	Normalized Intensity
NIR	Near-infrared
O_2	Oxygen Molecule
p	Momentum
p^+	Proton
PA	Patient A
PAC	Cancerous Colon Tissue Samples from Patient A
PAN	Normal Colon Tissue Samples from Patient A
PB	Patient B
PBC	Cancerous Colon Tissue Samples from Patient B
PBN	Normal Colon Tissue Samples from Patient B
PDT	Photodynamic Therapy
PpIX	Protoporphyrin IX
PVC	Poly Vinyl Chloride
R	Reference Intensity Reading
S	Sample Intensity Reading
σ	Standard Deviation
S_0	Singlet Ground State
S_1	Singlet Excited State
S_2	Singlet Excited State
SAD	Source to Axis Distance
SiO_2	Silicon Dioxide
SNR	Signal to Noise Ratio
τ	Fluorescence Lifetime
T	Kinetic Energy
UV	Ultraviolet
v	Speed of Light in a Medium
v_0	Ground State Vibrational Energy Level
v_1	Elevated Vibrational Energy Level
v_2	Elevated Vibrational Energy Level
V_a	Applied Voltage
V_{EtBr}	Volume of EtBr

Abbreviation	Full Name
V_{H20}	Volume of Water
VIS	Visible
v_n	Vibrational Energy Level
V_T	Total Volume (EtBr plus H_20)
θ	Angle of Incidents
θ'	Angle of Reflection
θ''	Angle of Refraction

APPENDIX II
UNIT CONVERSIONS

Units	Full Name	Conversion	Description
cm^2	Centimetres Squared	1 cm^2 = 1x 10^{-4} m^2	Area
µg/ml	Microgram per millilitre	1 µg/ml = 1x10^{-6} kg/l	Concentration
nm/pixel	Nanometre per Pixel		Dispersion
cGy	Centi Gray	1 cGy = 0.01 Gy = 0.01 J/kg	Dose
Gy	Gray	1 Gy = 1 J/kg	Dose
eV	Electron Volt	1 eV = 1.602x10^{-19} J	Energy
keV	Kilo Electron Volt	1 keV = 1x10^{3} eV	Energy
MeV	Mega Electron Volt	1 MeV = 1x10^{6} eV	Energy
Hz	Hertz	1 Hertz = 1 cycle/second	Frequency
cm	Centimetres	100 cm = 1 m	Length
mm	Millimetre	1 mm = 0.001 m	Length
nm	Nanometre	1 nm = 1x10^{-9} m	Length
µm	Micrometre	1 µm = 1x10^{-6} m	Length
M	Molar	1 mole substance/1 L solution	Molarity
mM	MilliMolar	1 mM = 0.001 M	Molarity
W	Watts	1 W = 1J/s	Power
Ω	Ohms	1 Ω = 1V/A	Resistance
K	Kelvin	K = °C + 273.15	Temperature
°C	Degrees Celsius		Temperature
min	Minutes	1 min = 60 s	Time
ns	Nanosecond	1 ns = 1x10^{-9} s	Time
s	Seconds		Time
hr	Hour	1 h = 3600 s	Time
m/s	Metre per Second	1 m/s	Velocity
V	Volts	1 V = 1 J/C	Voltage
ml	Millilitre	1 ml = 0.001 l	Volume
µl	Microlitre	1 µl = 1x10^{-6} l	Volume

APPENDIX III
PRODUCTS

Product No.	Name	Company
46047	Ethidium Bromide	Sigma-Aldrich Co.
430165	Polystyrene Cell Culture Dishes	Corning
48380068	Micro Cover Glass 22 mm No. 1	VWR International
11835-030	Gibco RPMI Medium 1640	Gibco
15249-062	Antibiotic-Antimycotic	Gibco
74-UV	Collimating Lens	Ocean Optics, Inc.
74-VIS	Collimating Lens	Ocean Optics, Inc.
B-3A	Filter Cube	Nikon Instruments, Inc.
Eclipse E400	Epi-fluorescence microscope	Nikon Instruments, Inc.
HTB-22	MCF-7 Breast Adenocarcinoma Cell Line	American Type Culture Collection
KX32ME	Cooled CCD Camera	Apogee Instruments, Inc.
L2	Detector Collimating Lens	Ocean Optics, Inc.
Leica CM 1850	Cryostat	Meyer Instruments, Inc.
LM1XY	X and Y Translating Lens Mount (+/- 1 mm)	ThorLabs, Inc.
LS-1	Tungsten Halogen Light Source	Ocean Optics, Inc.
OFLV	Variable Long Pass Order Sorting Filter	Ocean Optics, Inc.
S7810	Imaging Spacer	Sigma-Aldrich Co.
SM1A2	1" Tube to 2" Tube Adapter	ThorLabs, Inc.
SM1A3	Microscope Objective to 1" Tube Adapter	ThorLabs, Inc.
SM1L03	1" Tube 1/3" Deep	ThorLabs, Inc.
SM1L05	1" Tube 1/2" Deep	ThorLabs, Inc.
SM1SMA	SMA Fiber Adapter	ThorLabs, Inc.
SM1V05	1" Tube Rotating Adjustment Focus 1/2" Travel	ThorLabs, Inc.
SM2L05	2" Tube Lens Tube 1/2" Deep	ThorLabs, Inc.
SM2V10	2" Tube Rotation Adjustment Focus 1" Travel	ThorLabs, Inc.
1LX511	2048 Element CCD Array	Sony Electronics, Inc.
USB2000	Minature Fiber Optic Spectrometer	Ocean Optics, Inc.

Company Contact Information:

American Type Culture Collection
P.O. Box 1549
Manassas, VA 20108
Phone: (800) 638-6597
http://www.atcc.org

Apogee Instruments, Inc.
11760 Atwood Rd.
Auburn, CA 95603
Phone: (530) 888-0500
http://www.ccd.com

Corning
Phone: (800) 492-1110
http://www.corning.com/lifesciences/

Gibco
Invitrogen Canada Inc.
2270 Industrial St.
Burlington, ON L7P 1A1
Phone: (800) 263-6236
http://invitrogen.com/content.cfm?pageid=9371

Meyer Instruments, Inc.
1304 Langham Creek, Suite 235
Houston, Texas 77084
Phone: (281) 579-034
http://www.meyerinst.com/

Nikon Instruments, Inc.
1300 Walt Whitman Rd.
Melville, NY 11747-3064
Phone: (631) 547-8500
http://www.nikonusa.com/

Ocean Optics, Inc.
380 Main St.
Dunedin, FL 34698
Phone: (727) 733-2447
http://www.OceanOptics.com

Sigma-Aldrich Co.
2149 Winston Park Dr.
Oakville, ON L6H 6J8
Phone: (800) 565-1400
http://www.sigmaaldrich.com/

Sony Electronics, Inc
3300 Zanker Rd.
San Jose, CA 95134
Phone: (408) 432-1600
http://bssc.sel.sony.com/semi/

ThorLabs, Inc.
435 Route 206 North
Newton, NJ 07860
Phone: (973) 579-7227
http://www.thorlabs.com

VWR International
1310 Goshen Parkway
West Chester, PA 19380
Phone: (800) 932-5000
http://www.vwr.com

APPENDIX IV
DOSE CALCULATIONS

NWORCC Department of Medical Physics

Page 1/1 Patient Dose Calculation (v.6.4) 2003-Aug-20

Patient number: 000001C
Patient name: Actin GFP MCF-7
Date of calculation: 2003-Aug-20
Machine: C1

Total dose of 500cGy prescribed at 100.0%.

Field Number:	1
Field Description:	lat 1 brs
Energy:	1.25MeV
Col. Field (XxY):	10.0 x 10.0
Ref. Field (XxY):	10.0 x 10.0
Wedge:	None
Tray:	None
SAD:	80.0
Depth:	0.5
Field Weighting:	1.000
Field Daily Dose:	500.0
No. of Fractions:	1
Col. Eq. Square:	10.00
Ref. Eq. Square:	10.00
Unit Dose Rate:	98.0
Rel. Dose Factor:	1.000
Inv. Sq./Standoff:	1.000
T.P.R.:	1.416
Wedge Factor:	1.000
Tray Factor:	1.000
Compensator Factor:	1.000
Accessory Factor:	1.000
Beam Dose Rate:	138.8
Timer error (min):	-0.01

Time (min): 3.59

Page 1/1 Patient Dose Calculation (v.6.4) 2003-Jun-26

Patient number: 000001C
Patient name: H1 GFP MCF7 Cells
Date of calculation: 2003-Jun-26
Machine: C1

Total dose of 500cGy prescribed at 100.0%.

Field Number:	1
Field Description:	lat 1 brs
Energy:	1.25MeV
Col. Field (XxY):	10.0 x 10.0
Ref. Field (XxY):	10.0 x 10.0
Wedge:	None
Tray:	None
SAD:	80.0
Depth:	0.5
Field Weighting:	1.000
Field Daily Dose:	500.0
No. of Fractions:	1
Col. Eq. Square:	10.00
Ref. Eq. Square:	10.00
Unit Dose Rate:	100.0
Rel. Dose Factor:	1.000
Inv. Sq./Standoff:	1.000
T.P.R.:	1.416
Wedge Factor:	1.000
Tray Factor:	1.000
Compensator Factor:	1.000
Accessory Factor:	1.000
Beam Dose Rate:	141.5
Timer error (min):	-0.01

Time (min): 3.52

APPENDIX V
MEASUREMENT TIMELINES

Absorption Measurements of Colon Tissue

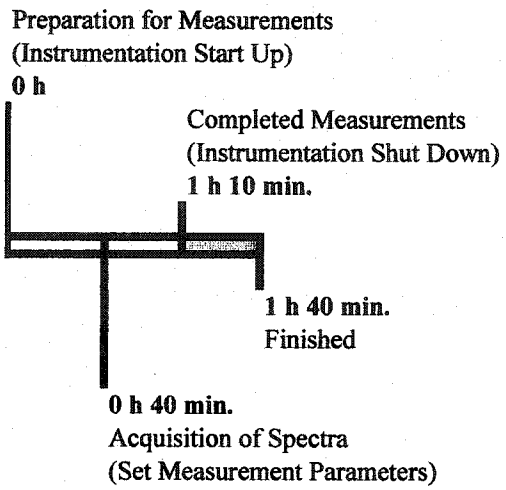

Fluorescence Measurements of Living GFP Tagged MCF-7 Breast Cancer Cell Line Samples Non-Irradiated or Irradiated [5 Gy].

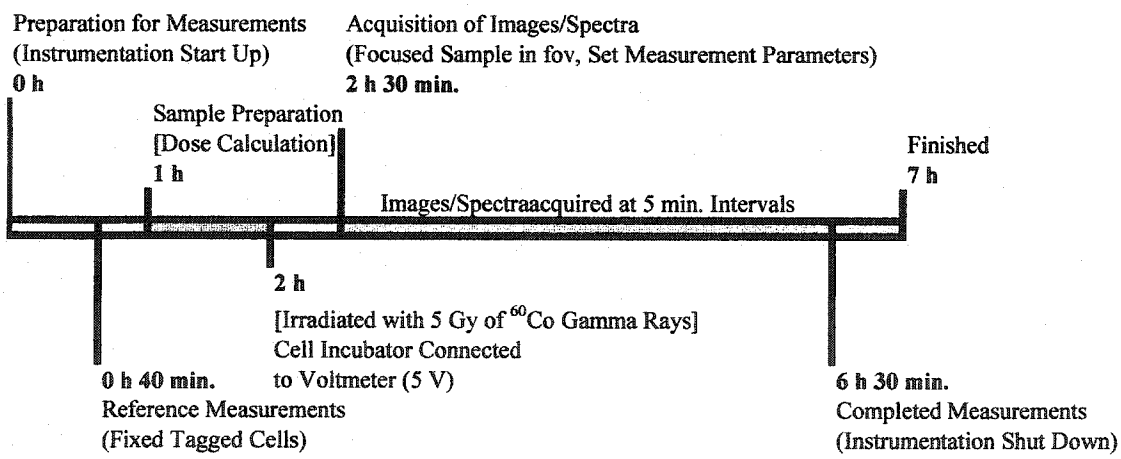

Fluorescence Measurements of Colon Tissue

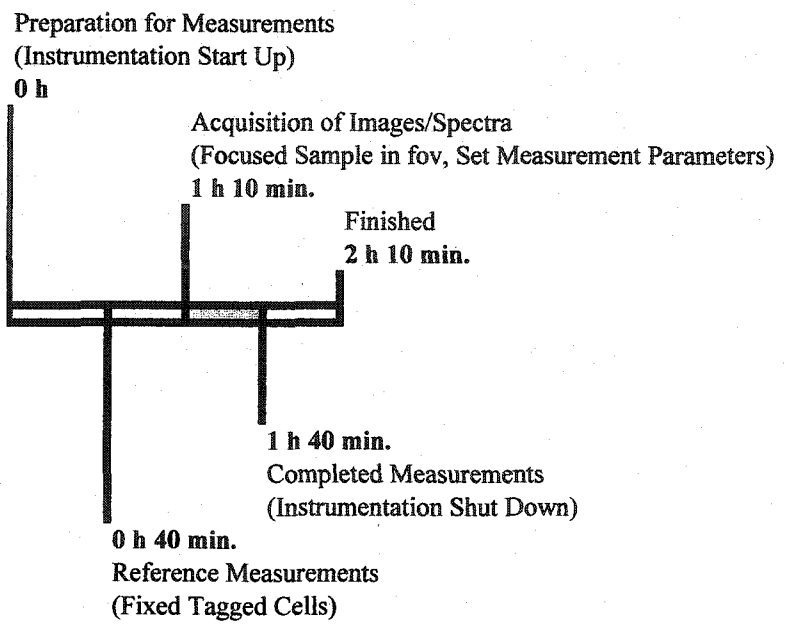

APPENDIX VI.i.
ANALYSIS SUMMARY FOR ABSORPTION SPECTROSCOPY FOR COLON TISSUE

Absorption Spectroscopy for Colon Tissue. (Re. Analysis and Results 6.1. pages 55-69)	
Raw Absorbance Spectra for Colon Tissue Samples	Three sets of fluorescence spectra and images were acquired for each of the normal and cancerous colon tissue samples from the two patients. Figures 6-1 and 6-2 illustrate the raw absorbance spectra for colon tissue of patients PA and PB respectively.
Calculation of the Spectral Area	Equation 6-1. (re. page 57) $\text{Spectral Area} = \sum_{\lambda} S(\lambda)$ $S(\lambda)$ is the intensity for the given wavelength range of 350 nm to 1000 nm. The spectral area was calculated as an alternative method to investigate the spectra.
Ratio of Area to Average Area	In Table 6-1 columns 3 and 5 show the ratios of the spectral area (equation 6-1) over the average spectral area for all spectral sets for each tissue type and patient. The spectral areas are calculated from the raw absorbance spectra in figure 6-1 and figure 6-2.
Normalized Absorbance Spectra for Colon Tissue Samples	Equation 6-2. (re. page 58) $NI = S(\lambda) \times \left(\frac{\text{Average Area}}{\text{Spectral Area}} \right)$ $S(\lambda)$ is the raw spectral reading for a given wavelength, the spectral area is calculated using equation 6-1, and the average area is calculated from the spectral areas obtained from each spectrum in a given spectral set. Normalization was carried out to obtain the same area under the curve for a given patient. The Normalization removed undesirable effects such as sample thickness
Renormalized Absorbance Spectra for Colon Tissue Samples	Equation 6-3. (re. page 59) $\text{RenormalizedNI} = \text{AverageNI} \times \left(\frac{\text{Average Area}}{\text{Average Normormalized Area}} \right)$ Term in the brackets is the renormalization ratio used to acquire the same spectral areas. Renormalization was carried out to facilitate comparison between (a) cancerous to normal colon tissue from the same patient, and (b) inter-patient comparison for the same colon tissue types (i.e. normal to normal and cancerous to cancerous). The renormalized spectra for patients PA and PB are illustrated in figures 6-3 and 6-4 respectively for the same patient comparison. The renormalized spectra for the inter-patient comparison are illustrated in figures 6-6 and 6-7.
Ratio of Renormalized Area to Average Area	In Table 6-2 column 4 shows the ratios of the renormalized spectral area (equation 6-1) over the average renormalized spectral area for all spectral sets for each patient. The spectral areas are calculated from the renormalized spectra in figure 6-3 and figure 6-4. In Table 6-5 column 4 shows the ratios of the renormalized spectral area (equation 6-1) over the average renormalized spectral area for all spectral sets for each tissue type. The spectral areas are calculated from the renormalized spectra in figure 6-6 and figure 6-7.

Spectral Difference between the Renormalized Spectra	Equation 6-4. Same patient Comparison (re. page 62) $SpectralDifference = \lvert RenormalizedC - RenormalizedN \rvert$ Equation 6-5. Inter-patient Comparison (re. page 67) $SpectralDifference = \lvert RenormalizedPA - RenormalizedPB \rvert$ The absolute values of the spectral differences were calculated for the two inter-comparisons to investigate variations between spectra. The spectral differences were plotted versus wavelength and a Gaussian fit was applied from the shape of the curves. For the same patient comparison the spectral difference is plotted in figure 6-5 and the Gaussian fit parameters are in table 6-3. For the inter-patient compa rison the spectral difference is plotted in figure 6-8 and the Gaussian fit parameters are in table 6-6. The errors for the spectral differences are calculated to the standard deviation (or root mean square). $\sigma = \sqrt{\frac{1}{N}\sum_{i=1}^{n}(x_i - \bar{x})^2}$ Where σ is the standard deviation, N is number of data points, x_i is a given difference and $\bar{x}$ is the mean difference.
Ratio of Area to Average Spectral Difference	Table 6-4 summarizes the ratio of the spectral area (Equation 6-1) of the spectral difference (Equation 6-4) to the average spectral difference for each spectral set for the same patient comparison. Table 6-7 summarizes the ratio of the spectral area (Equation 6-1) of the spectral difference (Equation 6-5) to the average spectral difference for each spectral set for the inter-patient comparison.

APPENDIX VI.ii.
ANALYSIS SUMMARY FOR FLUORESCENCE SPECTROSCOPY FOR ETHIDIUM BROMIDE

Fluorescence Spectroscopy for Ethidium Bromide (EtBr) (Re. Analysis and Results 6.2.1. pages 70-71)	
Raw Fluorescence Spectra for EtBr Samples	Fluorescence spectra were acquired for 5 concentrations of Ethidium Bromide (EtBr). EtBr was used due to its well known spectra, stability, and was readily diluted. The raw fluorescence spectra for the EtBr concentrations are shown in figure 6-9.
Calculation of the Spectral Area	Equation 6-1. (re. page 57) $\text{Spectral Area} = \sum_{\lambda} S(\lambda)$ $S(\lambda)$ is the intensity for the given wavelength range of 510 nm to 800 nm. An alternative method to investigate the spectra. Table 6-8 summarizes the spectral area (Equation 6-1) for each EtBr concentration.

APPENDIX VI.iii.
ANALYSIS SUMMARY FOR FLUORESCENCE MEASUREMENTS FOR FIXED TAGGED REFERENCE CELLS

Fluorescence Spectroscopy and Imaging for Fixed Tagged Reference Cells (Re. Analysis and Results 6.2.2. pages 72-74)	
Raw Fluorescence Spectra and Images for Fixed Tagged Reference Cells	Raw fluorescence spectra and images were acquired for the fixed tagged reference cells initially to align the eyepiece/fibre adapter, adjust the iris size to approximate the collection area of the fibre. Before fluorescence measurements of colon tissue and living cells the reference cells were used to adjust the iris size comparing the images and spectra to the initial results during adapter alignment. The raw fluorescence spectra are illustrated in figure 6-10 for the fixed tagged reference cells.
Calculation of the Spectral Area	Equation 6-1. (re. page 57) $\text{Spectral Area} = \sum_{\lambda} S(\lambda)$ $S(\lambda)$ is the intensity for the given wavelength range of 510 nm to 800 nm. The spectral areas (re. table 6-9) were calculated as an alternative method to investigate the spectra.

APPENDIX VI.iv.
ANALYSIS SUMMARY FOR FLUORESCENCE MEASUREMENTS FOR LIVING TAGGED MCF-7 CELLS

Fluorescence Spectroscopy and Imaging for Living Actin and H1 GFP Tagged MCF-7 Cells (Re. Analysis and Results 6.2.3. and 6.2.4. pages 74-83)	
Raw Fluorescence Spectra and Images for Living Tagged Cell Samples	Raw fluorescence spectra and images were acquired at 5 minute intervals for non-irradiated and irradiated living actin and H1 GFP tagged MCF-7 cells. The raw fluorescence spectra for actin GFP tagged MCF-7 cells were plotted in figure 6-12 and the raw fluorescence spectra for H1 GFP tagged MCF-7 cells were plotted in figure 6-13.
Calculation of the Spectral Area	Equation 6-1. (re. page 57) $\text{Spectral Area} = \sum_{\lambda} S(\lambda)$ $S(\lambda)$ is the intensity for the given wavelength range of 510 nm to 800 nm. The spectral area was calculated as an alternative method to investigate the spectra.
Ratio of Area to Average Area	In Table 6-11 column 4 show the ratios of the spectral area (equation 6-1) over the average spectral area for each cell type. The spectral areas are calculated from the raw fluorescence spectra in figure 6-12 and figure 6-13.
Renormalized Fluorescence Spectra for Living Tagged Cell Samples	Equation 6-3. (re. page 59) $\text{RenormalizedNI} = \text{AverageNI} \times \left(\frac{\text{Average Area}}{\text{Average Normormalized Area}} \right)$ Renormalization was carried out to compare between (a) the actin GFP tagged MCF-7 cells and (b) the H1 GFP tagged MCF-7 cells. The renormalized spectra for actin and H1 GFP tagged MCF-7 cells were plotted in figures 6-18 and 6-19 respectively.
Ratio of Renormalized Area to Average Area	In Table 6-12 column 4 shows the ratios of the renormalized spectral area (equation 6-1) over the average renormalized spectral area for each cell type. The spectral areas are calculated from the renormalized spectra in figure 6-18 and figure 6-19.
Spectral Difference between the Renormalized Spectra	Equation 6-6. (re. page 82) $\text{Spectral Difference} = \lvert \text{Renorm } S(\lambda) - \text{Renorm } S(\lambda) \rvert$ The spectral differences were calculated between N-N, I-I, and N-I. Where Non-irradiated (N), and Irradiated (I).
Ratio of Area to Average Spectral Difference	Table 6-13 summarizes the ratio of the spectral area (Equation 6-1) of the spectral difference (Equation 6-6) to the average spectral difference for N-N, I-I, and N-I. Table 6-14 summarizes the ratio of the spectral area (Equation 6-1) of the spectral difference (Equation 6-6) to the average spectral difference for N-N, I-I, and N-I.

APPENDIX VI.v.
ANALYSIS SUMMARY FOR FLUORESCENCE MEASUREMENTS FOR COLON TISSUE

Fluorescence Spectroscopy and Imaging for Colon Tissue (Re. Analysis and Results 6.2.5. and 6.2.6. pages 84-92)	
Raw Fluorescence Spectra and Images for Colon Tissue Samples	Two sets of fluorescence spectra and images were acquired for each of the normal and cancerous colon tissue samples from the two patients. Figures 6-20 and 6-21 illustrate the raw absorbance spectra for colon tissue of patients PA and PB respectively.
Calculation of the Spectral Area	Equation 6-1. (re. page 57) $\text{Spectral Area} = \sum_{\lambda} S(\lambda)$ $S(\lambda)$ is the intensity for the given wavelength range of 510 nm to 800 nm. The spectral area was calculated as an alternative method to investigate the spectra.
Ratio of Area to Average Area	In Table 6-15 column 3 shows the ratios of the spectral area (equation 6-1) over the average spectral area for each spectral sets and tissue type for each patient. The spectral areas are calculated from the raw absorbance spectra in figure 6-20 and figure 6-21.
Normalized Fluorescence Spectra for Colon Tissue Samples	Equation 6-2. (re. page 58) $NI = S(\lambda) \times \left(\frac{\text{Average Area}}{\text{Spectral Area}} \right)$ Normalization was carried out to obtain the same area under the curve for a given patient. The Normalization removed undesirable effects such as sample thickness
Renormalized Fluorescence Spectra for Colon Tissue Samples	Equation 6-3. (re. page 59) $\text{RenormalizedNI} = \text{AverageNI} \times \left(\frac{\text{Average Area}}{\text{Average Normormalized Area}} \right)$ Renormalization was carried out to facilitate comparison between (a) cancerous to normal colon tissue from the same patient, and (b) inter-patient comparison for the same colon tissue types (i.e. normal to normal and cancerous to cancerous). The renormalized spectra for patients PA and PB are illustrated in figures 6-23 and 6-24 respectively for the same patient comparison. The renormalized spectra are for the inter-patient comparison illustrated in figures 6-25 and 6-26.
Ratio of Renormalized Area to Average Area	In Table 6-16 column 4 shows the ratios of the renormalized spectral area (equation 6-1) over the average renormalized spectral area for all spectral sets for each patient. The spectral areas are calculated from the renormalized spectra in figure 6-23 and figure 6-24. In Table 6-18 column 4 shows the ratios of the renormalized spectral area (equation 6-1) over the average renormalized spectral area for all spectral sets for each tissue type. The spectral areas are calculated from the renormalized spectra in figure 6-25 and figure 6-26.

Spectral Difference between the Renormalized Spectra	Equation 6-4. Same patient Comparison (re. page 62) $SpectralDifference = |RenormalizedC - RenormalizedN|$ Equation 6-5. Inter-patient Comparson (re. page 67) $SpectralDifference = |RenormalizedPA - RenormalizedPB|$ The absolute values of the spectral differences were calculated for the two inter-comparisons to investigate variations between spectra. The errors for the spectral differences are calculated to the standard deviation (or root mean square). $\sigma = \sqrt{\frac{1}{N}\sum_{i=1}^{n}(x_i - \bar{x})^2}$ Where σ is the standard deviation, N is number of data points, x_i is a given difference and $\bar{x}$ is the mean difference.
Ratio of Area to Average Spectral Difference	Table 6-17 summarizes the ratio of the spectral area (Equation 6-1) of the spectral difference (Equation 6-4) to the average spectral difference for each spectral set for the same patient comparison. Table 6-19 summarizes the ratio of the spectral area (Equation 6-1) of the spectral difference (Equation 6-5) to the average spectral difference for each spectral set for the inter-patient comparison.